A Thesis entitled

THE APPLICATION OF ELECTRON-OPTICAL IMAGING DEVICES TO TIME RESOLVED SPECTROSCOPY

by

SAMPANNA MAJUMDAR M.Sc., D.I.C.

Submitted for the

degree of Ph.D. in the University of London

Applied Physics Section
Physics Department
Imperial College
London S.W.7.

June 1966

ABSTRACT.

Problems in time resolved spectroscopy using scanning techniques in the submicrosecond region for plasma and laser spectroscopy are introduced. Advantages of using an image-converter-intensifier system with electron storage for nanosecond time resolution in spectroscopy are discussed.

A new "multiple beam" image converter tube which accomplishes framing and storing of the electron image simultaneously and without leaving any time gap between consecutive frames is described. Different methods of employing the tube in practice are discussed.

The effect of internal electronic time dispersion in the tube has been studied theoretically and experimentally.

Possible exploitation of this internal time dispersion so as to achieve a greater time resolution in spectroscopic work has been demonstrated.

Problems in electronic control and synchronisation are considered and an all transistor delay and control system has been constructed.

Details of techniques of construction of the multiple beam tube in its developmental and final form are given.

Preliminary work on the extension of the spectral range of the tube to the vacuum ultraviolet as well as to transients with low photon output by adding intensifier stages is described.

Use of the multiple beam tube for general high speed photographic work of transient phenomena is discussed and illustrated with 50 nanosecond frames of an argon spark discharge.

Possible future developments are discussed, including the use of the multiple beam principle for producing a sensitive wide band (1500 mc/sec) oscilloscope capable of recording single electrical transients.

CONTENTS.

	Page.
Chapter 1. Introduction.	
Scanned Interferometers for Time Resolved Spectroscopy.	1
Rotating Mirror and Drum Cameras	4
Magneto-Optic and Kerr Cell Shutters	5
Electron Optical Devices	6
Application of Storage Techniques to Image Tubes	10
Image Dissection	10
Chapter 2. Evaluation of Image Tubes for Time Resolved Spectroscopy and Choice of System.	
Optical Requirements and Set Up.	11
Design of a New Tube.	16
Chapter 3. Photo Electronic Techniques.	
Basic Components of an Image Converter or Intensifier	18
The Envelope	19
Electrodes	19
Metallising Paints	19
Metal Electrodes	20
Electrodes for Evaporation of Metals and Compounds used in Making Photoelectric Surfaces	21

Page.

Windows 24

Photo-Emissive Surfaces 26

Antimony Cesium Photocathode 28

Application of Lallemonde Techniques 29

Trialkali Photocathodes 31

Bi-Ag-O-Cs Photocathode Cesium Iodide Solar Blind 32

Photocathode 33

Production of Photocathodes in Ampoules 35

Fluorescent Screens 35

The Image Tube 41

Experimental Single Stage Tube for Ultraviolet

and Visible. 41

Fall in Cathode Sensitivity 46

Test on a Photocell of the Effect of Pumping a

Photocell to a very Low Pressure 48

Special Two Stage Cascaded Image Intensifier with Externally

Processed Photocathodes and Phosphor-Photocathode Sandwiches 52

Chapter 4. The Multiple Beam Tube - Principle of Operation.

Basic Consideration - Use of Small Width Cathode 56

Operation as a Framing Camera, Principal Mode 56

Saliant Features and Advantages 62

Time Dispersion 63

Way to Minimise Time Dispersion 66

Chopped Mode of Operation 68

Page.

Streak Operation 72

Utilisation of Time Dispersion to Achieve Higher Time Resolution in Spectroscopy. 74

Chapter 5. Electronics.

General Electronic Requirements 82

Avalanche Mode of Operation for a Transistor 83

Design and Construction of Electronic Circuits 87

Improvement of Electronic Circuits 91

General Layout of the Electronic and other Variable Electrical Outputs 98

Spurious Triggering and Shielding 101

Chapter 6. Design and Production of High Speed Tubes.

Electrode Assembly for the first Tube Design 102

New Assembly System Using Ceramic Rods 104

Fixing the Metal Assembly Inside the Pyrex Carcase and Assembly of the Whole Tube. 110

Introduction of Photocathode inside the Tube. 115

Loss of Photocathode Sensitivity after Seal Off. 115

Recesiation Inside the Tubes 117

Redesign of the Tube with an Internally Processed Photocathode 118

Monitoring Evaporation and Processing by Reflection 121

Processing of the Image Tube 121

Chapter 7 Evaluation of the Performance of Multiple-Beam Tubes.

The Demountable Tube with Thermionic Cathode 124

Tube with Photocathode 134

Tube with Photocathode Processed Inside 138

Recording of a Luminous Transient Phenomenon 157

Chapter 8 Discussion and Future Developments.

Limit of Time Resolution Achievable with a Multiple Beam Tube 161

Improvement in Tube Design 164

Use of Multiple - Beam Principle for Producing Wide-Band and Sensitive Oscilloscopes 166

Conclusion 177

Acknowledgments 178

References 179

CHAPTER I.

INTRODUCTION.

Scanned Interferometers for Time Resolved Spectroscopy.

In the past decade great interest has arisen in rapid spectral measurement with the growth of laboratory plasmas and subsequently with the invention of lasers with very high spectral purity, coherence and extremely short time duration. In plasma diagnostics, rapidly changing phenomena needed spectrometers with very short recording times.

Conventional photographic methods of spectrum analysis ~~was~~ were found incapable of meeting this requirement for two reasons: 1) The insensitivity of photographic emulsion and reciprocity failure at low light levels. 2) Lack of proper shuttering mechanism to select and record an event with enough accuracy in a very short time scale. On the other hand the linearity of response and very high quantum efficiency coupled with signal amplification available in a photomultiplier seemed to be the ideal solution to the problem if scanning techniques could be developed for display of the spectral line profiles on an oscilloscope screen.

Jaquinot (1948) developed a scanning Fabry-Perot interferometer which could scan a line profile in a few minutes by varying the air pressure between the etalon plates. This technique, with enhanced speed was suited most to high time resolved work because of the superiority of a Fabry-Perot interferometer over other dispersive systems due to its high angular dispersion and light gathering power (Jaquinot, 1954).

Tolansky and Bradley (1959) and Bradley (1962)described new oscillating Fabry-Perot systems where one of the two etalons was oscillated electromechanically. A time resolution of 100 μsec could be achieved by this system. A further increase in scanning speed was obtained by Cooper & Grieg (1962), and Ramsay (1962) and others by using piezoelectric drive. Cooper and Grieg claim to achieve a scanning period of 0.1μ sec for one spectral line profile.

A serious disadvantage of such a system is the fact that time and wave number dispersions are superposed. Thus the scanning time has to be much faster than the rate of change of the phenomenon observed. If N is the interferometer finesse, the scanning rate has to be N (about 20) times faster than the rate of change of the phenomenon under study. Another defect of the system is that only a point source is utilised and continuous monitoring of the event is not possible. Both these factors lead to a decrease in signal to noise ratio attainable with a given source.

Thus for resolution below about 0.5 microsecond this system of time resolved spectroscopy becomes useless.

A much higher time resolution is demanded in plasma diagnostic spectroscopy, specially with the development of the new laser light sources of very short duration and high power (Ascoli-Bartoli 1965). With the advent of lasers capable of producing giant pulses for time duration shorter than 10 nanoseconds (peak power tens of megawatts) one problem of plasma diagnostic spectroscopy in the nanosecond region becomes simpler if Q-spoilt lasers are used as a tool - there are enough photons

available to allow recording of fringes on a photographic plate with exposures as short as one nanosecond. But for some scattering experiments amplification of the signal will still be required.

The study of the phenomenon of Q-spoiling has itself become of great importance and for this purpose a spectral resolution of less than 0.01 cm^{-1} with continuous monitoring of the event with time resolution in the nanosecond region is required. Because of the abundance of photons in these experiments no light gain is required in the spectroscope although synchronisation becomes very critical.

A different system of high resolution spectroscopy than scanning Fabry-Perot system is therefore required for these types of experiments The most obvious solution to this problem is going back to photographic techniques which have developed very rapidly in the post war period. If very short duration exposures of a Fabry-Perot fringe system were achieved, the two disadvantages of scanning Fabry-Perot spectrometers would be obviated. This is because in such a system (Bradley, Majumdar et.al. 1964) the wave number and time dispersions are crossed and not superposed. Also, full advantage of the high light gathering power of a Fabry-Perot system can be taken because the whole fringe pattern can now be imaged. The purpose of the present work was to explore the possibilities of employing high speed photographic techniques to time resolved spectroscopy in the visible as well as ultraviolet range of spectrum (From 7000 A^{o} to 1700 A^{o}) and to devise a suitable time resolving camera which could be used for nanosecond resolution in conjunction with a Fabry-Perot interferometer.

In order to do this a study of the present art of high speed photography was first made, as will be discussed in the following section.

Two excellent reviews of the subject were prepared by J.S. Courtney-Pratt (1957) and K.R. Coleman (1963) which were of great assistance in this study.

The two oldest types of shutters for short exposures and time selection were the mechanical shutters (Corco, 1962) and the cine cameras. But neither of these types of camera can achieve time resolution even in the microsecond region.

Rotating Mirror and Drum Cameras;

Rotating mirror cameras have in the past decade found extensive uses in high speed framing and streaking operation. Schardin (1956) has shown theoretically that in a rotating mirror camera the ultimate time resolution is limited by the strength and the density of the mirror material and that the limit of time resolution that could be achieved with such a system is well below one nanosecond. Coleman (1963) reviews the different techniques quite comprehensively. In the last two years the techniques of rotating mirror cameras have been perfected. It was suggested by Buck (1960) that use of Beryllium as the mirror material would improve performance of rotating mirror cameras as this material distorts less at high speeds. This was in fact found to be so by Landre (1964) and Beckman and White now makes rotating mirror camera systems with beryllium mirrors coated with aluminium and silicon monoxide for framing times as small as 3 nanoseconds. Hargrove and Courtney-Pratt (1965) reported using one of these cameras to study the light output

from an intracavity modulated He-Ne gas laser, with a time resolution of about 3 nsecs. The mirror was driven byadry air turbine at 2000 revolutions per second. When used at 4000 r.p.s., the mirror vibration became very serious and the image was badly distorted. The problem of mirror vibrations was studied by Winker (1964) who showed that mirrors could be designed to avoid resonance at any particular revolution rate upto about 10000 revolutions per second, using steel as mirror material.

Rotating mirror cameras are almost always used with photographic film for direct recording of the transient event, some times with a moving film. A system like this will prove useful to record spectrograms from a strong laser source because no intensification of the image is required. Also, since the beam divergence in a laser beam is small, the system does not get aperture limited.

But to obtain continuous monitoring of an event a rotating mirror camera is only useful when used as a streak camera. Besides, for use in plasma dianostics where the available number of photons is not large, photographic recording becomes impossible unless some sort of image intensifying device is employed before photographing. Fatora (1965) surveyed a number of commercial cameras manufactured in the U.S.A. and the U.K. which are useful for users of such cameras.

Magneto-Optic and Kerr Cell Shutters.

Amongst non mechanical shutters, work has been done on magneto-optic shutters employing Faraday effect by several authors (Edgerton 1961, Weedon 1962, for example). Shutter speeds in the region of one hundred nanoseconds could be achieved by this method.

Many authors have successfully employed a Kerr cell for very short exposures in a single shot or in a sequence of shots. Thus, Goss (1960) reported a Kerr cell camera capable of producing 6 frames each of 5 nanosecond duration and with 15 nanosecond seperation, using an optical delay tank in conjunction with only one Kerr cell. Eylon (1962) reported a Kerr cell camera which could take 4 shots, each of 5 nanoseconds duration. A twelve channel Kerr cell camera was designed by Barnsley (1962). Leibig & Frungel (1960) describe a coaxial Kerr cell system capable of 5 nanosecond framing.

Although very fast exposures could be achieved with these cameras, the transmission of the cell when turned on by switching the high voltage pulse on only reaches about 15%. Continuous monitoring of an event without any time gap between consecutive frames is also not possible.

Electron-Optical Devices.

These type of devices form one of the most studied and promising branches of high speed cameras. In the first phase of its development, image converter tubes developed during the second war were used to obtain single shot exposures, as well as framing and streak operation (for example, Courtney-Pratt, 1952 , Hogan 1951). Mullard Limited introduced image converter cameras specifically for high speed photography (Jenkins and Chippendale, 1951) and many authors used this tube for all three types of operation - single shot, multiframing and streaking. Exposure times as short as 7 nsec have been achieved by Saxe and Chippendale (1955), while King and Hett (1960) have used these tubes for a framing rate upto 2×10^6 pictures per second with 4 to 8 images displayed on the

phosphor screen.

Stondenheimer and Moor (1957) at R.C.A. developed an electrostatic image converter incorporating focussing and shuttering grids as well as deflecting plates. They claimed an exposure time of 10 nanoseconds. Space Technology Limited of U.S.A. has made a high speed camera commercially available with facilities for streak and framing operation using this R.C.A. tube. Minimum framing time of 5 nanoseconds is claimed. At this speed the resolution of the tube is very poor. Another commericial firm Beckman and Whitley (1965) has marketed image converter diodes with proximity focussing. The voltage on the diode is gated on for an exposure. Single shot exposures of 5 nanoseconds are claimed.

Butslov et.al. (1958) described very interesting tube designs with stages of intensification built inside the tube in cascade (named PIM3 and PIM 4). They used two pairs of deflecting plates on opposite sides of an aperture for gating. One pair produces short exposures by deflecting the electron beam across the aperture while the other pair compensates for the movement of the image on the screen. Two pairs of oscilloscope type deflecting plates are used to deflect the image in rows and columns. with Exposure times as short as 15 nanoseconds with a repetition rate of 3×10^7/- sec . Simonov et.al. (1960) used these tubes with a novel mismatched transmission line staircase voltage generator to obtain 5 nanosecond framing time at a rate of 10^8 pictures per second.

These tubes were the first ones with an incorporated light gain of about 8000, thus enabling high speed photographic work at lower light levels, as required in many experiments in diagnostic spectroscopy.

Malyshev et.al. (1963) have in fact used this type of camera with streak operation for diagnostic spectroscopy.

A different mode of operation of this tube was described by Zavcisky et.al (1956) where sinusoidal voltages of right phase were applied to the deflecting plates to obtain a sweep in a circle on the phosphor screen. A time resolution of 10^{-10} seconds is claimed and possibilities of extending it to 10^{-14} seconds is suggested.

Walter (1962) made tubes in England with PIM3 techniques to achieve $\frac{1}{2}$ nsec time resolution in streak operation. Huston and Walter (1962) proposed a tube design which employs PIM3 techniques for framing and time resolution with television camera type read out of the framed and time resolved image with signal amplification (Chippendale and Folkes, 1960).

Huston (1964,1965) described an image converter camera which employs modified PIM3 type tube with an ingenious electronic system to obtain 10 nsec frames at a repetition rate of 2×10^7 pictures/sec. Image converters with better time resolution as well as with an ultraviolet optical system are also designed by the same group at A.W.R.E.

Use of television cameras for high speed photography has also been explored by several authors (Saxe et.al. 1949). Most sucessful camera of this type has been described by Hopmann(1965) - capable of achieving frames with times as short as 10 nanoseconds. Special type of image converters were used by Drecescamp and Burton (1959) to sweep a small beam of photo electrons across a small phosphor screen to obtain nano-

second time resolution in experiments on decay time measurement of fast phosphors. The same technique with further sophistication was employed by Yguerabidi (1965) to obtain time resolution of 10^{-10} secs in measuring rise times of nanosecond light sources. Although the authors call the tubes image converter cameras, essentially the imaging is to the same extent as the imaging of an electron beam in a C.R. oscilloscope.

In all the cameras reviewed above, shuttering and framing is accomplished by highly sophisticated electronic control and high voltage pulsing. Even the simplest framing camera in this category (Huston 1964) needs an electronic shuttering system of quite involved nature to ensure linearity and reliability. This particular tube is quite suitable for time resolved laser spectroscopy by streak operation if photocathodes of suitable spectral response are used (like BiAg-O-Cs or Ag-O-Cs cathodes for ruby or neodymium glass lasers). Also transients like the generation of sparks in different gases with very high power solid state lasers can be studied with this tube, with subnanosecond time resolution. But for experiments where available number of photons is limited tubes with incorporated gainstages will be more useful (like the Russian tubes.)

One draw back of all these tubes is, even the low inertia of electrons is too much to synchronise the camera to an event. Hence either the event has to be triggered from the tube or an optical delay has to be introduced between the object and the camera objective. For example, with Huston's tube, an optical delay of about 50 nanoseconds is required (Key, Stokes, 1966) if the camera has to be triggered from the event.

Application of Storage Techniques to Image Tubes.

Hill (1962) suggested electron storage with low voltage photo-electrons to overcome this triggering problem. McGee (1962) proposed such a system with an equipotential storage section at 300 volts. A magnetically focussed cascaded image intensifier has been described by McGee et.al. (1966) which employed such storage section with gating facilities employing the mesh technique developed by Mandel (1960). Framing time of 5 nanoseconds has been achieved with such a system and it could be triggered from the event. The authors claim that 10^{-9} frames/sec is possible with this device. The advantage of Mandel's gating mesh is that it needs only a few volts to turn on from 'off' position.

Image Dissection.

Many authors worked on image dissector cameras and Courtney-Pratt (1964) gives a comprehensive bibliography on the subject. He (1957) suggested that combination of image-converters and image dissection techniques could produce time resolution as high as 10^{-14} sec. But a system with full advantages of the method is yet to be devised.

CHAPTER 2.

EVALUATION OF IMAGE TUBES FOR TIME RESOLVED SPECTROSCOPY AND CHOICE OF SYSTEM.

Optical Requirements and Set Up.

As explained in Chapter I, the best system having high spectral resolution and light gathering power is a Fabry-Perot interferometer. The interferometer system to be used in a high speed photographic system is diagramatically illustrated in Fig.(2.1.). A slit is placed crossed with the interference fringes and the slit image is then allowed to fall on the time resolving apparatus for recording the time resolved image. This could basioally be done in two different ways - slit image could either be swept at right angle to its length and a line is obtained on the photographic emulsion corresponding to every fringe element in the slit, (Fig.2.2.a.) or the image could be seperated into a number of descrete frames each representing a fraction of the time for which the image was allowed into the time resolving camera.(2.2.b.). In case of spectroscopy with laser sources with plenty of photons available, direct recording of the time resolved image of either type is possible in the submicrosecond region, using either a rotating mirror or an image converter camera. As is obvious from the review in chapter I, these are the two most suitable cameras for this type of work. When the work described in this thesis was started, nanosecond time resolution with continuous monitoring was not practicable in either of these cameras, although there were possibilities of their extension to these regions.

The two systems of time resolution described become more difficult

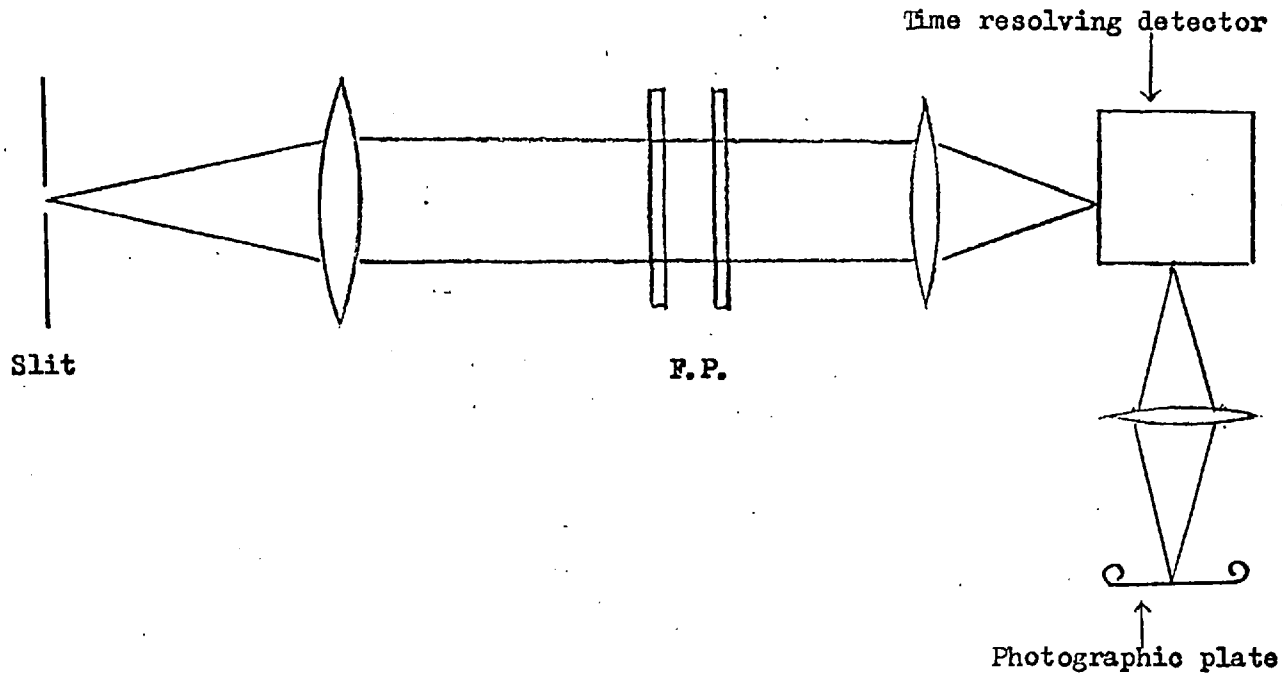


Fig 2.1.

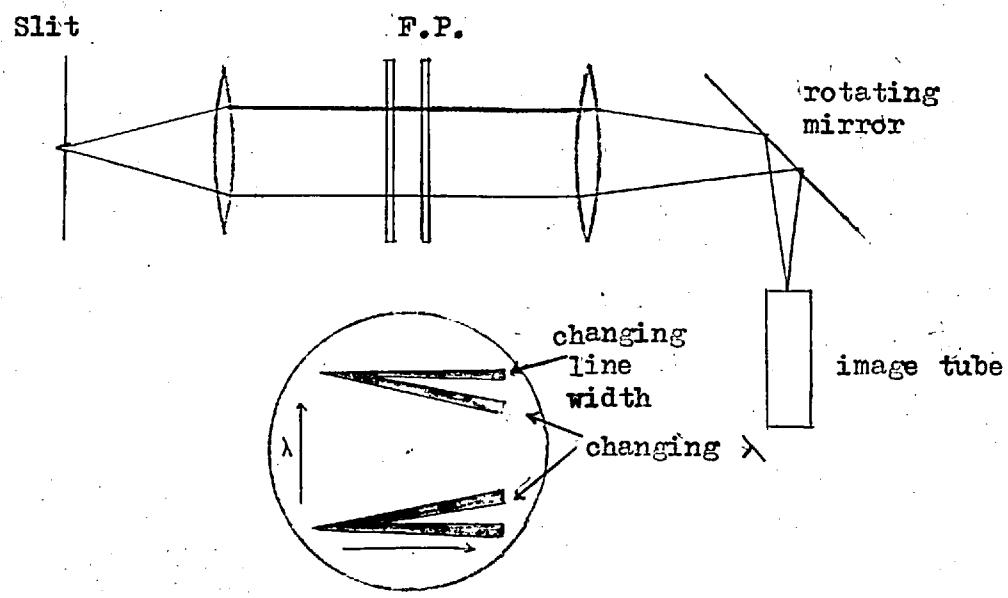


Fig 2.2.a

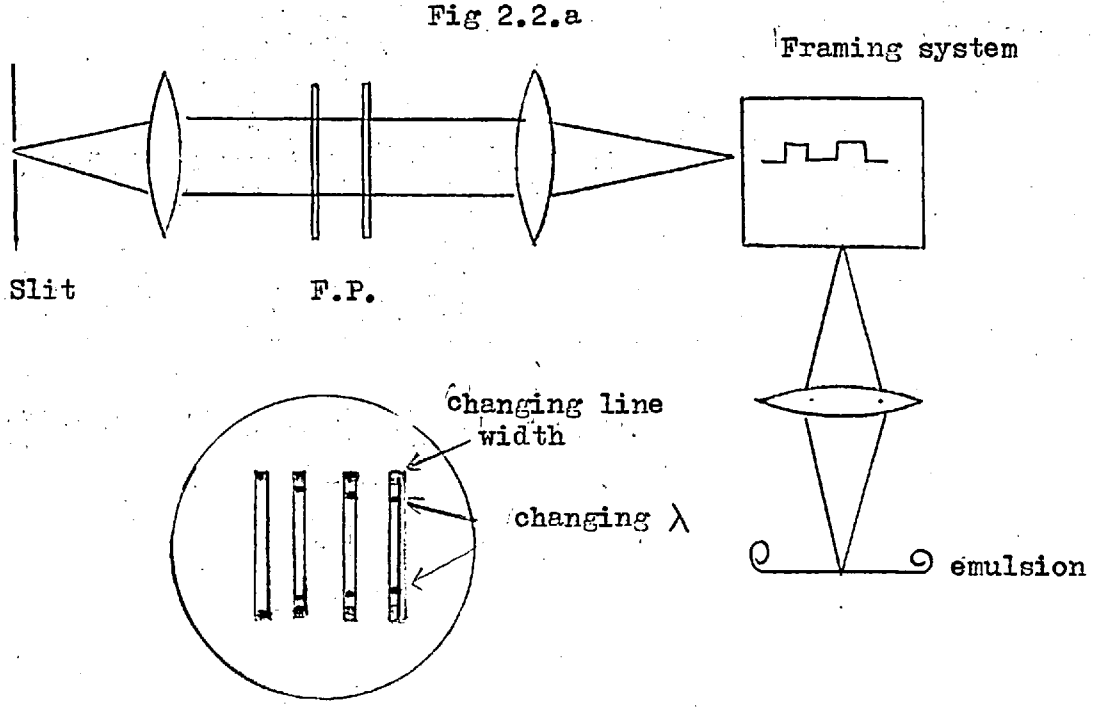


Fig 2.2.b

when the intensity of light is low. In such cases the image of the slit has first to be time resolved and then intensified for photographic recording (Bradley, Majumder et.al, 1964). Thus,whether one uses an image converter or a rotating mirror camera, an image intensifier has to be incorporated in the system. This is a point where an image converter-intensifier system scores and the Russians have used such systems for this purpose (Malyshev et.al. 1963). Also, the electron-optical time resolving system can at least in theory give better time resolution than a rotating mirror camera, and hence holds more promise for future development. Synchronisation problems are more serious in rotating mirror cameras because they need time to get a steady speed. Image tubes, specially those with storage techniques should be best suited for any form of ultra-high speed photography, let alone time-resolved spectroscopy. All these considerations were sufficient to make a decission for developing an image converter type camera with built in storage facilities. It was also decided to explore possibilities of devising a simple and efficient framing system in such a camera so that a number of frames can be obtained without any time seperation between frames. Although in conventional image converter cameras employing synchronised deflection such consecutive framing is not possible, employment of a storage section in an image tube opens up such possibilities.

As has been pointed out by Bradley et.al. (1963), to obtain best performance with a system comprising a Fabry-Perot and an image tube camera the linear resolution g of the image tube has to be matched to that of the projected fringe half width. This requires, for the pth

ring from the centre a focal length $f = 2gN\sqrt{p.s.\nu}$, where N is the finesse, s the interferometer separation and ν the wave number. Maximum use of the photocathode area of an image tube is made if the interferometer is tilted, so that only half of the ring pattern employed. It is best to start from the first order fringe outwards because angular dispersion decreases from the centre. Maximum number of rings which can then be displayed can be shown to be $(p_2 - p_1) = \frac{1}{2} gN$, independent of p_1 or p_2 if g is matched to p_2. If the light gathering power is to be utilised most, the width of the slit has to be kept at its maximum possible value. This is determined by the curvature of the fringes inside a slit, and for streak operation, the maximum width that is permissible can be derived from the angular width α of the slit:

$$\alpha = 2\sqrt{N.s.\nu}, \quad \text{so that linear width}$$

$$a = 4g\sqrt{N.p.}$$

using practical numerical values of

g = .01 cm (7 line pairs/mm), N = 20, p = 5, we get

a = 0.4 cm.

This slit width can be further reduced at the expense of the light gathering power. The length of the slit need only be about 1 cm. If such an image is swept 2 cmswithin a period between 50 to 100 nanoseconds (which is well within practical limits) about 200 resolution elements will be available for each fringe giving sub nanosecond time resolution. Also, 5 seperate frames can be accommodated in ths 2 cm space if the width of the slit is 0.4. cms, and more for narrower slits.

Design of a New Multiple Beam Tube.

The design and testing of a multiple beam camera described in this thesis exploits the fact that such a small cathode area, specially the width, is all that is required. As will be described in Chapters 4,5, 6, and 7, framing and sweeping of an image electron optically can be done with great simplicity in such a system which has the added advantage of perfect synchronisation because framing and sweeping is accomplished simultaneously with electron storage. The two other aspects of the problem i.e. extension of the spectral range to cover wavelengths from 1700 A° to 8000 A° (and subsequently to 11000 Å for neodymium lasers), and intensification of the image were taken up separately because of two reasons: 1) It is easier to construct a simple multiple beam image converter tube for general testing and evaluation of the design. 2)Intensifying tubes developed independantly with ultraviolet windows and special photocathodes can later be incorporated easily in a multiple beam tube to extend its range of use. This work was part of a project which also undertakes extension of Fabry-Perot interferometry to vacuum ultraviolet. Image tubes were made with ultraviolet windows and developmental work on different types of cathodes were also made to facilitate this work (Bradley, Majumdar et.al. 1964)[4,6]

In order to maintain the continuity of discussion of the main part of the work (i.e. development of the multiple beam tube) these two aspects along with the electron tube and photoelectronic techniques employed generally in this work are described in the next chapter, before going into the principle and designs of the high speed camera (Chapters 4 to 8).

Although the multiple beam tube has been developed for use specially in spectroscopy, any type of transient event with small image area can also be studied with it, with all the advantages of the multiple beam system. The only transient event so far has been recorded with a multiple beam tube is in fact one such event of high speed photography, with sufficent intensity for framing without intensification, i.e. an argon spark discharge (Chapter 7.).

CHAPTER 3.

PHOTO ELECTRONIC TECHNIQUES

3.1. Basic Components of an Image Converter or Intensifier.

An electron optical device like an image converter or image intensifier essentially consists of the following:

i) An envelope to maintain high vacuum.

ii) A system of electrodes to focus and control the photoelectrons, whose potential can be externally adjusted.

iii) A photoemissive surface to produce photoelectrons when an optical image is focussed on it.

iv) A suitable window to let the optical image fall on the photocathode.

v) A Fluorescent screen to reconvert the electron image to an optical image.

The choice of components depends on the type of work for which the device is required but in all cases some features like the following are desirable.

a) The system should have highest quantum efficiency.

b) Signal to noise ratio, i.e. contrast should be high.

c) The device should be stable and durable, and easy to handle.

The other factor which decide the choice of components is the availability of materials and techniques.

Choice and fabrication of different components along with progressive designs are described in the following sections.

3.2. The Envelope.

Pyrex tubing was chosen for envelopes and most of the glass works because of its good mechanical and electrical properties and more important, low quantity of ~~these~~ harmful gas content which could spoil the photoemissive surface and deteriorate the vacuum inside. This was of particular importance since almost all the photoelectric surfaces lose their efficiency and die in presence of water vapour, oxygen, hydrogen, chlorine and other active vapours.

In industry in the U.K., Kodial glass is mostly used for this purpose since matching alloys are available to make glass to metal seals which are rigid and could be very conveniently used to form an electrode system inside the vacuum chamber with provision for external connection.

No such properly matched metal or alloy exist for pyrex although small diameter tungsten pins or thin tapes of platinum can be used to connect internal electrodes to the outside. Pyrex glass system was still used because of the availability of such a system and associated techniques.

3.3. Electrodes.

Two types of electrodes were used,

a) Thin layers of metallising platinum or silver applied to the glass wall and

b) Metal electrodes fixed inside the tube and connected to the outside by tungsten pins or thin platinum tapes passing through the tube.

a) Metallising Platinum:

Two types of metallising platinum were used, both are products of

Johnson Mathey and Co.Ltd., One was the metalising paint, which had to be painted on the tube wall, and then cured by baking it up to the annealing temperature of the glass in the presence of ample air supply, which burnt out the organic suspension, leaving a very thin and shiny metallic layer of platinum. The other platinum preparation was a paste which was applied and dried before curing in the same way as the paint. This produced layers of platinum which could be 2 to 3 mm.thick. On the surface of this layer after it had been cured appeared a scum which could be cleared by buffing.

Silver pastes: These were also Johnson Mathey and Co. product and were used to produce metallic silver electrodes on the outside of the glass wall to which electrical connection could be made by soldering.

b) Metal Electrodes.

For external connections of internal electrodes, either tungsten pins or thin platinum tapes were used as described below. Tungsten and pyrex haveexpansion coefficients that are slightly mismatched, and could be used as a glass to metal seal with pyrex safely if the diameter of the tungsten pin is not larger than 2 mm. An oxide layer formed on the tungsten pin was most important for making a good leakproff seal

(This seal had to be handled carefully as it was not capable of withstanding mechanical shocks, specially impulses.

The seal of platinum tape through pyrex was also a mismatch - to a much greater extent than that in a pyrex-tungsten seal. But it could be used if the tape was narrow and thin . . This seal often produced a small leak after the glasswork had undergone the

necessary baking and annealing processes. To avoid such leaks, silver chloride was applied to the point where the tape came out from the tube body when the tube was at 455°C (melting point of Silver Chloride) during cooling down in the last annealing operation. As a final protection against the appearence of a leak, a leak sealing compound Gevac (General Electric ~~Motors~~, U.S.A.) was applied to these points and cured by baking for an hour at 200°C just before the final processing of a tube or an experimental photocell. Use of these seals in tubes for making experimental photocells and image tubes has been described in later sections.

Electrodes for Evaporation of Metals and Compounds used in making Photo-Electric Surfaces:

Fixed electrodes were used when the envelope was to contain the evaporant permanently inside it. These consisted of small boats of tantalum, molyldenum or a tube of nickel(in case of mixtures generating alkali metals) connected between two tungsten pins.

Movable electrodes carrying boats were used to evaporate metals onto the photocathode substrates in envelopes which could not contain these evaporators after processing had been completed. Magnets were used to move these evaporators, parts of which were made of magnetic materials, inside a vacuum system.

Three types of evaporators were used during the whole work as will be described below.

1. Nickel Evaporators, without any External Connections.

Fig.3.1.a. illustrates this type of evaporator, which employed eddy current heating for the purpose of evaporation. The evaporant

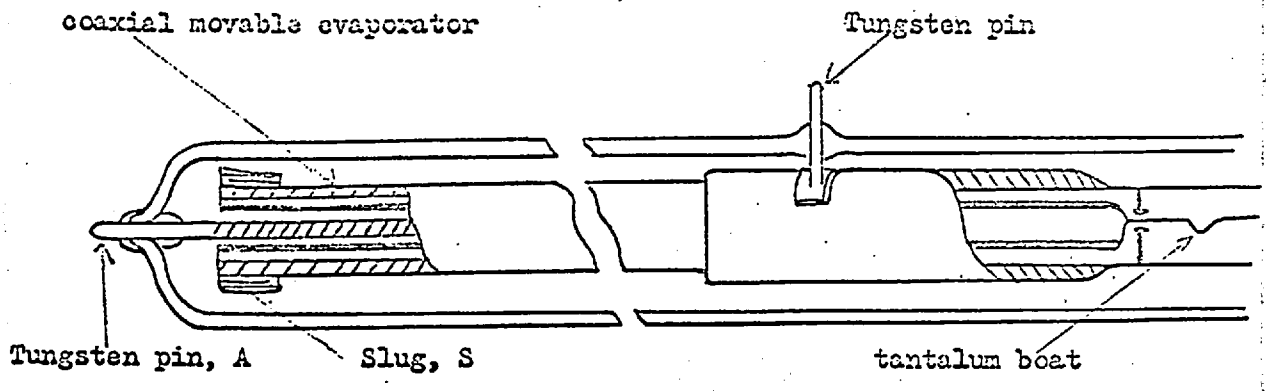


Fig 3.1.b

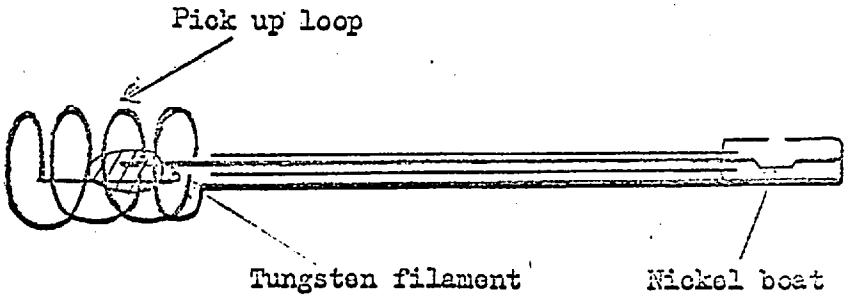


Fig 3.1.a

was loaded in a boat of very thin nickel sheet, shielded inside a rectangular box of nickel, with one end connected to the shield. The other end was connected to a one mm thick nickel wire, sleeved by a glass tube which entered the nickel box through a hole as shown. This wire was connected to the box via a pick up loop, also made of the same wire, and a small tungsten filament which was used to control the current through the boat. A small hole opposite the load in the boat in the shield allowed directional evaporation. When an output coil of a high frequency heater was brought near the pick up loop of the evaporator, both the boat and the tungsten filament were heated up and the load was evaporated. The heat and hence the rate of evaporation could be controlled by varying the amount of pick up or the power of the r-f heater. Extreme care was needed to control the amount of load evaporated. This type of evaporator was used during the early part of the work.

2. Coaxial Evaporator. Better control of evaporation was possible if the filament was heated by direct electrical connection so that the current could be measured. The coaxial evaporator, shown in Fig.3.1.b. was designed by the author to serve this purpose. The movable evaporator unit slided between two electrodes connected to the outside by tungsten pins. Two cylindrical stainless steel tubes with a pyrex glass tube between them were bound together by silver chloride to form the movable part, which had the evaporator head as an integral part, the sheild of which was formed by the outer stainless steel tube (Fig.3.1.b.). A tantalum filament was connected between the two concentric tubes inside the head as shown. A small hole in the outer tube opposite the filament

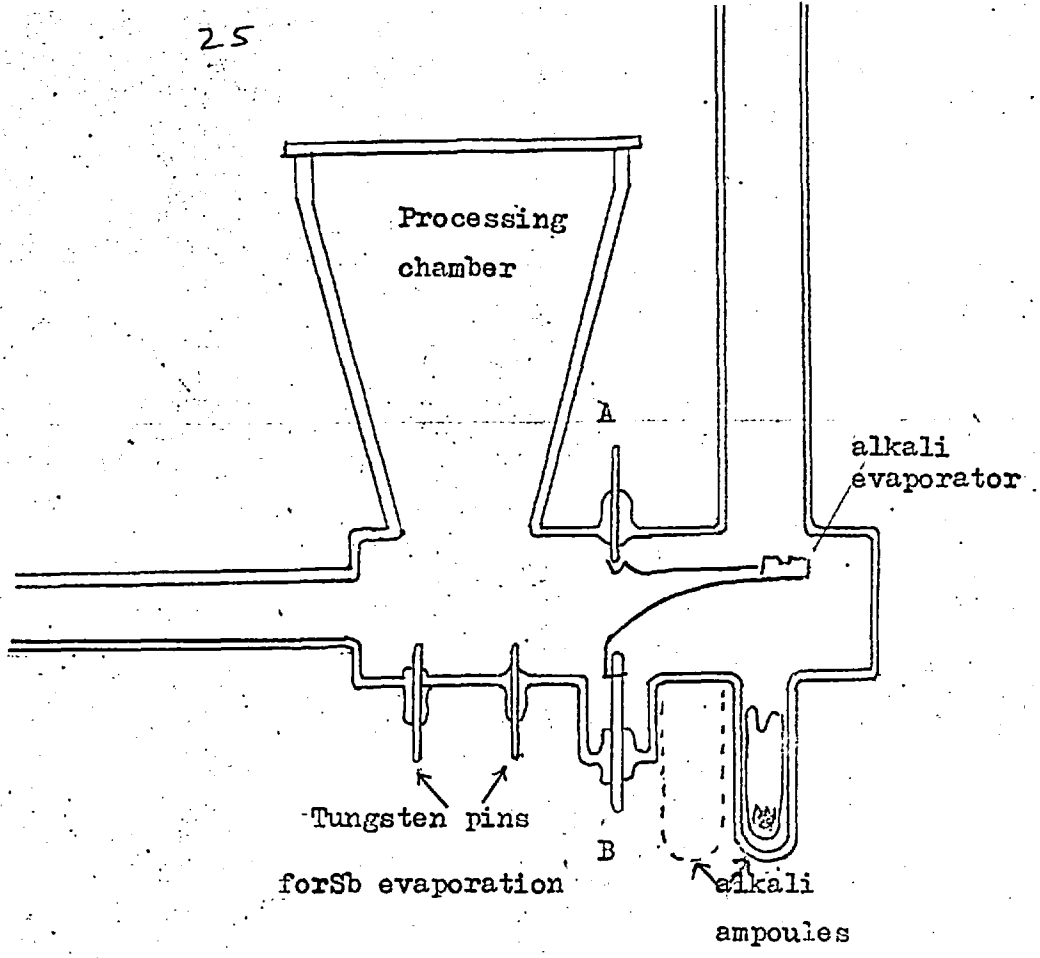
allowed directional evaporation.

A long tungsten pin A which slided through the inner tube constituted one electrode for external connection while another tungsten pin B which held a short cylinder of nickel through which passed the whole evaporator assembly constituted the other electrode. A cylindrical magnetic slug S of soft iron was fixed to the rear end of the evaporator for moving it with the help of a magnet. This evaporator, like the previous one, could be rotated about the axis through 360 degress. Control of evaporation was easy and straight forward with this evaporator.

3. Swinging Evaporator. This evaporator was designed by the author to evaporate three alkalies from one boat, by controlled electrical heating, and was used for processing trialkali cathodes (Fig.3.2.). As illustrated in Fig.3.2. the boat, similar in design to the one described in (1), is revolved about two tungsten pins A and B which also were the electrical contacts. The figure shows the system for trialkali processing. One of the alkalies was picked up from the ampoules K, Na, Cs by respective dippers and was loaded on the boat at will. Then the boat was swung round to face the cathode surface for evaporation. The boat could be cleared by emptying its charge by evaporation. Full details of operation are given in a following section.

3.5. Windows:

The range of spectrum in which interest was limited had been from 1700^{o}A in the vacuum ultraviolet to about 7000 A^{o} in the far red. For tubes to be used in the visible region of the spectrum pyrex windows were used. Image tubes with fused quartz windows (Spectrosil B, supplied by Thermal Syndicate Limited) were constructed for experimental purposes.


Processing
chamber
A
alkali
evaporator
Tungsten pins
forSb evaporation
B
alkali
ampoules

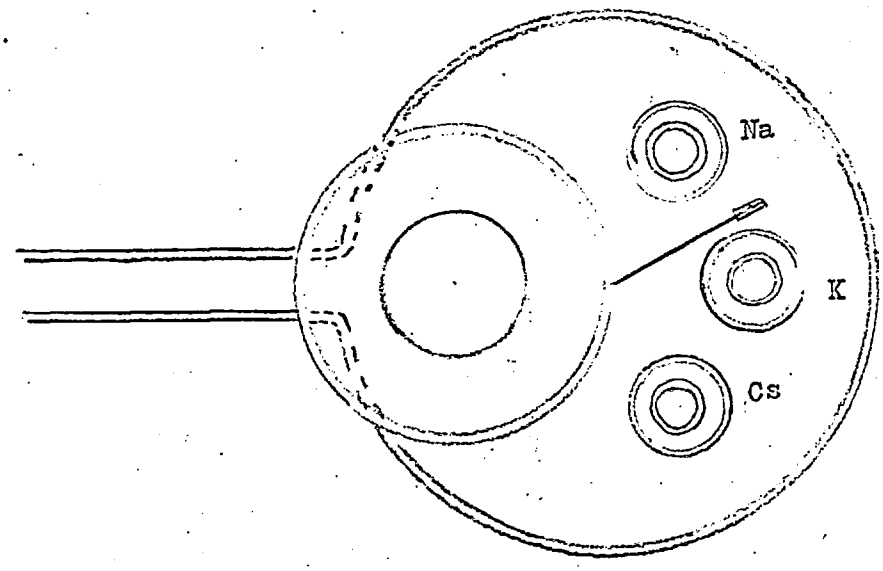

Na
K
Cs

Fig 3.2.

Whereas no problem was involved in sealing a pyrex window to the pyrex tube body, special sealing techniques had to be employed to seal a spectrosil window to the pyrex tube body. The best solution to this problem wasagraded seal, but the large diameter of such seals required for this purpose was prohibitive in their prices. Hence silver chloride seals with silver "washers" were used for sealing. This was done in two ways (Fig.3.3.)

Fig. 3.3.a. shows the technique used when a spectrosil plate was sealed to the ground and polished end of an image tube. A 0.005" thick annular sheet of silver was used between the plate and the polished end of the tube so that some strain was eased by the bellowing action of the silver sheet. Once silver chloride had melted and seal made, it was cooled down to room temperature very slowly ($3\frac{1}{2}$ hours).

Fig.3.3.b. shows a more satisfactory technique where a spectrosil plate was sealed to a pyrex plate slotted out in the centre. Silver washers were used between the spectrosil and the pyrex as before. Similar precaution was taken during the cooling down after silver chloride had melted and the seal made.

Since silver chloride did not run well on bare surfaces of spectrosil or pyrex, liquid platinum paint was applied to them in the region where seal was to be made. The paint was cured by baking in atmospheric pressure upto $600^{\circ}C$ for pyrex and $800^{\circ}C$ for spectrosil.

3.6. Photo-Emissive Surfaces:

The choice of photo-emissive surfaces were made with the following consideration:

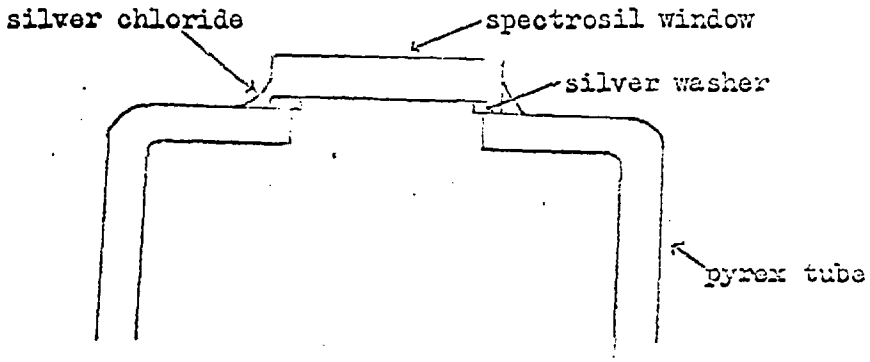


Fig 3.3.b

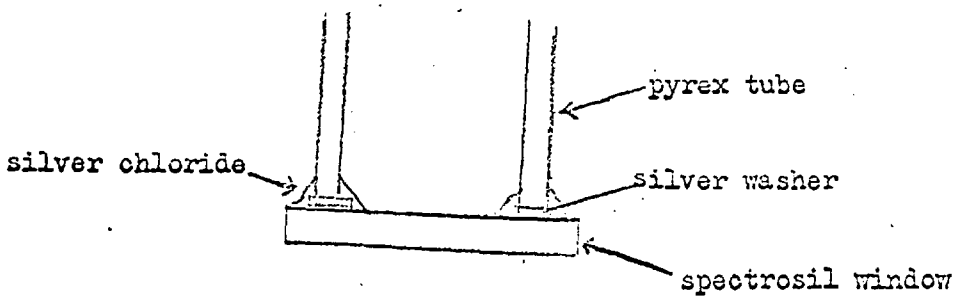


Fig 3.3. a

1. Maximum Quntan efficency in the region of spectrum interested.

2. Signal to noise considerations because of incident photons from unwanted region of spectrum.

3. Comparative ease of preparation of surfaces.

4. For high speed photographic work, conductivity of the photo-emissive layer.

In the general work on image intensifiers for intensification of the time resolved image, best possible photocathode was a trialkali photo-cathode For use in the vacuum ultraviolet region of the spectrum, solar blind cathodes like CsI could be extremely useful. For laser works, either trialkali or BiAgOCs cathodes were more suited because of their higher sensitivity in the red region. For image intensifiers used to study spectrum from 1700 A^{o} up-to 6000 A^{o} antimony cesium photocathodes have high guantum efficiency. BiAgOCs cathodes were the best when conductivity of the layer was most important.

Techniques were developed for making all these types of photocathodes for different uses.

Antimony Cesium Photo-cathode:

Antimony cesium photocathodes are the most commonly used ones in photoemissive devices. These were made for the preliminary single stage image converters with ultraviolet transmitting windows described in a following section. A layer of antimony was first evaporated on the spectrosil cathode substrate. The thickness of the evaporated layer was monitored by fall of transmission of white light through the substrate. A fall of about 25% in transmission was found to give best sensitivity.

Pure oesium was introduced while the substate was at 140°C and photo emissive surface was formed. Doses of cesium was introduced into the tube as the temperature was brought down to 70°C after which the system was rapidly cooled down.

Application of Lallemonds Technique to SbCs, processing.

Lallemond (private) reported that semitransparent S - 9 photocathodes of very high sensetivities could be obtained if processing was done by evaporating alternate layers of Sb and Cs onto the substrate. Processing in this way was tried for the following reasons.

i) To find out whether such a photocathode could be processed at room temperature by directional evaporation of Sb and Cs. If succesful, this method of processing could be applied to make image tubes with an end window photocathode (see sec.3.8.)

ii) To master evaporation techniques of alkalies and Sb for processing trialkali photocathodes, which are difficult to process in the conventional way on laboratory basis.

iii) To investigate the possibility of making highly sensitive antimony cesium photocathods as claimed by Lallemond.

Fig.3.4. illustrates the set up used. Antimony was evaporated from a fixed evaporator, A. The movable shield between the evaporator and the substrate was used to protect the substrate when antimony was pre-evaporated for cleaning purposes. Cesium was kept in an ampoule B beneath a dipper D which broke the thin glass membrane of the ampoule and dipped into pure molten cesium. The dipper was then lifted up and the coaxial evaporator E was brought up so that its filament was placed

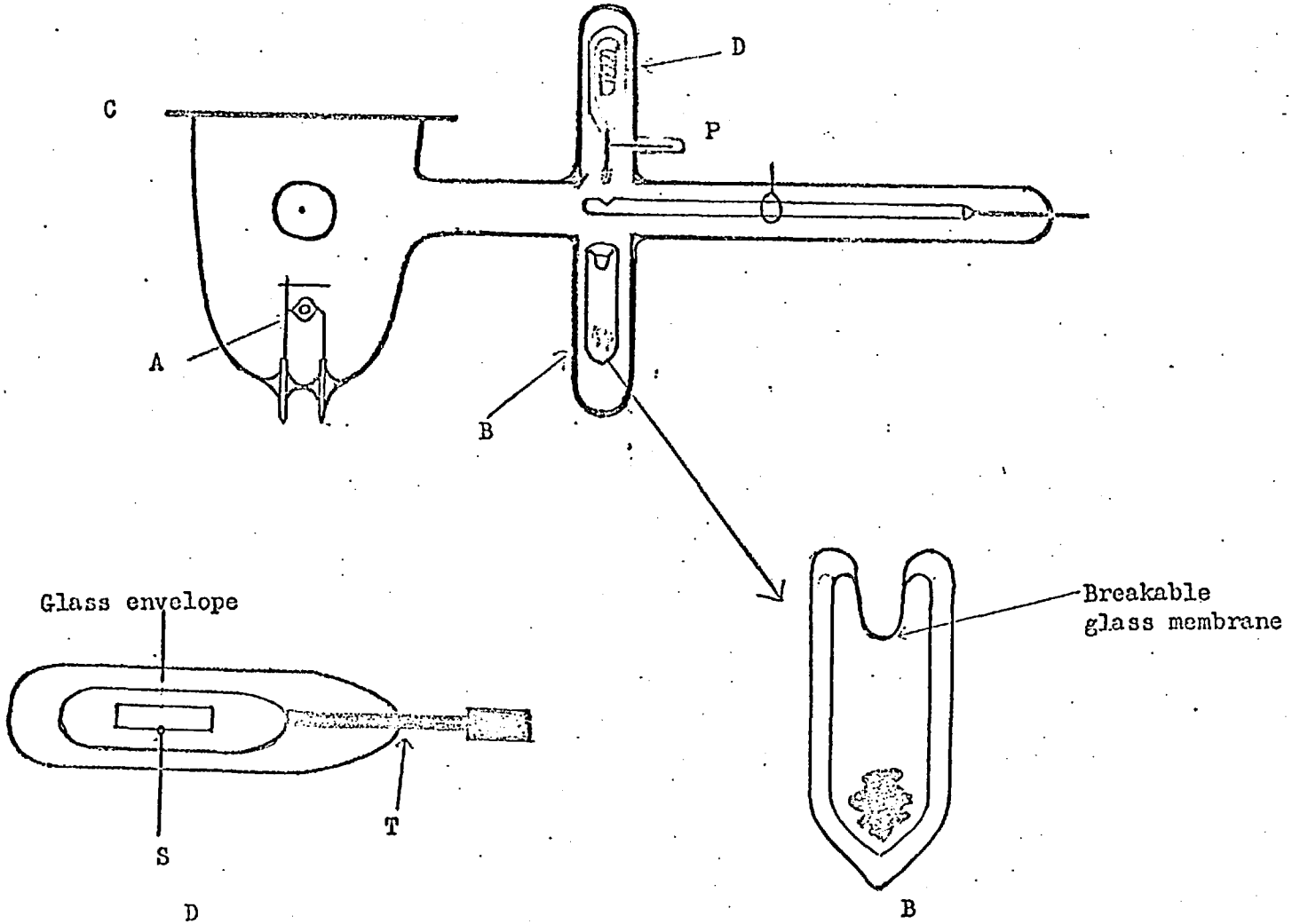


Fig 3.4

just underneath the pin of the dipper. The dipper was now lowered down to rest on the filament to load it with cesium from its tip and then lifted and locked into position with the locking pin P. The evaporator, thus loaded was taken inside the cell whenever cesium was to be evaporated onto the substrate C.

Photosensitivities in excess of 40 μA/lumen could be obtained using this system when processing was carried on either at room temperature or at an elevated temperature in the usual way. Processing at room temperature was found to take longer since the reaction was much slower. Slight heating of the substrate (to 45°C) increased the reaction speed substantially.

Tri-Alkali Photocathodes (Sb-Na-K-Cs.)

Processing of Trialkali photocathodes were first attempted in the conventional way (Sommer 1960) but reasonable sensitivities (anything in excess of 75 μA/lumen) could not be obtained consistently, and the rate of failure was very high. Hence evaporation of alkalies in the Lallemond technique was adapted in the hope that processing could be done at low temperatures, as opposed to the very high temperatures (250°C) needed in the conventional system. Fig.3.2. shows the set up of this system, where a swinging evaporator was used to evaporate all three alkalies. Everytime a different alkali was to be loaded into the evaporator, the latter was cleaned by evaporating off any residual alkali from the previous loading. As is shown in the diagram, the evaporator could be moved in a circle on whose circumference were three sets of ampoules and dippers for the three alkalies. After loading the evapor-

ator in the way described before, it was swung round to face the cathode substrate C for evaporating alkali onto it. Antimony was evaporated from a fixed filament between two tungsten pins placed directly facing the substrate.

Temperature of the substrate and the cell containing it was brought upto 135°C and antimony was evaporated to drop the transmission by 10%. Potassium was now evaporated, in small doses when the sensitivity rose slowly to a peak and started to climb down with slight more of potassium. Potassium evaporation was stopped. Antimony was evaporated again when sensitivity rose and then fell again. Now alternate layers of sodium and antimony were evaporated until the sensetivity rose to a plateau around 45μ A/lumen. The process was stopped with a final layer of sodium. Now cesium was evaporated onto the surface when the sensitivity rose to a new peak and started to fall down due to over cesiation. When the sensitivity had dropped to about 75% of the peak due to overcesiation, processing was stopped and the system cooled down as quickly as possible. Sensitivities above 80μA/lumen could be achieved fairly consistently in this way. Maximum sensitivities of 120μA/Lumen could be obtained. One interesting point was, cesium was found not to react with the surface at temperatures below 130°C. Thus was in agreement with Sommer's findings. (Sommer, 1944).

Bismuth Silver Oxide Cesium Photocathode:

This photocathode was used in multiple-beam tubes because of their high conductivity and red response characteristics. The set up for processing was similar to that for $SbCs_3$ (Fig.3.4.) except that it had

two side arms carrying two coaxial evaporators for bismuth and silver and another side arm for annular potassium chlorate used to generate oxygen. The processing cell could be seperated from the rest of the pumping system with the help of a movable plug used to cut down the conduction of the pumping time to very low values. This was done during oxygenation of the substrate.

A silver layer dropping the transmission of the glass substrate to 40% was first evaporated while the cell was at 145°C. The cell was now seperated from the pumping system and oxygen was generated by electrically heating the bulb containing potassium chlorate. When the pressure of oxygen in the cell was about 0.1 mm of Hg, oxygen generation was stopped and high frequency discharge was created inside the cell by a Tesla coil. This oxidised the silver layer, rising the transmission of the substrate. Oxidation was stopped when transmission rose to 60%. Bismuth was then evaporated on the surface to bring down the transmission to 40% again. The substrate was now cesiated in the usual way for a peak sensitivity monitered with red light of wavelength above 6000 A°, and then cooled down. Maximum sensitivity of 28 μA/lumen was obtained in this way although the average was 15 μA/lumen. The conductivity of the layer was measured by a system shown in Fig.3.5. Usually the resistance was around 200 per square although half the value could be achieved if sensitivity is sacrificed by making the A_g layer thicker and with less oxidation

Cesium Iodide Solar Blind Photocathode:

Cesium iodide is a stable and insulating material, the energy gap between the valence and conduction bands being 6.3. electron volts,

The cathode substrate, painted in 4 quadrant with liquid platinum

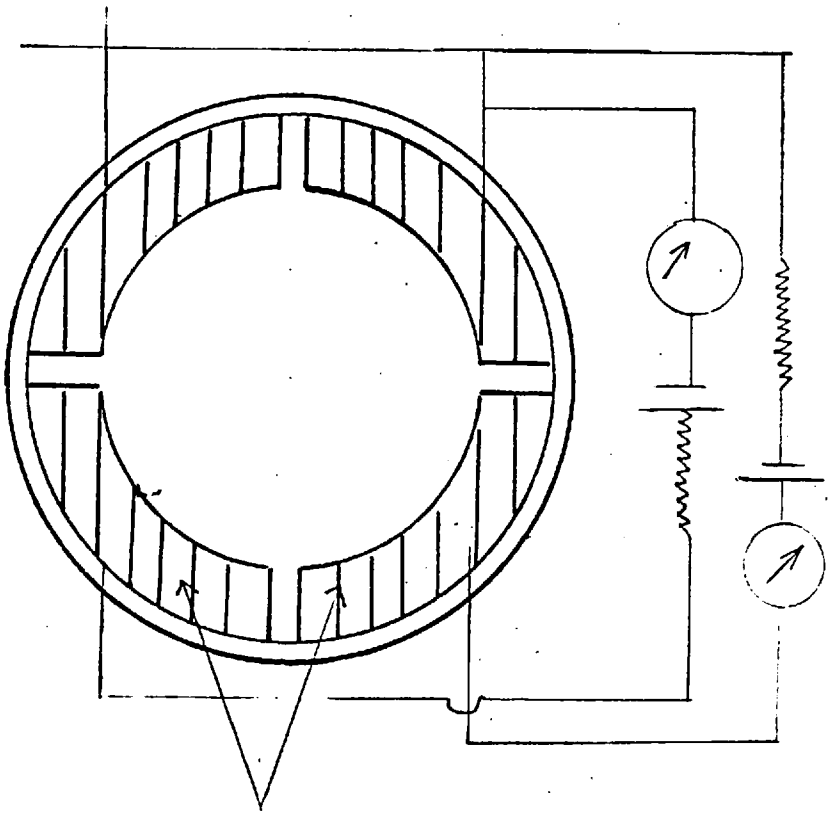


Fig 3.5.

corresponding to a photoelectric threshold of 2000 A^{o}. Sommer (1964) used a tungsten layer as a conducting backing to the CsI photoemissive surface. Nickel and palladium were used for this purposes too (Doughty et.al.1962). A layer of nickel was evaporated onto the spectrosil substrate which dropped its transmission by 20%. Cesium was then evaporated while the sensitivity was monitered all the time with a spectroline pencil lamp which had a fairly strong emission line at 1849 A^{o}. Quantum efficiency was estimated to be roughly 0.6% at 1849 A^{o}.

3.7. Production of Photocathodes in Ampoules:

It is known that (Folkes,1962) transferable photocathodes which are processed seperately and kept in an ampoule for subsequent introduction into a tube have definite advantages in production of quality image tubes. Such ampoules of photocathodes were made for use in the single stage tubes, the two stage cascade tube and the multiple beam tube.

Fig.3.6.a. shows the basic scheme of such a cathode production system where the cathode substrates were mounted on movable carriers (shown in Fig.3.6.b.) and could be carried into an 'ampoule' with a thin glass membrane (Fig.3.6.c.) brakable with the help of a magnetic slug when required. Carriers and empoules for photocathodes of various dimensions (for use in different types of tubes) were constructed. Fig. 3.7. shows a few such ampoule with processed photocathodes inside.

3.8. Fluorescent Screens:

Silver activated Zinc sulphide (P - 11) phosphors were used through-

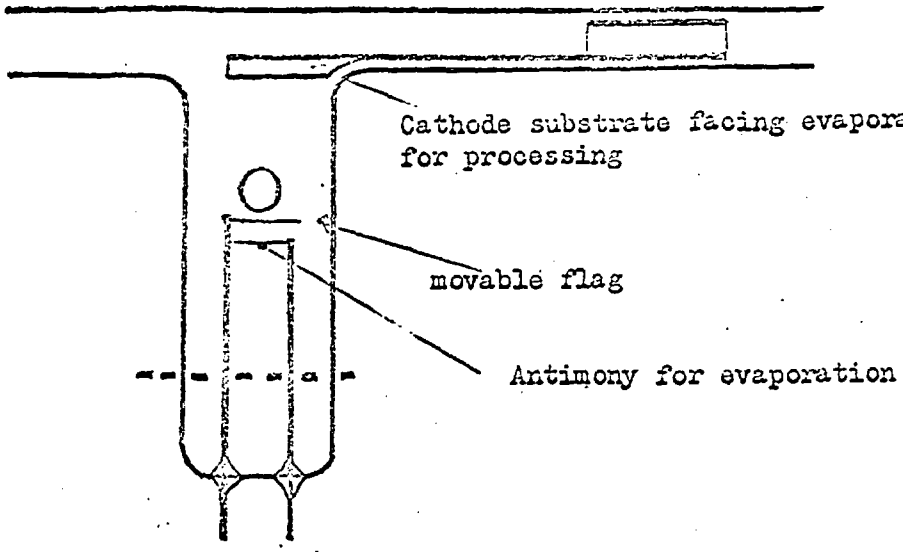


Fig 3.6.a

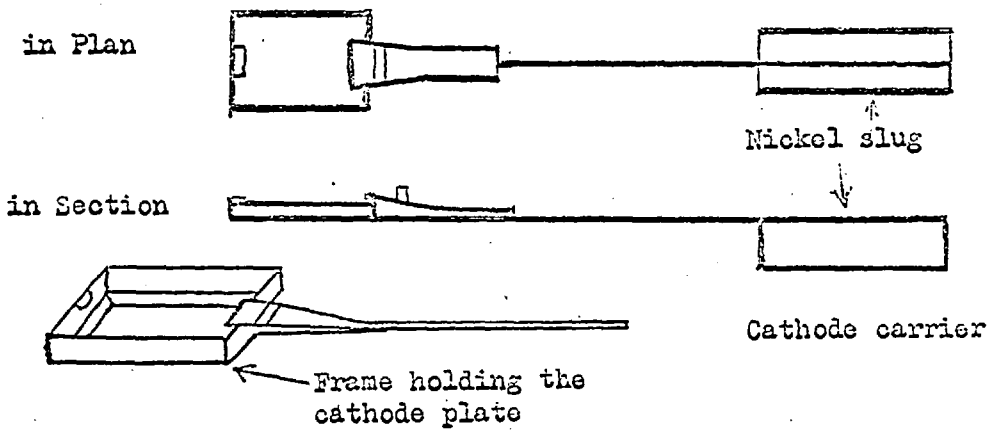


Fig 3.6.b

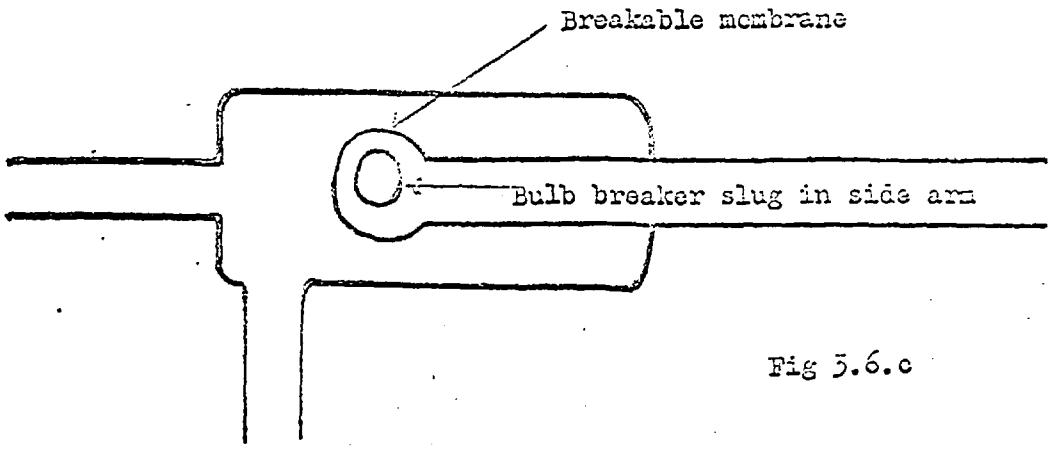


Fig 3.6.c

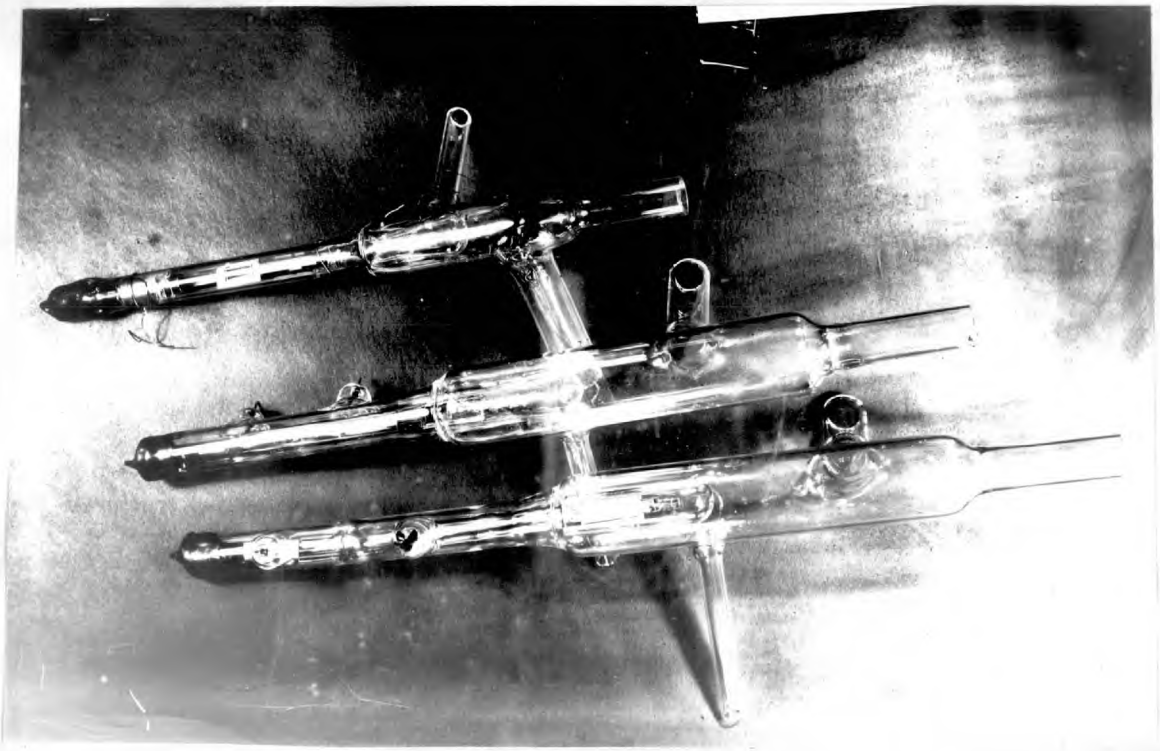


Fig 3.7

out. Two methods of depositing the phosphor screen was used viz. i) Settling by gravitation ii) Electrophoresis, described below:

i) Settling by Sedimentation: In this process of phosphor screen preparation two solutions were used, the electrolyte and the binder (solns A. and B respectively):

Soln A: 0.22 gm/litre solution of pure barium nitrate in double distilled water.

Soln B: 10% solution of potassium silicate (sp.gr.1.225 and molar ratio 2:1) supplied by Levy and West Ltd.

Phosphor Suspension: 1.188 gms of phosphor was measured and poured into a flask containing $\frac{1}{8}$" glass balls for milling the phosphor grains. 3 cc of solution B was poured into the flask the paste of phosphor so formed was milled for about ten minutes to disperse the phosphors evenly. 62 cc of solution B was now poured into this flask.

239 cc of solution A was poured into a 'monax' dish of 17 cm diameter, at the bottom of which was placed the phosphor substrate. 80 cc of soln A was also poured into another flask.

The phosphor suspension was thoroughly mixed and allowed to stand for one minute after which 41 cc of the suspension was decanted into the flask containing 80 cc of solution A, mixed thoroughly and the whole mixture poured into the monax dish containing the substrate. The posphor was now allowed to settle down for about three hours and the supernatant liquid was then syphoned off. The phosphor screen thus deposited on the substrate was now allowed to dry in a vertical position. In this way a relatively fine grain phosphor screen was prepared with about1.8 mgm of

of phosphor per square centimetre of the screen even when coarser grain phosphor material was used. This was because most of the large size phosphor grains were left out when the 41 cc of the suspension was decanted.

b) Electrophoresis (Cataphoresis).

The technique developed by Airy (1964) for cataphoretic deposition of phosphor was employed in making the fine grain high efficiency phosphors used in latter tubes. A conducting film of aluminium was first evaporated onto the substrate, which was to form the negetive electrode in the process. Two solutions were used to prepare the phosphor suspension:

Solution A: Annalar quality thorium nitrate (0.6 gm) dissolved in the 10 cc of "analar" iso-propyl alcohol.

Solution B: A 50 - 50 solution of analar iso-prophy alcohol and glycerol.

500 mgm of phosphor (E.M.I. type 210) was measured into a clean flask containing a few $\frac{1}{8}$" glass balls: ten drops of soln.A and 2 cc of soln. B was added to it and the mixture was ball milled for 10 minutes. 95 cc of analar isopropyl alcohol and 5 cc of double distilled water was added to it and the mixture shaken very well. Now 3 cc of soln A was added to make the suspension which was agitated for 5 minutes in an ultrasonic agitation bath. The suspension was poured into the cataphoresis bath. A clean stainless steel disc electrode was placed at the bottom of the bath and was connected to the positive terminal of a variable stabilised power supply. The substrate on which phosphor had to be deposited was mounted on a stainless steel guard ring used to provide a good electrical contact between this and the aluminium conducting layer on the substrate. Negetive

terminal of the power supply was connected to the guard ring and the latter was immersed into the suspension, with the aluminium layer facing downwards. Now a controlled amount of current was passed between the two electrodes and phosphor was deposited uniformly on the aluminium layer ; the thickness of the layer deposited depended on the current density and the time for which the current was passed. Electrophoresis was stopped when the phosphor deposition was about 1 mgm/cm^2 on the substrate (known from previous experiments).

Now the substrate was removed from the mount, cleaned in doubled distilled water and placed in an etching solution to etch away the conducting aluminium layer. The composition of the etchant was

8 grams of ammonium phosphate

40 cc of ammonia solution

200 cc of double distilled water.

The aluminium layer cleared off within 15 minutes and the phosphor screen was thoroughly cleaned in running double distilled water. Then the screen was allowed to dry in a vertical position.

Aluminium Backing: Floated aluminium backing was used in both the types of phosphor (Aslam 1965.). An aluminium film, about 1000A° thick was evaporated on a plate glass substrate onto which a very thin layer of salt (NaCl, annalar) had been evaporated previously.

The aluminum film so deposited was now floated by slowly immersing the substrate in distilled water which dissolved the thin layer of salt between the substrate and Al film. The phosphor screen was immersed into a 4.5% solution of potassium silicate (specific gravity 1.225), taken out

and kept upright for a while to allow the excess potassium silicate solution to drip away. Now the phosphor screen was gently immersed into the water on which the aluminium film was floating and was carefully lifted up with the aluminium film on top of it. It was then dried and baked for one hour at 350°C to drive away any water and also to increase the adhesion of the aluminium film to the phosphor due to potassium silicate.

The phosphor screen was now mounted on stainless steel annular ring electrode which had springs fitted in it for fixing at the output end of the image tube.

Efficiency: Efficency of the phosphors were measured in terms of light gain that could be obtained from such a phosphor in an image intensifier if a 10μA/lumen photocathode and accelerating potential of 15 KV were used (R.W. Airy 1965). Both the settled (G.E. type, grain size 1 to 5μ) and certaphorised phosphors (E.M.I. fine grain, grain size 1) had gains between 25 and 30. Spatial resolution of the fine grain E.M.I. phosphor was much higher than that of the G.E. phosphor. Fig.3.8. shows the various stages of phosphor preparation and assembly.

3.9. The Image Tube:

Experimental single stage tube for ultraviolet and visible.

Single stage tubes with spectrosil window and photocathode substrate were made with a seperate processing chamber (Fig.3.9.). Antimony cesium photocathodes were processed in the conventional way. i.e. with cesium vapour at about 140°C. The spectrosil window was sealed as illustrated in Fig.3.3.a. (Section3.5.). The image section of the tube

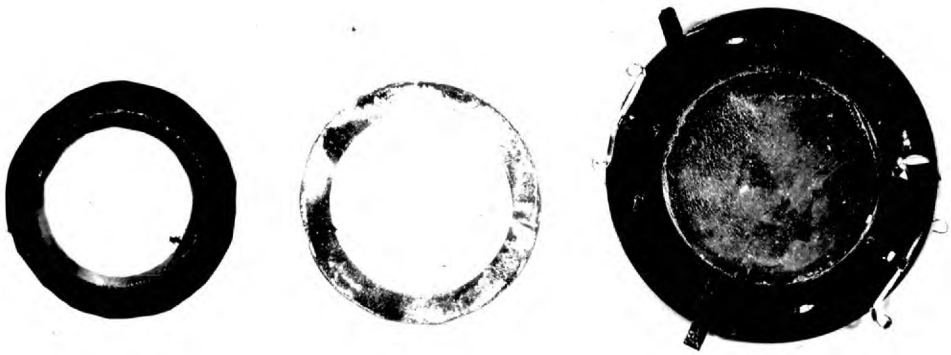


Fig 3.8

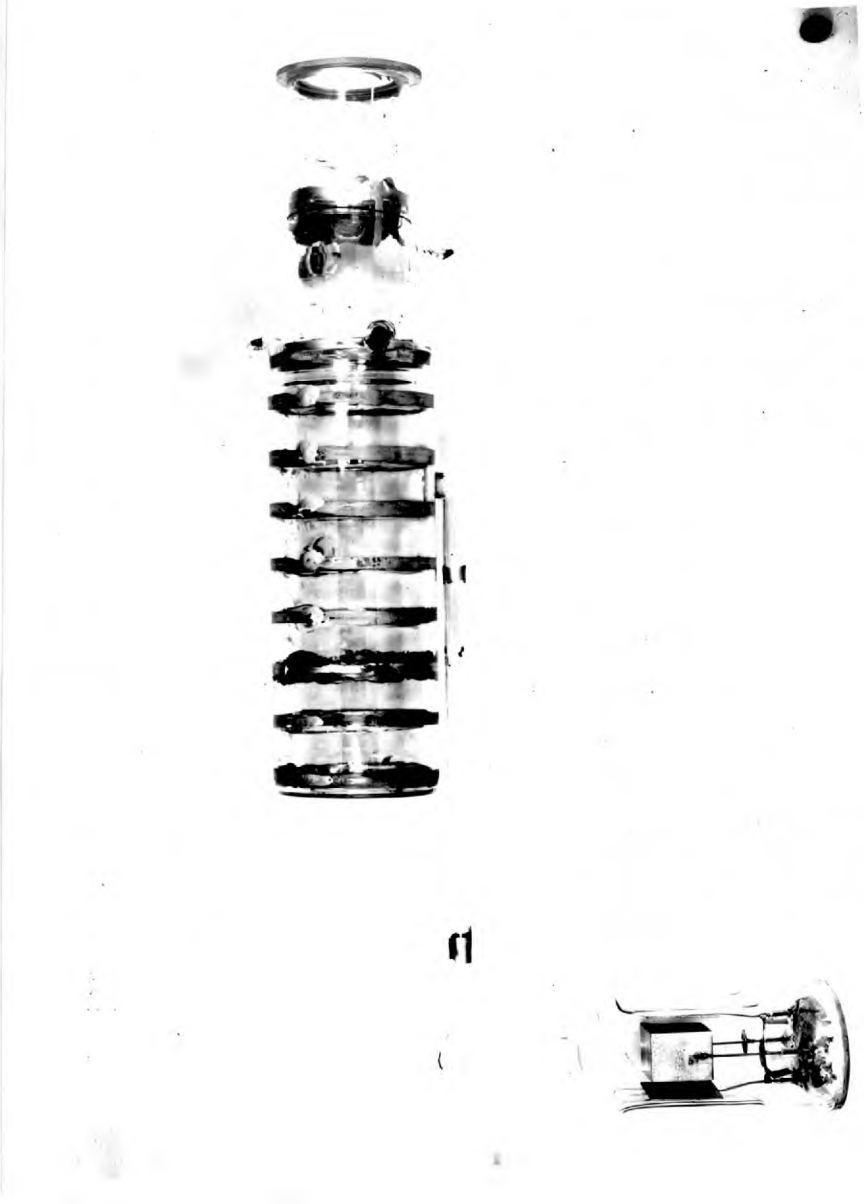


Fig 3.9

was seperated from the processing chamber by the cathode shelf which had a skirt that fitted closely to the tooling down of the tube in this region (Fig.3.10.a.). The shelf was supported on three tungsten pins. The cathode shelf was fixed on it by springs and could be released, reversed and set in again facing the image section by tapping the tube.

Platinum tapes were sealed through the tube wall in the image section at 2 cm. intervals and rings of platinum were pasted on the inside wall of the tube over this tape using type T177 platinum paste. Silver paste types X 351 and X 353 were painted around the tube on the outside, just opposite to the inside rings of platinum, except the point where the platinum tape emerged from the tube body. Bright platinum paint was applied to these points. Groves were cut on the inside wall adjascent to the rings of platinum by a diamond cutting wheel Fig.(3.10.b.). Stainless steel annular electrodes were fixed inside the tube at right angle to the tube axis with the help of springs which fitted into the grooves cut on the tube wall. Another inconel spring connected each of these metal electrodes to the adjascent platinum ring electrically. Accelerating potential was applied to the tube through these electrodes. The stainless steel discs constituted baffles to cut down background caused by secondary emission from the wall of the tube (McGee 1962). All the metal parts used inside the tube were electropolished to smooth out any sharp points in them and degassed by baking upto 1000^{o}C in vacuum. The phosphor mount also was fixed inside the tube by the same technique of grooving the tube wall. An ion pump was incorporated in the tube to pump away any surge of gases generated insdie the tube.

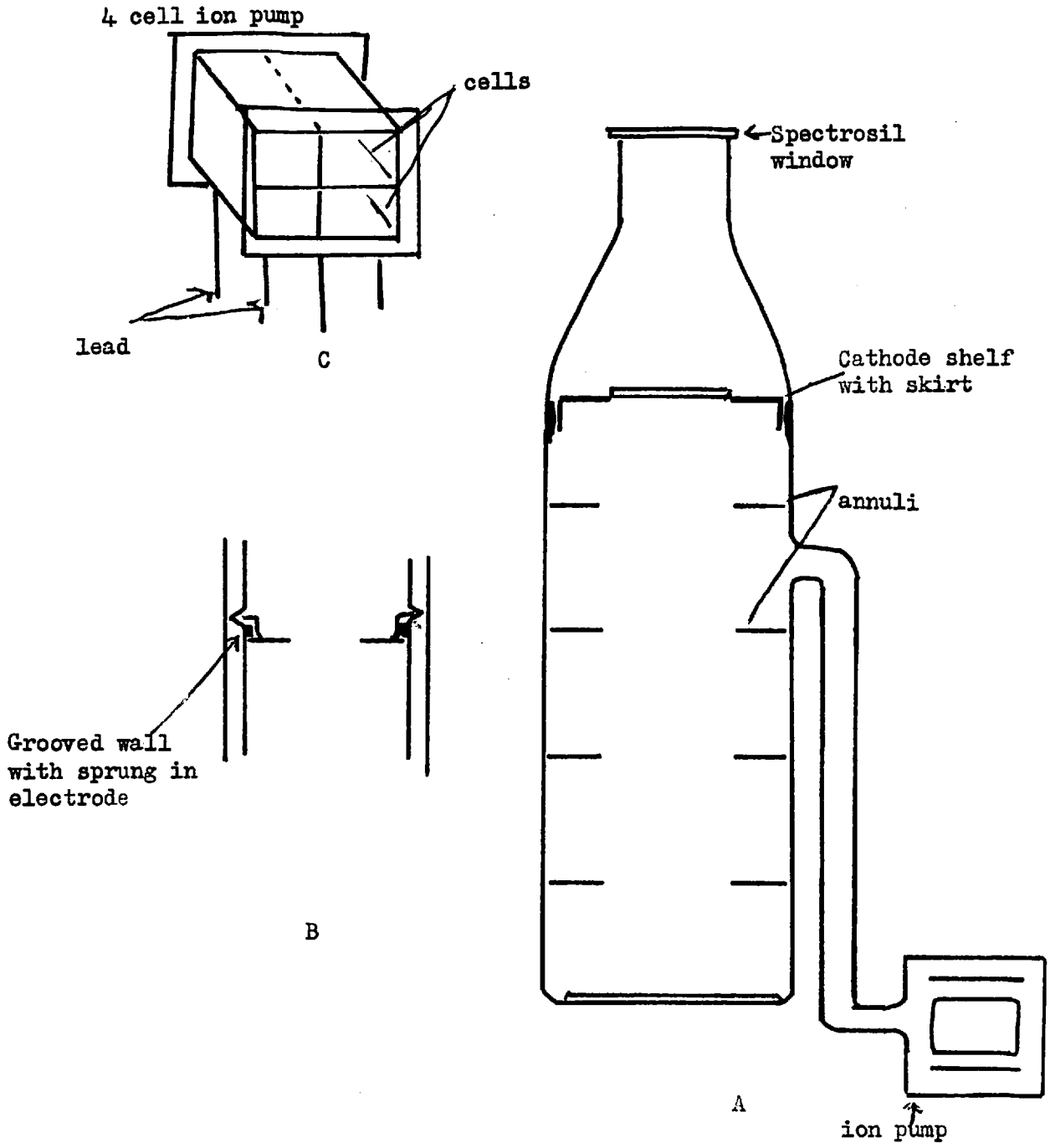

4 cell ion pump
cells
lead
C
Spectrosil window
Cathode shelf with skirt
annuli
Grooved wall with sprung in electrode
B
A
ion pump

Fig 3.10

Fig.3.10.c. shows its structural details. It had four cells and when operated at 3 KV with a 1.5 kilogauss magnet the pumping speed was nearly 1 litre/sec. It was also used to measure pressure inside the tube. Fig.3.11. shows the pressure calibration curve for this pump. After assembling the tube it was connected to the high vacuum system and was degassed at 320°C for 15 hours at pressures below 10^{-6} mm. of Hg. Generally at the end of this glass bake the pressure was around 10^{-7} mm of Hg. Any further fall in pressure when the tube was cooled down was a measure of residual gas in the system, and if it was found considerably large the tube was again baked for some more time until the pressure while it was hot decreased further. Before processing the photocathode, the tube was thoroughly checked for leaks. These tubes showed satisfactory performance and had spatial resolution of 30 line pairs/mm. Three tubes were made and were used for work in vacuum ultraviolet instrumentation (Bradley, Bates, Juulman, Majumdar, 1964).

Fall in Cathode Sensitivity. It was observed on the first two tubes that cathode sensitivity dropped slowly but continuously over a few days while the photocathode was facing the image sides, but this drop could be arrested if the cathode was reversed to face the processing chamber which had cesium and antimony on its walls. It was anticipated that at very good pressures (as was the case in these tubes, better than 10^{-7} due to pumping with the ion pumps after seal off), cesium moved off from the photocathode and sensitivity fell. In the processing section however, there were cesium on the walls and a dynamic equilibrium was established in cesium migration, thus arresting the cesium loss and hence

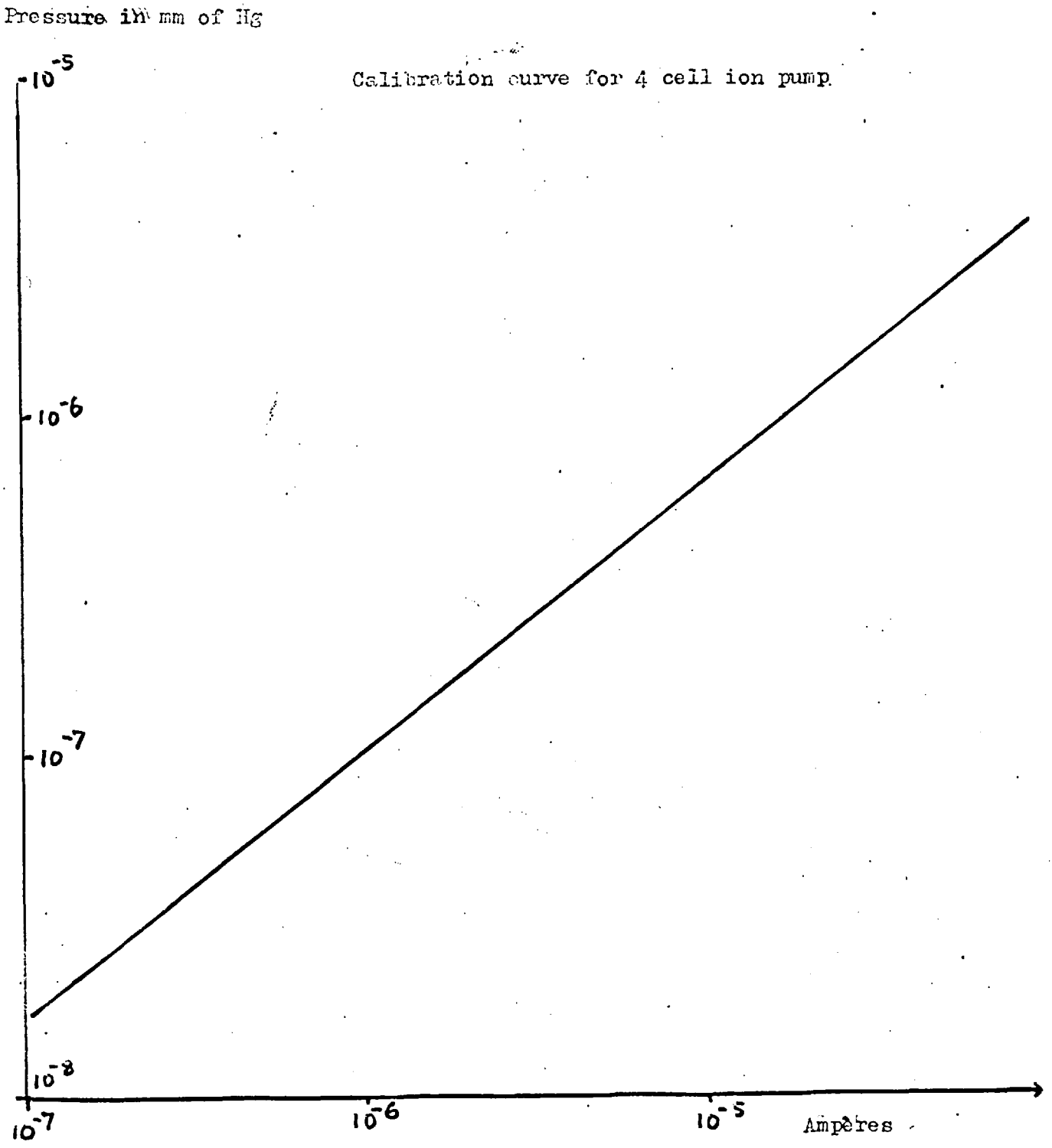

Pressure in mm of Hg
Calibration curve for 4 cell ion pump
10^{-5}
10^{-6}
10^{-7}
10^{-8}
10^{-7}
10^{-6}
10^{-5}
Ampères

Fig 3.11

the sensitivity was retained.

Test on a photocell of the effect of pumping a photocell to a very low pressure. A test cell was made with two ionpumps connected to it which could pump the pressure down to below 10^{-8} mm. of Hg(Fig.3.12.) The pressure and sensitivity variation with time as observed in this experiment is illustrated in Fig.3.13. A clear fall in sensitivity followed a fall in pressure, with a slight delay. It was also observed that both pressure and sensitivity rose to higher value when pumping was stopped, although sensitivity never reached the original value.

This experiment suggested that cesium seemed to move away from the surfaces but in an enclosure with cesium all around, a dynamic equilibrium existed which helped the photocathode to retain its original photo-sensitivity. It was observed that cathode sensitivity started to fall at pressures below 10^{-7} mm. of Hg. Thus, the purpose of the experiment to find out whether pressure did have an effect, and if so, at what pressure it became prominent, was fulfilled. It showed that in a clean system (without any possibility of contamination and poisoning) sensitivity dropped even in the presence of Cs around if the system was pumped below 10^{-7} mm. of Hg. Thus, in subsequent tubes, final pressure after seal off was never brought below 10^{-7} mm. of Hg by pumping with ion pumps.

Single State Tube with photocathode processed on the end wall by evaporation

Fig.3.14 shows the sketch of this tube, constructed to test the functioning of a tube without a seperate processing chamber when the photocathode was made by evaporation as described in Section 3.6. This tube was also designed with corregated glass wall, which were to

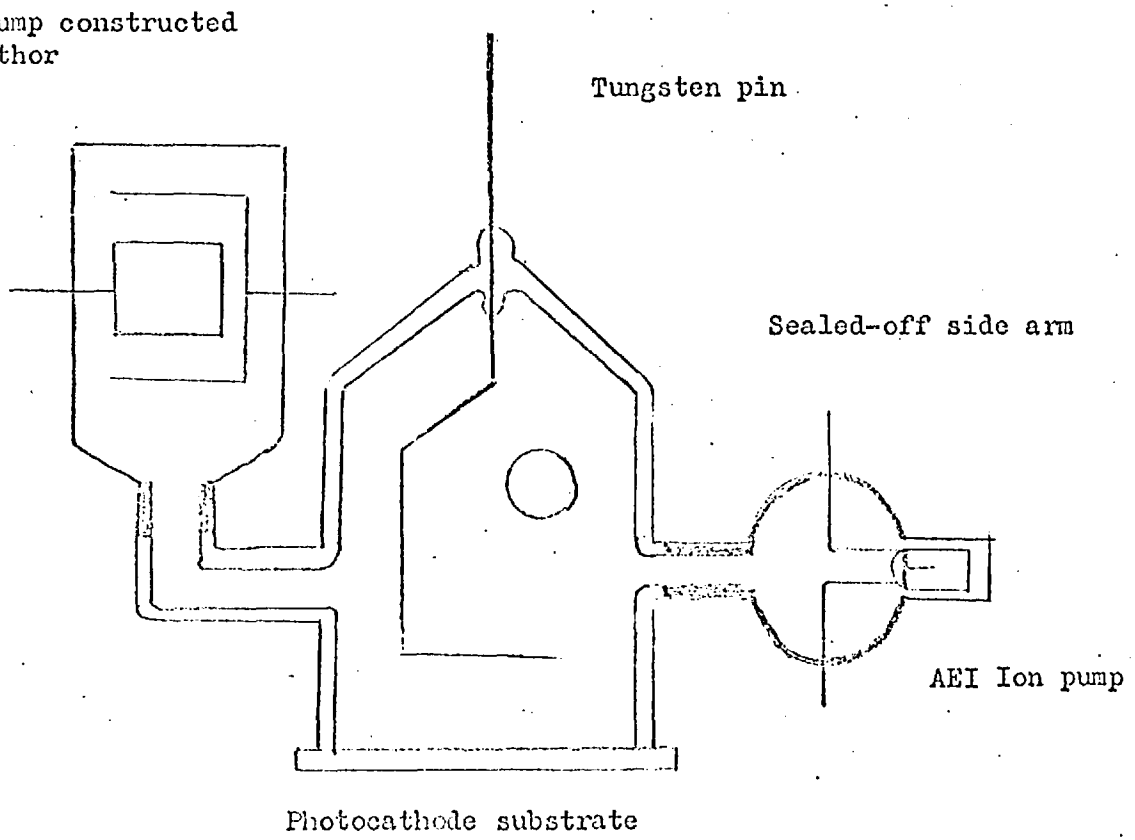

Ion pump constructed
by author
Tungsten pin
Sealed-off side arm
AEI Ion pump
Photocathode substrate

Fig 3.12

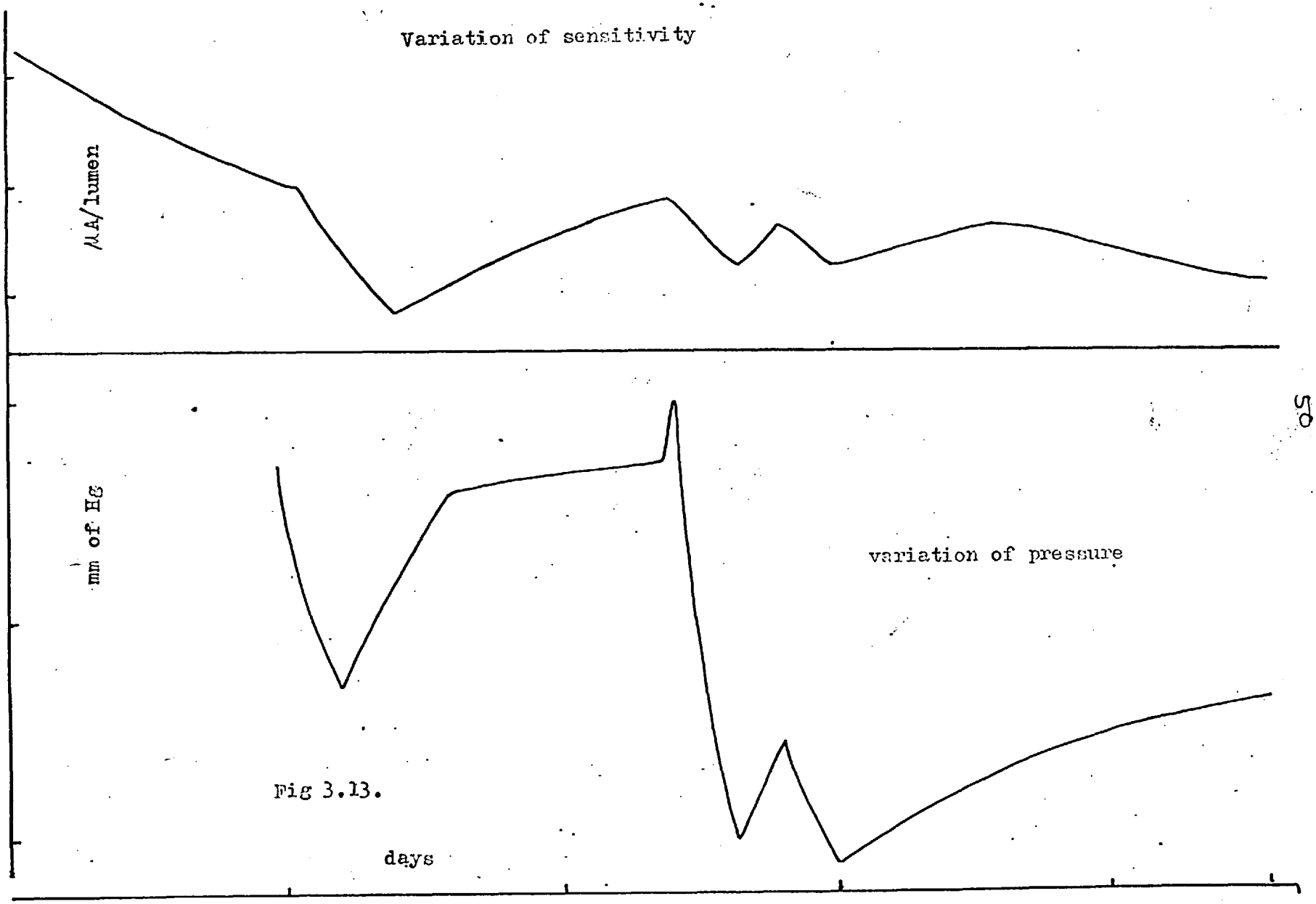

Variation of sensitivity
μA/lumen
mm of Hg
variation of pressure
days

Fig 3.13.

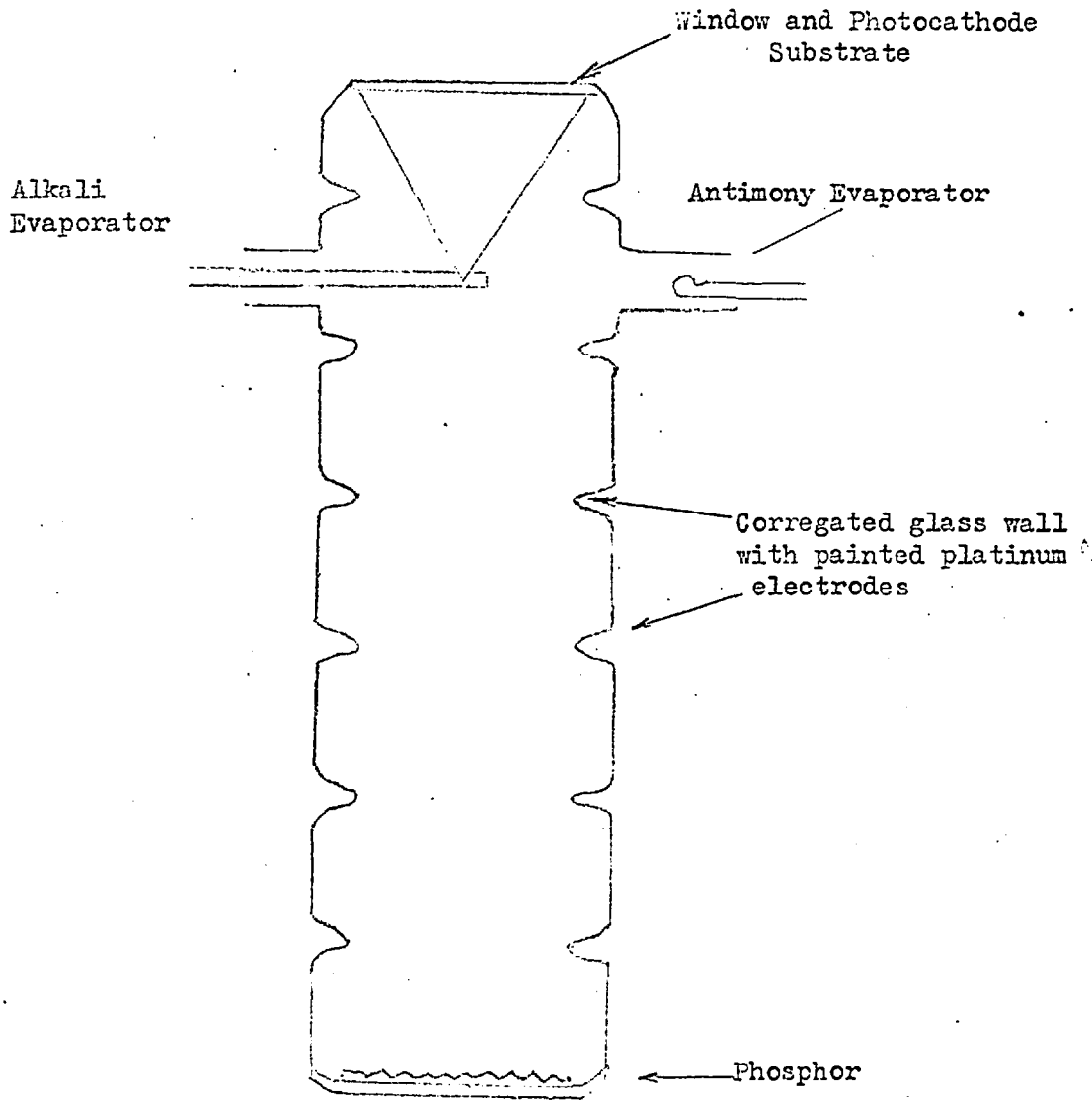

Window and Photocathode Substrate
Alkali Evaporator
Antimony Evaporator
Corregated glass wall with painted platinum electrodes
Phosphor

Fig. 3.14.

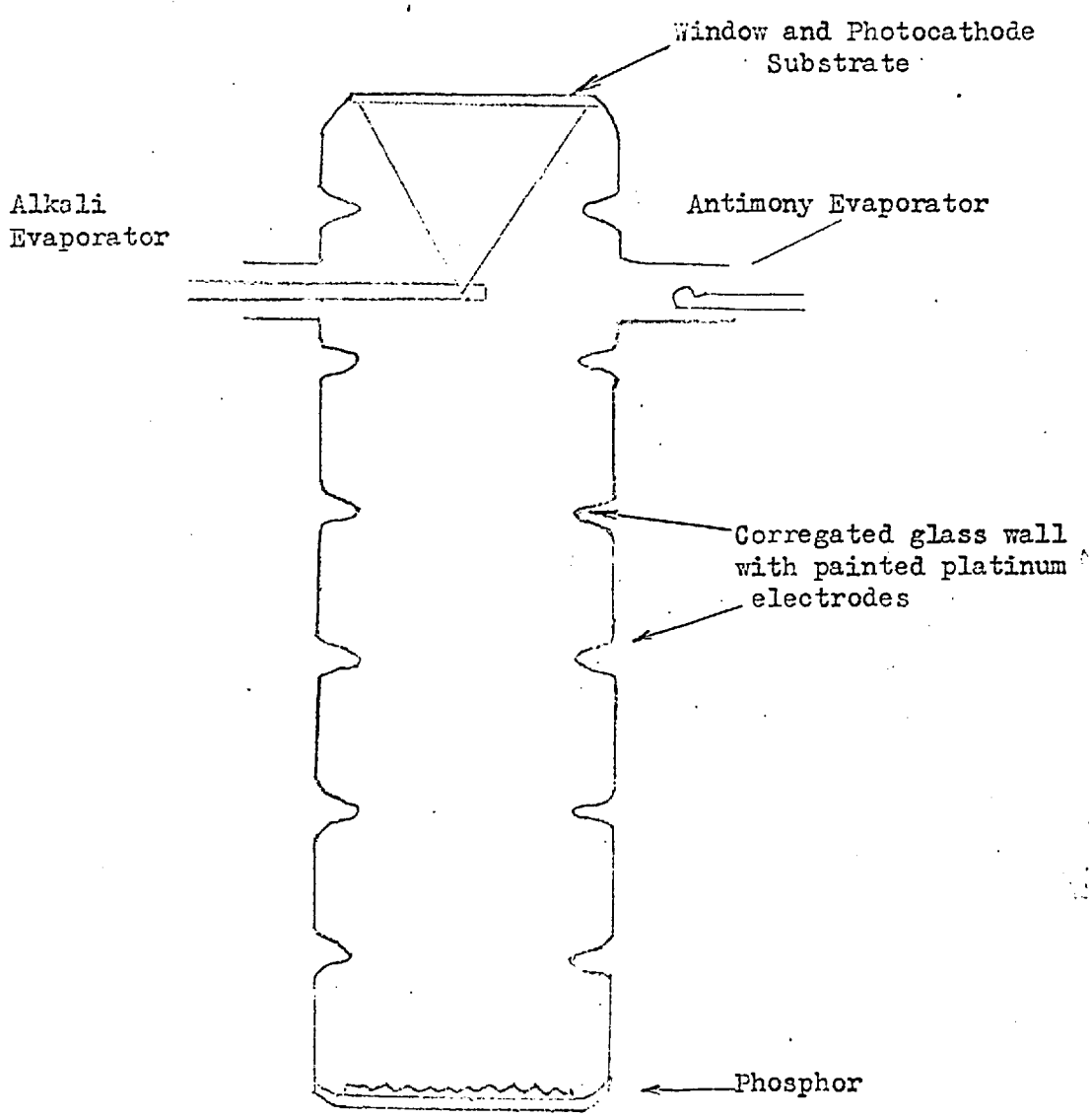

Window and Photocathode Substrate
Alkali Evaporator
Antimony Evaporator
Corregated glass wall with painted platinum electrodes
Phosphor

Fig. 3.14.

act as substitutes of metal accelerating electrodes, held inside by springs. This design, if sucessful, could make the construction of more complicated tubes simpler. Degassing from metals would also be minimised.

It was found after testing the tube that both these changes in tube production and design were sucessful. The tube had a resolution of 35 line pairs/mm and could stand an overall potential of 20KV without much background. Beyond 20 KV, of course, background got worse rather rapidly

Both the multiple beam tube and the two-stage cascaded tube were designed to have corregated glass wall accelerating electrodes in the image section.

Special two-stage cascaded image intensifier with externally processed photocathodes and phosphor-photocathode sandwich.

Fig. 3.15. shows the design of such a tube. The novel features in this design were

1) Two different types of cathodes to be used at the input window - a CsI and an antimony cesium one of which could be used at a time.

2) Tube was to have all its cathodes and sandwiches externally prepared and introduced later.

3) Spectrosil window and cathode substrates were used for versatility.

4) A gating mesh following the first photocathode for high speed single shot operations.

Cathodes and gain stages were prepared and preserved in ampoules as discussed in section 3.7. (Fig.3.7.). The gainstage was an antimony-Cesium photocathode, (continued on next page.)

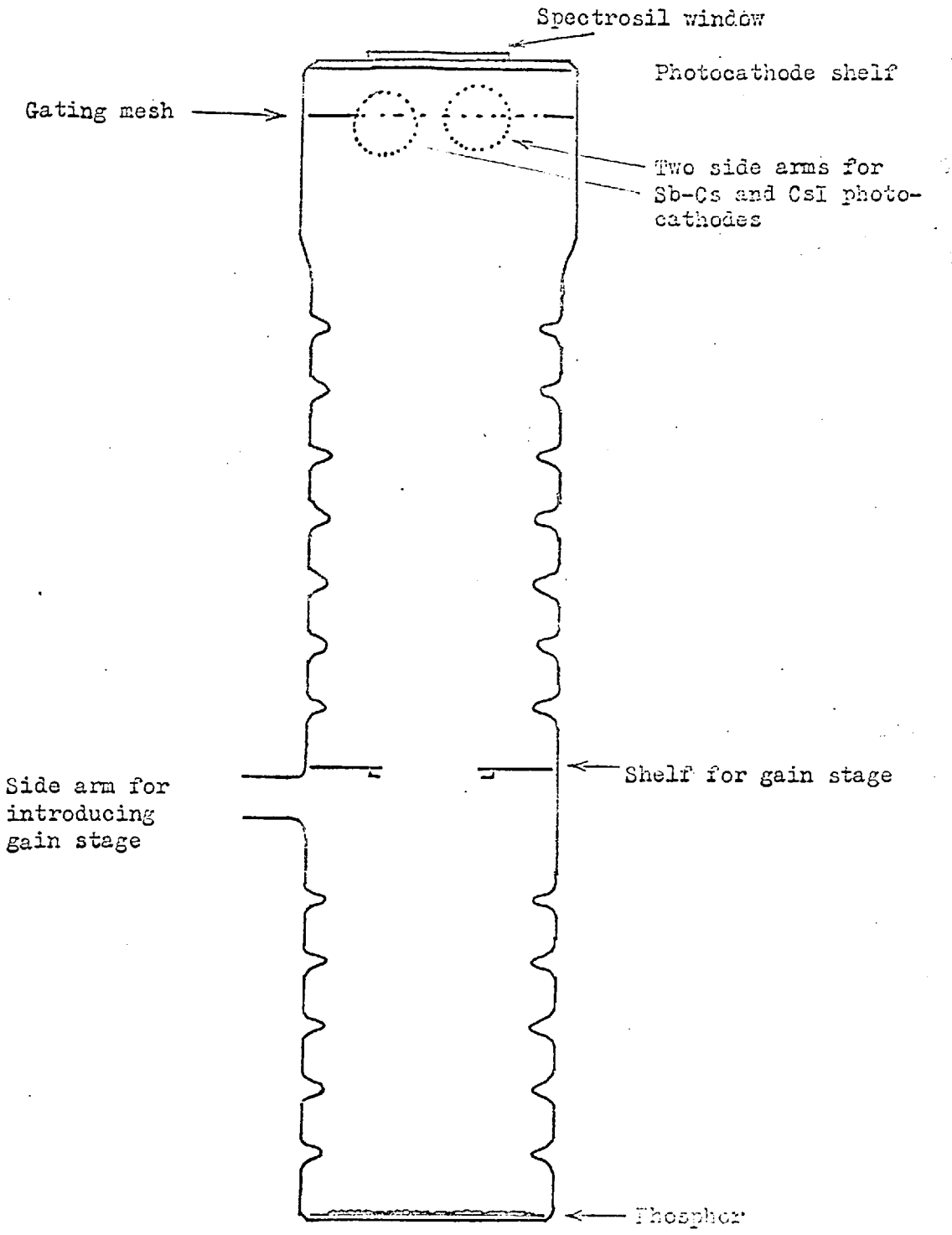

Spectrosil window
Photocathode shelf
Gating mesh
Two side arms for Sb-Cs and CsI photo-cathodes
Side arm for introducing gain stage
Shelf for gain stage
Phosphor

Fig. 3.15.

and a cataphorise P-11 phosphor prepared on two sides of a rectangular piece of 4 micron thick mica (25 mm x 10 mm) sealed on a titanium frame with solder glass (390). The procedure for making a sandwich was quite involved. Phosphor was first deposited on one side while the other side was protected from contamination by covering it. This was necessary because the other surface, on which photocathode was to be processed had to be kept meticulously clean. Also, during processing of the photocathode, the phosphor had to be protected from cesium vapour which would otherwise poison the phosphor screen. Fig.3.16.a. shows the diagram of a gain stage in its carrier. The first photocathode mount inside the tube is shown infFig.3.16.b. Two photocathodes were to be mounted side by side on a sliding cradle in this mount. Either of the cathodes could be lined up with the phosphor of the gain stage by sliding the cradle, using gravity. The metal parts in the tube, the cathode mount, the gain stage mount, the gating mesh and the output phosphor mount (Fig.3.16.) were all fixed by springs inside the tube. One attempt was made to assemble and produce such a tube, but the gain stage shattered because of a mechanical shock. We hope to produce tubes of this design in the near future, and use it as an intensifier to the multiple beam tube or for ultraviolet spectroscopy.

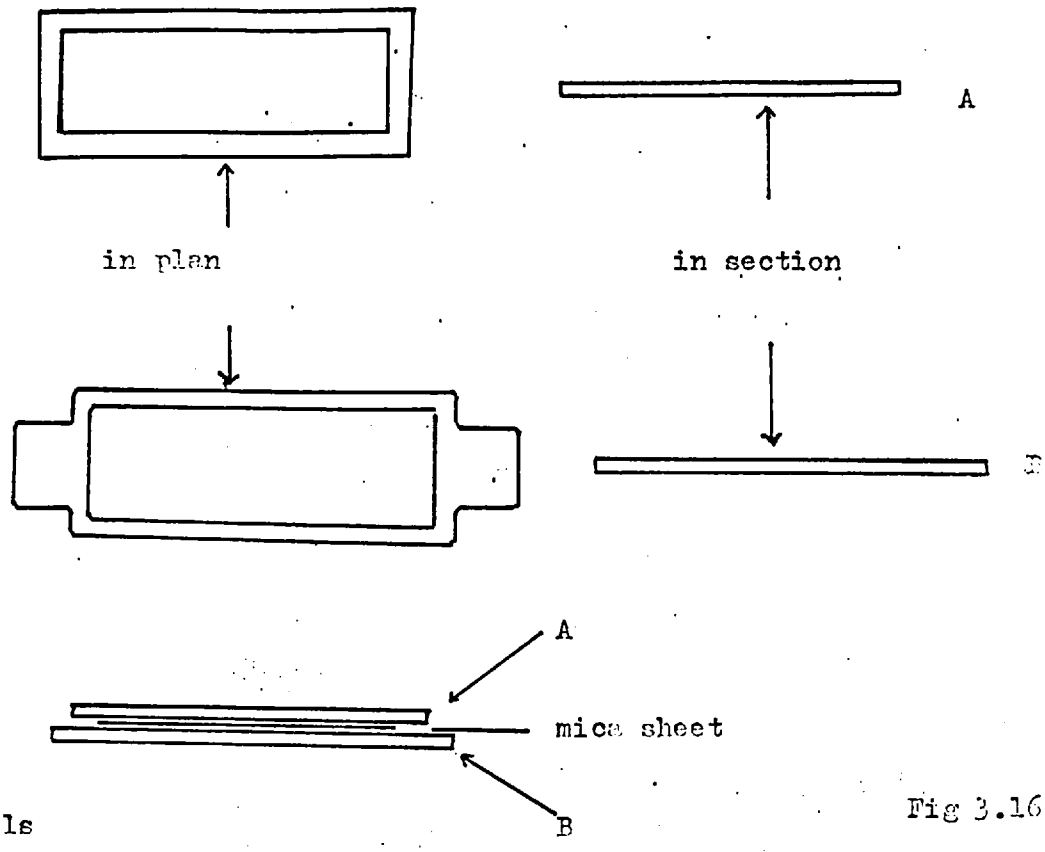


Fig 3.16. a

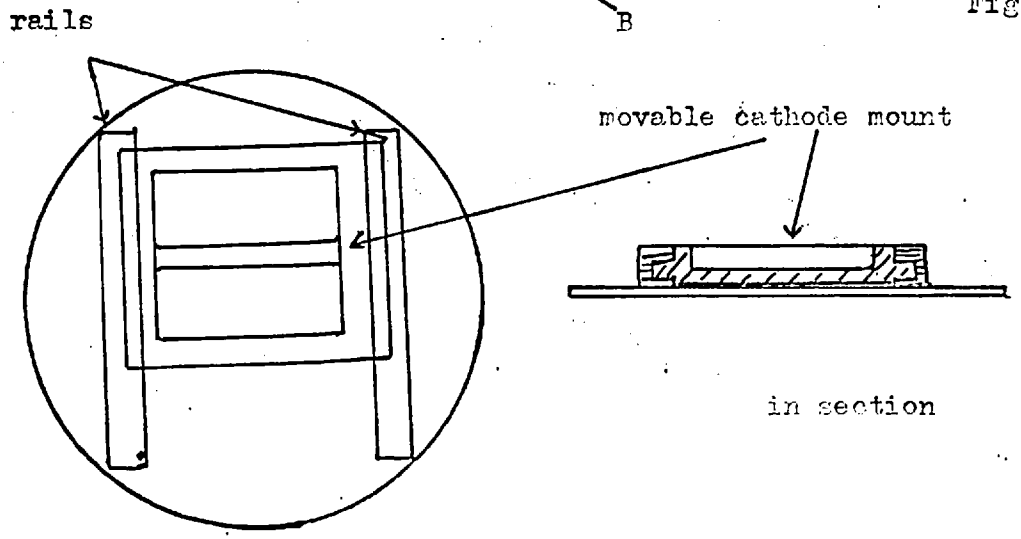


Fig 3.16.b

CHAPTER 4.

THE MULTIPLE BEAM TUBE - PRINCIPLE OF OPERATION

4.1. Basic Consideration - Use of Small Cathode Width.

Work on high speed photography was started with a view to using it for time resolved diagnostic spectroscopy in the nanosecond region. As it has been discussed in Chapter (2), a slit image, crossed with Fabry Perot interference fringes, has many advantages for high resolution spectroscopy where high light gathering power is required. Thus, such a system was kept in mind while designing the high speed camera, because the number of photons available is in many cases a limiting factor in the time resolution that could be achieved in high speed photography.

The use of a slit image crossed with Fabry-Perot fringes cuts down the useful area on the photocathode to the dimension of the slit. The fact that such a small image area is all that is required for diagnostic spectroscopic work was exploited in designing the framing and storage system which will be described below.

4.2. Operation as a Framing Camera - Principal Mode.

Basically, the system employs the mesh gating technique developed by Mandel (1961) and the storage obtained with the help of such meshes (J. McGee J.Beesly et.al, 1965) along with a three element einzel lens system immersed in an axial magnetic field, and a deflecting field inside the storage section to achieve framing of the image while it is being

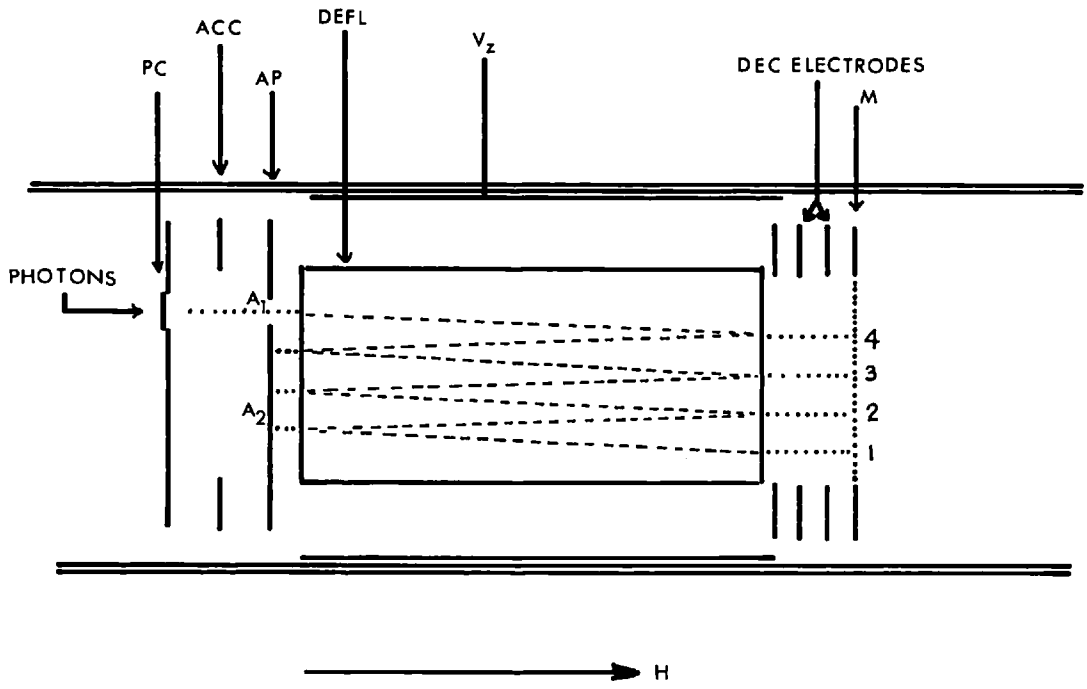
stored. Fig.(4.1.) explaines the basic principle of operation of this system.

A slit image, crossed with Fabry-Perot interference fringes is focussed onto the photo-cathode PC placed off axially inside the tube, and the resulting photo electrons are first accelerated through the first accelerating electrode and then allowed to pass into an equipotential storage section through the rectangular aperture A_1, made in a stainless steel disc A_2. The first accelerating electrode, the aperture following this, and the drift section on the other side of the aperture electrode form the three electrodes of the said einzel lens system. Both the first accelerating electrode and the potential on the drift section are positive while the "aperture" electrode between them is at a slightly negative potential (Fig.4.2.). Such a system of electrodes will allow electrons to pass through A_p when the negative potential on the aperture electrode does not exceed the value.

$$V_A = KV \qquad (1)$$

Focussing of the photoelectrons is maintained by an axial magnetic field H_Z over the whole length of the tube, supplied by a solenoid. Under this condition electrons approaching the aperture electrode anywhere other than at the aperture A_1 will be reflected back while those approaching it at A_1 will pass through it.

As soon as the electrons enter the drift section they acquire the potential of this section; they then enter the transverse field Ed due to the deflecting plates and get shifted in a direction perpendicular to


ACC
DEFL
V_z
PC
AP
DEC ELECTRODES
M
PHOTONS
A_1
A_2
4
3
2
1
H

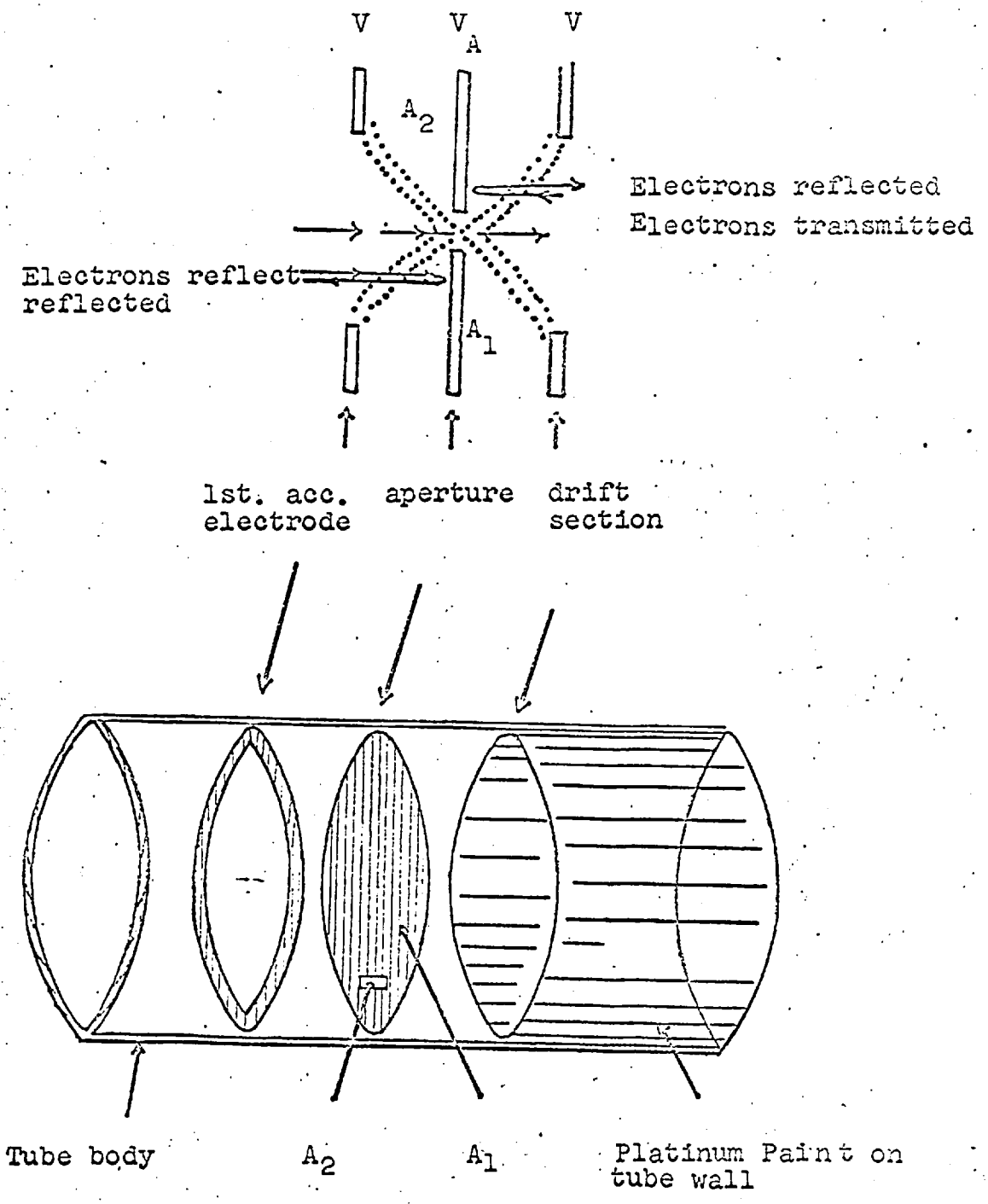

V
V A
V
A2
Electrons reflected
Electrons transmitted
Electrons reflect
reflected
A1
1st. acc. electrode
aperture
drift section
Tube body
A2
A1
Platinum Paint on tube wall

Fig. 4.2.

both the magnetic and transverse electric field as they pass across the deflecting field parallel to the tube axis (Z - direction). The deflection velocity V_d is given by,

$$V_d = \frac{E_d \wedge B_z}{B_z^2} \qquad (2)$$

Where Bz is the axial magnetic field. At the end of the deflecting field, the electrons are decelerated by a set of decelerating electrodes as they approach the gating mesh M, kept at a slightly negative potential. As a result, the photoelectrons lose all their energy in the close proximity of the mesh and are reflected back. The photo electrons then regain their original velocity as they go back through the same set of decelerating electrodes (now acting as accelerating electrodes), towards the aperture electrode, undergoing a further deflection away from the aperture while passing through the deflecting field for the second time (Fig.4.1.). By the time this backward moving beam of electrons reaches the end of the deflecting field, it has been deflected away from the aperture area A_1 into the negative region A_2 of the electrode; this causes the beam to reflect back again at the aperture electrode. This system of deflection was used by Rose & Imaus (1939) in the image orthicon television camera. The process of reflection between the aperture electrode and the gating mesh continues together with the deflection while photoelectons from the photocathode keep on entering the storage section through the aperture A_1.

Now, consider that T is the time a photoelectron takes to move from

the aperture to the mesh so that time taken by it for a double transit is 2T, during which time it comes back to the aperture after one journey. Everytime a photoelectron approaches the mesh, it must have completed an odd number of transits through the storage section. Let (2 n + 1) be the number of such transits the front edge of the electron beam complets before it gets deflected away from the working region of the tube. The time it has taken to do this since it entered the storage section is then

$$T_D = (2n + 1) \; T \qquad (3)$$

If a very fast rising positive square pulse with a pulse width of 2T is applied to the mesh at this point, all the photoelectrons which have entered the storage section during the last T_D secs will be extracted through the mesh at n + 1 different positions, constituting (n + 1) frames. The electrons in their (2n + 1) and 2n transits will come out in the (n + 1)th,frame, those in (2n - 1) and (2n - 2) transits will come out in the n th frame and so on, the "oldest" frame being the (n + 1) th. The 1st frame will hold information for a time 2T,the last half of which has entered the storage section after the gating pulse has been applied to the mesh. In Fig.(4.1) n = 3. The photoelectronic image is retained by the axial magnetic field applied, which constrains the electrons into light helical paths. These extracted frames are now accelerated and imaged onto a fluorescent screen for photographic recording.

4.3. Salient Features and Advantages.

The characteristic features of such a framing and storing system can be summarised as follows:

i) Fairly long storage time may be achieved in a small space.

ii) Storing and framing is achieved simultaneously without application of any changing potentials in the system.

iii) All the frames are extracted by a single gating pulse.

iv) The gating pulse need only be of the order of ten volts, making the electronics simpler.

v) Framing time is defined by the drift time of the electrons in the storage section which can easily be altered by altering the drift voltage in this section.

vi) There is no time gap between two consecutive frames.

vii) Time selection is easily done by simply varying the delay between the initiation of a trigger from the event and the mesh gating pulse. Thus, any part of the event under test may be recorded by gating the tube with a trigger pulse obtained from the event itself. The inherent delay in the storage section allows any part of the event starting from the very begining to be recorded without any need of pre-triggering the camera.

viii) If the total time of the transient phenomenon is less than T_D of eqn.(3), the gating pulse need only have a sharp rise and a flat top equal to or longer than 2T, provided the transient is much brighter than the background illumination. This is also true if the length of the event to be recorded is determined by a gating pulse which will open the aperture kept biased beyond cut off (eqn.1). In this case time selection

is achieved at the input by gating the aperture on for only a specified period.

For time resolved spectroscopic work such a tube will be extremely useful because of the simplicity of its operation and its capability of extremely fast framing . So far we have assumed that all the photo-electrons inside the drift section have equal energies so that they all have equal transit times,T. It is evident that to obtain highest time resolution, the transit time has to be the smallest which can be achieved by making the storage section short and applying maximun possible voltage in the drift section. Maximum number of frames is obtainable if the separation between two consecutive frames is minimum i.e. Ed is minimum. Maximum spatial resolution is obtained if B_z is maximum since "brute force focussing" rather than proper magnetic focussing is employed.

4.4. Time Dispersion

Further complication arises because in practice there is bound to be variations in transit times due to the presence of a deflecting field along the length of the slit image which will cause appreciable time dispersion along the length of the slit. The situation is studied in detail below. A much less serious time dispersion is also present in the system which is due to variation in the emission energy of photo-electrons from the photocathode.

Situation arising from the presence of deflecting field Ed is explained with the help of the simplified diagram in Fig.(4.3.). In this diagram, the lower deflecting plate is shown electrically connected

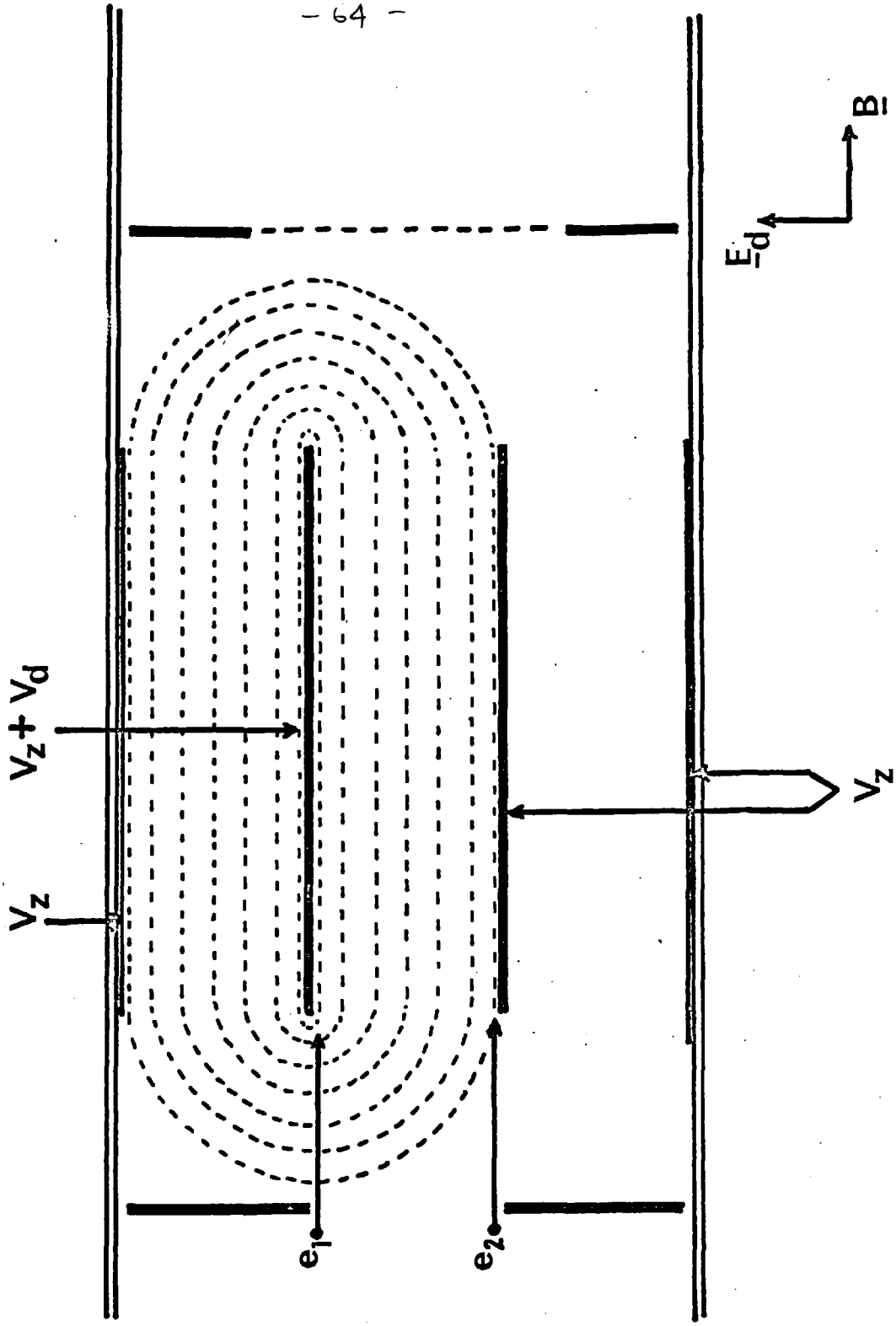


Fig 4.3.

to the drift potential while the upper one is at a potential $+V_d$ with respect to the other deflecting plate, thus producing a deflecting field $E_d = \frac{V_d}{S}$ between the electrodes, where S is the separation between the deflecting plates. Equipotentials due to this impressed deflecting field are shown by dotted lines around the upper deflecting plate. Now, consider two photoelectrons entering the storage section, one infinitely close to the upper deflecting plate and the other infinitely close to the lower deflecting plate, both having the same initial velocity. As soon as they enter the drift section, they both acquire the drift velocity $v_z = \sqrt{2 \frac{e}{m} V_z}$, where V_z stands for the potential applied to the drift section. The electron entering the drift section. The electron entering at the bottom continues to move with this velocity v_z until it is slowed down by the decelerating electrodes as they approach the mesh. But the upper electron crosses a number of equipotentials and will be energised to a velocity $v_z' = \sqrt{\frac{2e}{m}(V_z + Vd)}$ by the time it reaches the front edge of the upper deflecting electrode, and continue at this velocity until it is decelerated by the decelerating field near the gating mesh.

As a result, the photoelectron entering the storage section near the top deflecting plate complets its transit at a lesser time than the corresponding electron entering the storage section near the bottom deflecting plate. Thus, while the framing time of a portion of image infinitely near the bottom plate is

$$t_1 = 2 \frac{\left(2(d_1 + d_2) + 1 \right)}{\sqrt{v_z}} = \frac{k}{v_z} \qquad (4)$$

that for the portion infinitely near the top deflecting plate is

$$t_2 = 2 \frac{(2(d_1 + d_2) + l}{\sqrt{V_z'}} = \frac{K}{\sqrt{V_z'}} \qquad (5)$$

where d_1 and d_2 are the lengths on either side of the deflecting electrodes inside the storage section and l is the length of the deflecting plates. The difference in framing times between these two portions of the image is

$$\Delta t = t_1 - t_2 = k \left(\frac{1}{\sqrt{V_z}} - \frac{1}{\sqrt{V_z}} 1 \right)$$

Substituting for V_z'S,

$$\Delta t = k^1 \left(\frac{1}{\sqrt{V_z}} - \frac{1}{\sqrt{V_z + V_d}} \right) = \frac{k^1}{\sqrt{V_z}} \left(1 - \frac{V_z}{\sqrt{V_z + V_d}} \right) \qquad (6)$$

where $k^1 = \frac{k}{\sqrt{\frac{2m}{e}}}$ and $t_1 = \frac{k^1}{\sqrt{V_z}}$

So that, the time dispersion between the top and the bottom is,

$$\frac{\Delta t}{t_1} = 1 - \left(\frac{V_z}{V_z + V_d} \right)^{\frac{1}{2}} \qquad (7)$$

4.5. Way to Minimise Time Dispersion.

It follows from equation (7), that the time dispersion is negligible if $V_z \gg V_d$. Thus, we arrive at another very important conclusion that

V_d has to be kept at as low a value as practicable, to minimise time dispersion, which could otherwise be a very serious problem.

Equation (7) also suggests that, for this time dispersion to be negligible, the storage section should be designed for $V_z \gg V_d$. In fact this can be achieved if the framing time is sacrificed. Since the velocity and hence the framing time depends on V_z one has to increase the V_z to $4V_z$ in order to increase v_z to $2v_z$. Thus, if the length of the deflecting plates is doubled we will have the electrons energised to $4V_z$ but still keeping the time during which they get deflected the same, leaving deflection per frame and V_d unchanged. The net result is, V_d has been reduced with respect to V_z by a factor of 4, and hence the time dispersion has also been reduced. Since the value of V_z applicable is limited by the constructional features of the tube, the framing time consequently has to be larger than what could be attained with a tube having shorter deflecting plates.

In the case where $V_z \gg V_d$, eqn.(7) can be rewritten as

$$\frac{\Delta t}{t_1} = \frac{1}{2} \frac{V_d}{V_z} \qquad (8)$$

neglecting 2nd and higher order terms, This equation shows that for low value of $\frac{V_d}{V_z}$, the time dispersion along the length of an image is linear.

This variation of the transit time of electrons in the storage section produces the further effect of tilting the image because the electrons stay in the deflecting field for different lengths of time at

different parts along the length of the image. From eqn.(2), the variation of deflection at the top and bottom is: (Bradley & Majumder 1966b).

$$\frac{\Delta d}{d} = 1 - \left(\frac{V_z}{V_z + V_d}\right)^{\frac{1}{2}} \qquad (9)$$

$$\simeq \tfrac{1}{2} \frac{V_d}{V_z} \qquad (9a)$$

This effect results in a fitting of a line image through an angle

$$\tfrac{1}{2} \tan^{-1} \left(\frac{\Delta d}{S}\right) = \tfrac{1}{2} \tan^{-1} \frac{E_d . d}{2V_z} \qquad (10)$$

Where S = separation between the two plates.

Both time dispersion and tilting of the image are cumulative and increase linearly with the number of passes. If for example, V_z = 1000 V and V_d = 50 Volts, $\Delta t = 0.05\ t$, after two passes, that is, for one frame. Thus, after 20 frames, time dispersion along a length S could equal to the framing time t_1.

This time dispersion along the length of the image, is from eqn.(8) linear, and in fact could be turned to advantage to increase the overall time resolution by a factor $\frac{t1}{\Delta t}$, for a Fabry plot slit image. This will be discussed in sec.(4.8.)

4.6. Chopped Mode of Operation.

So far, the operation of the tube has been discussed for the main type of framing operation, where framing time is governed completely by

tube geometry and applied potentials.

Shorter exposure times for each frame can be achieved if the mesh gating pulse is used to control the framing time, the pulse width being less than the time taken by the electrons for a double pass in the storage section. In fig.(4.4.) the portion of the electron beam which can pass through the mesh during the time the gating mesh stays open is shown in continuous lines, while the dotted portion is lost inside the storage section. As a result, a time gap occurs between consecutive frames.

If T_G = Gating time, then according to eqn.(3) and the following discussion, the n th frame will contain information for a time T_G starting from

$$T_D - (2n-1) \quad T \quad = T_D - \quad (2n-1)\,T \qquad (10A)$$

after the first photoelectrons have entered the storage section. The time gap between two consecutive frames is given by (Fig.4.5.)

$$= 2T - T_G \qquad (11)$$

In this way it should be possible to have a framing time as short as the gating pulse would allow, i.e. of the order of one to 5 nano-seconds.

When the tube is operated in this mode, points (V), (VI) and (VII) discussed in section (3) are no longer valid. An event of relatively long duration could in this way be analysed with a number of very short exposures at equal intervals.

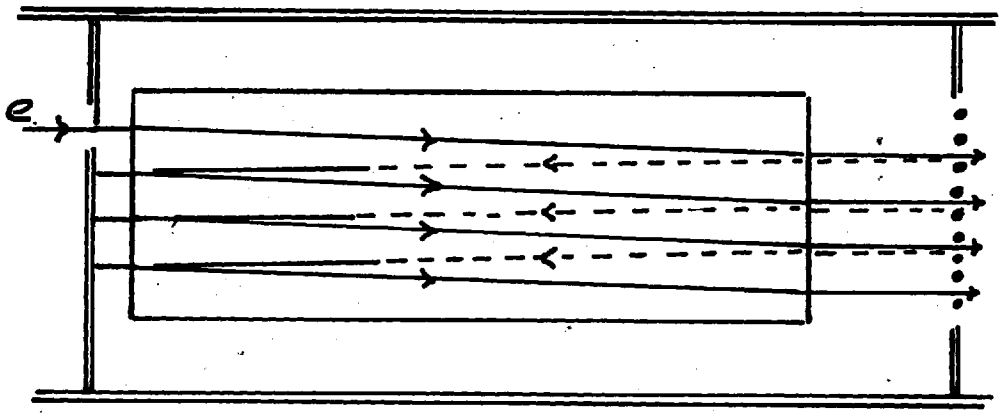


Fig. 4.4.

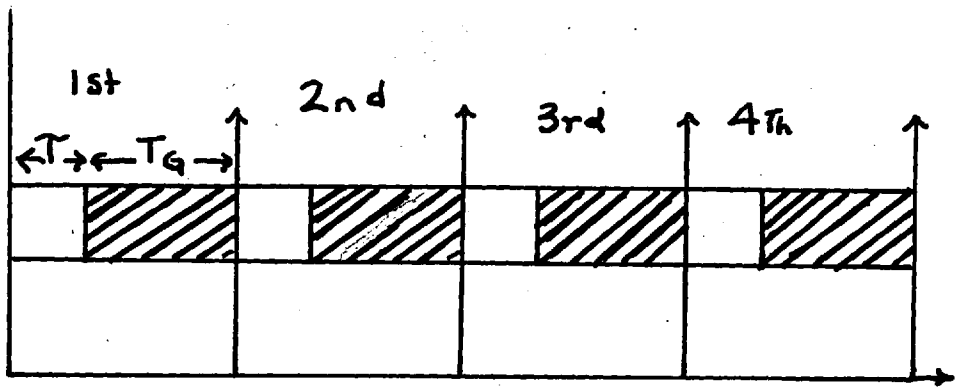
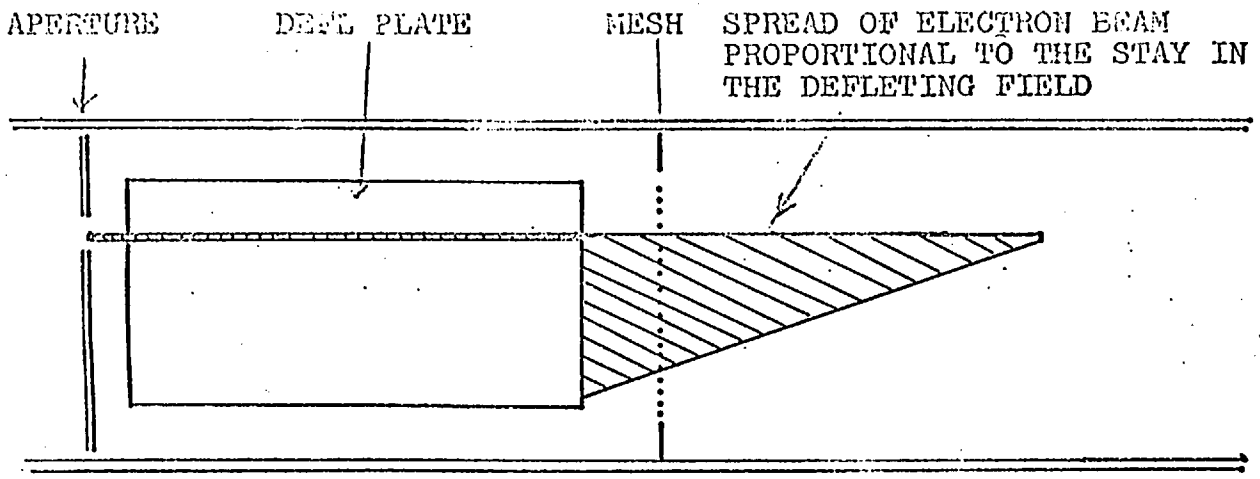
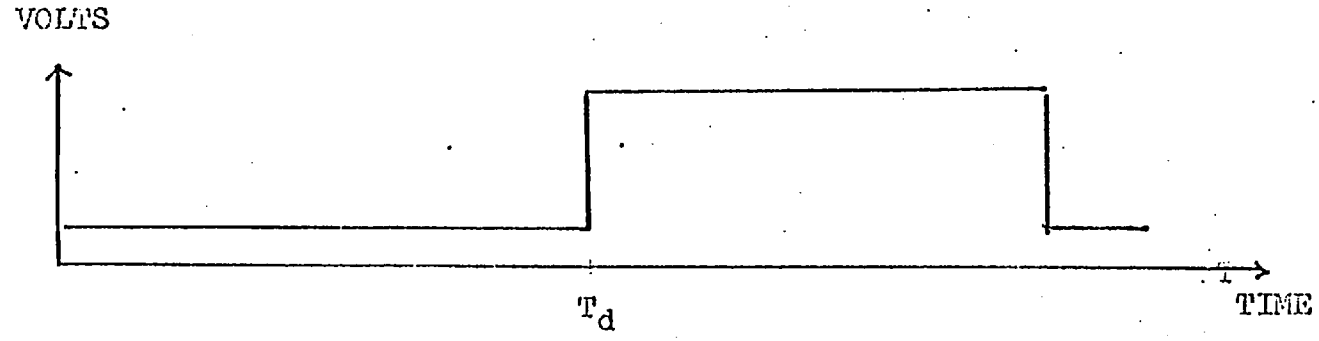


Fig. 4.5.

CHOPPED MODE OF OPERATION, PRODUCING TIME GAPS BETWEEN FRAMES.



DEFLECTION OF ELECTRON BEAM FOR STREAK OPERATION



DELAYED PULSE ON DEFLECTING PLATES

Fig. 4.6.

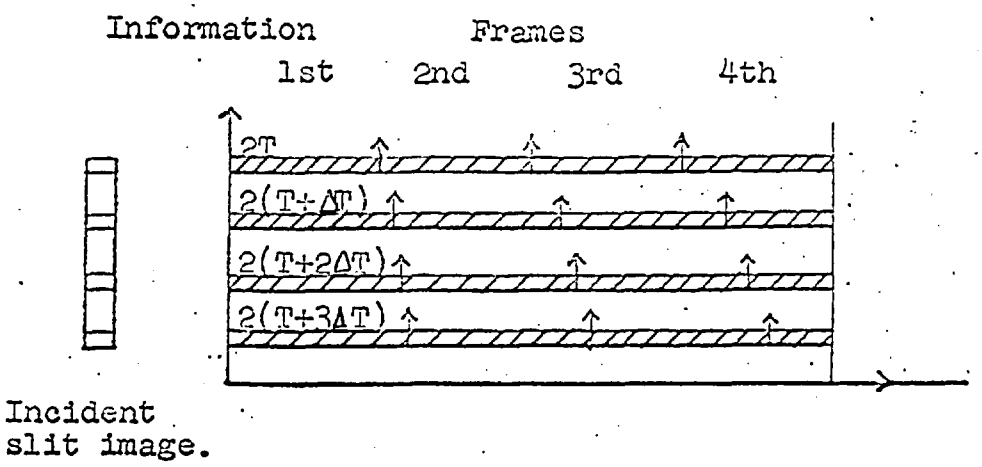
4.7. Streak Operation.

Fastest time resolution could be achieved when the system is used as a streak camera. The presence of a long deflecting field in the storage section opens up a novel way of operating the tube for streak operation where high writing speed is feasible with relatively low voltages. In this mode of operation, gating properly of the aperture alone is utilised, the mesh being kept open all the time. Fig.(4.6.) explains the principle.

A slice of information lasting for T_S seconds is allowed to pass into the storage section. The length of time T_S is so selclected that $T_S \leq T_{defl}$. Where T_{defl} represents the time taken by an electron to cross the deflecting field,

$$T_{defl} = \frac{L}{v_z} .$$

When the front edge of this beam of photoelectrons is just about to leave the deflecting field i.e. when it reaches point B, the whole beam is inside the deflecting field. At this point, a square pulse of height V_d and width not less than T defl is applied between the deflecting plates. This will deflect different parts of the beam in proportion to the time of their stay in the deflecting field. Since the deflection velocity remains constant, this produces a streak image which should inherently be linear with time over the the whole image had there not been any time dispersion associated with the deflecting pulse. But as discussed, time dispersion may be made negligible for an image of small height.



Storage of electrons in different frames.

Fig. 4.7.A

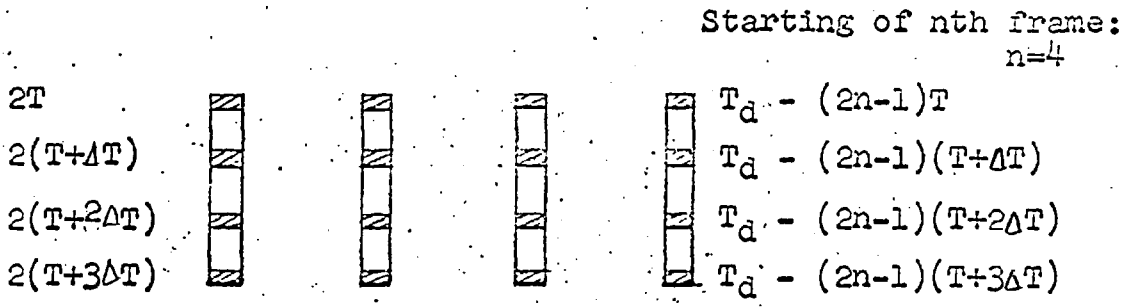


Fig. 4.7.B

4.8. Utilisation of Time Dispersion to Achieve Higher Time Resolution in Spectroscopy.

When used for spectroscopy, since the slit pattern will only have small patches of light at different heights, time dispersion along one such Fabry-Perot line would be infinitely small. As a result, if there are n orders displayed in the slit, we shall get streaks which would have different lengths because of the different lengths of time they would stay in the deflecting field, even though the total time displayed in each streak would be the same. Thus a streak interferogram should be obtained where different order fringes will have different time resolution. The beauty of such a system is its inherent linearity within each streak image.

Writing speed can be calculated from equ.(2) and in the following manner

If t = time taken by the electrons at the higher velocity end to cross the deflecting field,

$$\text{Total defl } d = v_d \cdot t = (E_d \wedge B_z) / B_z^2 \cdot t.$$

$$= \frac{V_d}{S.B_z} \cdot \frac{L.}{v_z} = \frac{V_d}{S\,B_z} L\sqrt{\frac{e}{2m}} \frac{1}{\sqrt{V_z + V_d}}$$

$$\text{or } d = K \frac{V_d}{\sqrt{(V_z + V_d)} \cdot B_z} \qquad (12)$$

$$\text{where } K = \frac{L}{S}\sqrt{\frac{e}{2m}} .$$

The deflection at the slowest part of the image would be

$$d_1 = d + \Delta d \qquad (12a)$$

as obtained from eqn. (9).

Eqns. 12 and 12a suggest that the time dispersion effect could in fact be utilised to get better time resolution when slit images crossed with Fabry-Perot fringes are used for streak operation.

The same should be true in the case of framing as has been suggested in a previous section. Let the slit image consist of fringes of different orders (Fig.4.7a). The width of each fringe is so small that the time dispersion is negligible compared to the framing time. But there could be a time dispersion Δt between this and the next fringe which would be an appreciable fraction of the total framing time, so that the framing time for this fringe is $t + \Delta t$ and so on. Thus the time over which the image of each segment is integrated varies incrementally from frame to frame. Hence any change in the event during these incremental times would be recorded between different orders in the same frame.

If, for example, in a frame containing four orders of an F.P. interference pattern, each having a framing time of

$$2T, \quad 2(T + \Delta T), \quad 2(T + 2\Delta T) \text{ and } 2(T + 3\Delta T)$$

The nth frame will display in these four lines information starting respectively at

$$T_d - (2n - 1)\,T, \quad T_d - (2n - 1)\,(T + \Delta T),$$

$$T_d - (2n-1)\,(T + 2\Delta T) \text{ and } T_d - (2n - 1)\,(T + 3\Delta T)$$

following the same argument as used in deriving expression -(10 A). The effect is diagramatically shown in Fig.(4.7.B.). It is seen that

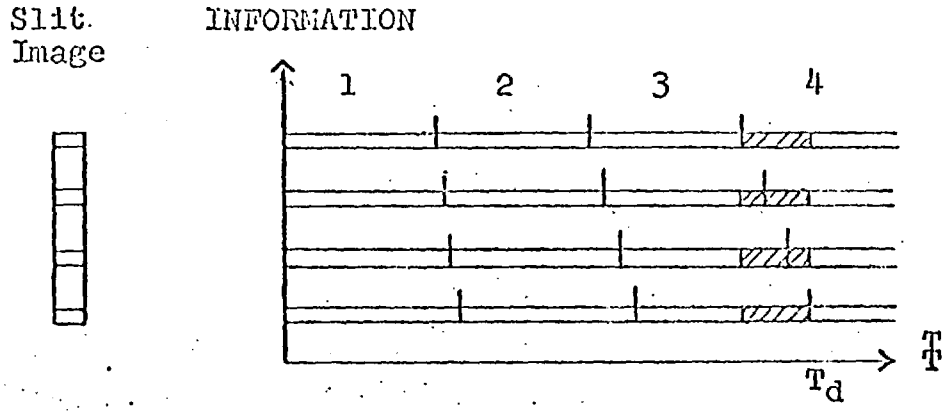


Fig. 4.8.A

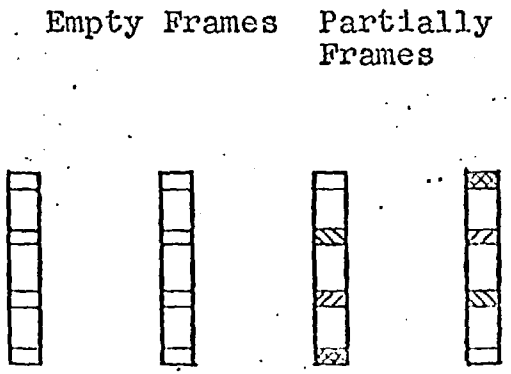


Fig. 4.8.B

each segment of a frame represent a seperate time of the event, with sufficient overlaps. A qualitative estimation of a transient phenomenon is possible in time ΔT in such a case, as the information is superposed on the event happening over a much longer time.

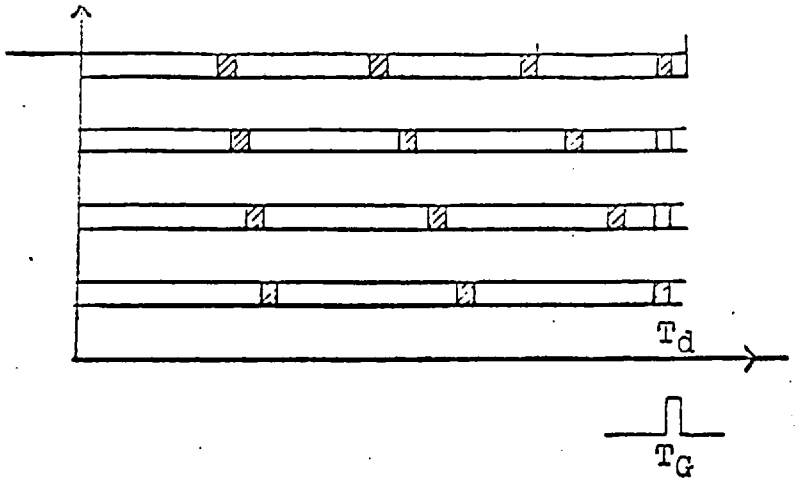
But once with such an experimental set up the time scale and its period of occurrence is "roughly" (within a few nanoseconds) known, it is possible to use the system in a slightly different way to analyse the transient on a fine time scale clearly.

In this case, time selection is performed by gating the input aperture, while fine time resolution is achieved with the help of a delay T_d as will be explained below Fig.(4.8.a.).

A section of information containing the short transient to be time resolved is first let in through the aperture with proper timing of the aperture gate. Let T_{in} be the time for which information is allowed into the storage section. Since higher time resolution than the framing time is sought, T in is made shorter than the framing time 2T, where as the width of the mesh gating pulse is kept $T_G \gtrsim 2T$.

Let T, $T + \Delta T$, etc be the transit times for the segments 1,2, etc, starting from the top. The condition that the last bit of information in the 1st. segment will just have entered the nth frame when the mesh is gated after a time delay T_d, is that the last photoelectron entering the storage section will just have completed $(2n - 2)$ transits during this time T_d.

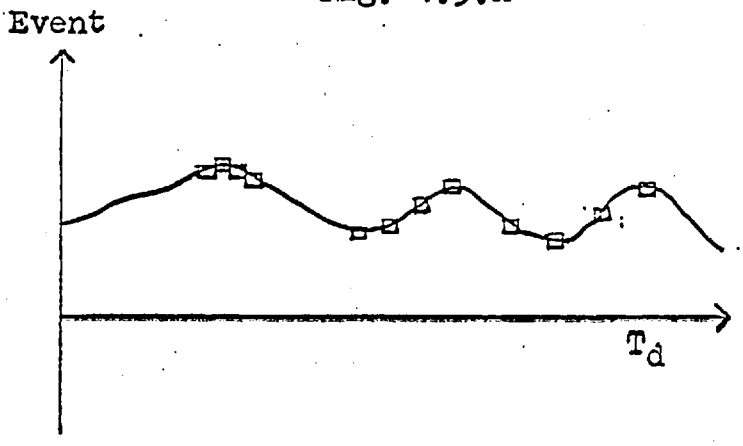
Thus, $$T_d = (2n - 2)\, T + T_{in} \qquad (13)$$



Shaded portions show information output at each frame.

Information allowed in for a time T_d.

Fig. 4.9.A



Portions of the event sampled are shown by squares.

Fig. 4.9.B

If in the same time the 1st photoelectron entering the storage section in the pth segment just arrive at the mesh in the $(n-1)$th frame,

$$T_d = 2(n-1)-1)(T + (p-1) \qquad (14)$$

from (13) and (14),

$$T = (2n-3)(p-1)\ T - T_{in} \qquad (15)$$

But $T_{in} = (p-1)\ T$

Therefore $T = T_{in}\ (2p-4) \qquad (16)$

Fig.(4.8.b.) is an example where $p = 4$, $n = 4$ therefore $T_{in} = \frac{1}{4}\ T$.

and $\Delta T = \frac{1}{3}\ T_{in} = \frac{1}{12}\ T$.

Thus, as Fig.(4.8.b.) explains, T is resolved between segments, thus producing a time resolution $\frac{T}{\Delta T} = 12$ times higher than the framing time.

The device could be used in still another way if the transient is periodic.

This is the chopped mode of operation explained in section (4.6.) but with the time dispersion so arranged that in the frame which is deflected most, the slowest segment is just lost, as illustrated in Fig.(4.9.a.). Here, each frame produces a series of segments of duration T_G but representing different parts of the event close together (Fig.4.9.b.).

In all these calculations, we have not taken into consideration the effect of variation of electron emission energies. But this error

is negligible for time resolution above 1 nanosecond. If one is using the tube for high resolution spectroscopy in the nanosecond region, this time dispersion due to electron emission energy variation is even more neglible, as, in this case the electron energy spectrum is narrow due to the use of highly monochromatic light. Thus for laser plasma diagnostics, extremely high time resolution should be possible.

All along in this theoretical analysis, time selection is done by variation of pulse widths and/or variation of the delay T_d; consequently extremely precise synchronisation as well as fastest rise and fall times are of pariamount importance.

CHAPTER 5

ELECTRONICS.

5.1. General Electronic Requirements.

It has been established from the theoretical considerations, that the control and operation of the camera would need an electronic system capable of fulfilling the following requirements:-

1. It must be able to produce extremely fast switching pulses - a rise time of less than a nanosecond with a voltage swing of a few tens of volts would be adequate.

2. An extremely accurate delay system capable of producing hundreds of nanoseconds delay with an accuracy of a small fraction of one nanosecond. It is convinient to have the delay system variable.

3. The width of the gating pulses should be variable.

4. A repetitive master pulse generator which will be used to test the electronic circuits as well as to test the performance of the tube at low light level by repetitive pulsing.

5. To test and operate the tube for streak operation, fast pulses of several hundred volts would be required.

All these requirements are best fulfilled by using an all transistor electronic system. It is now known for several years that transistors designed for high frequency work, when properly picked, could be employed to function in the avalanche mode to produce pulses much faster than those obtained from the same transistor operated in the conventional way. (Beale et.al. and Chaplin et.al.)

5.2. Avalanche mode of operation for a transistor.

The principle of operation is explained here in brief. The increase in gain and frequency response when a transistor is biased very near its collector breakdown voltage V_{CB} is caused by two effects.(Fig.5.1.)

1. Avalanche multiplication in the collector-base depletion layer.

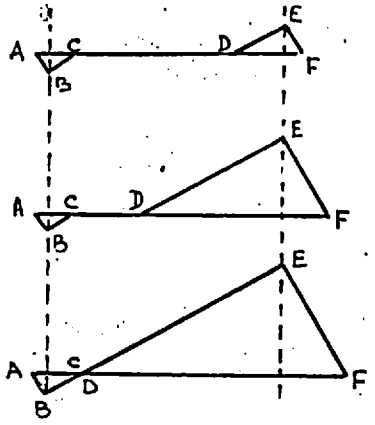
2. Shortening of transit time of minority carriersfrom the base to the collector region.

Shortening of transit time:

When a transistor is biased in its normal way (fig.5.1.a.(the depletion layers at the emitter and collector juntions are fairly small, and the field distribution is also not very high. But when the collector-base junction is biased near the breakdown voltage V_{CB}, the depletion layer at the collector-base junction expands and also the electric field in this region becomes very high, as shown in fig.(5.1b.) The diffusion length CD is therefore reduced. Thus, if any minority carriers are injected into the base region near the base emitter junction, they only have to drift through a short length CD before getting swept across the collector-base depletion layer because of the high electric field present in this region. The net result is a shortening of the transit time of the minority carriers across the base region.

Avalanche Multiplication:

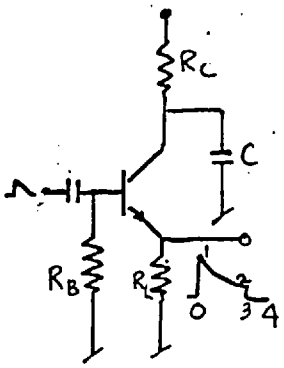
If the field in the depletion layer is high enough, secondary electron-hole pairs are produced by the collission of the minority carriers with the crystal lattice. The process continues in a way similar to ionisation in a gas discharge. This multiplication process increases

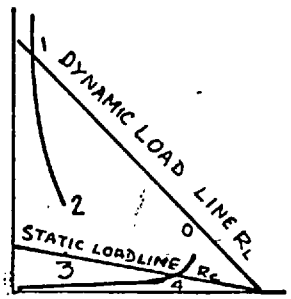


a

b

c





d. Basic avalanche circuit and the working cycle

Fig 5.1.

the current gain substantially, the multiplication M of the current gain being emperically given by (Miller and Ebbs.)

$$M = \frac{1}{1 - \left(\frac{V_C}{V_A} \right)^3} \quad \text{for germanium transistors.}$$

where V_C = Collector voltage

V_A = Voltage at which complete breakdown occurs.

This expression shows that by making the collector voltage very close to breakdown voltage, larger values of M could be obtained.

The way of making the transistor determines whether it will avalanche or not. For example, if the base resistance is very high (i.e. the base region is very slightly doped with impurity), the collector depletion layer may have to extend up to the emitter depletion layer (fig.5.1.c.) to neutralise the voltage before the field reaches near the avalanche breakdown level. This is known as "punch through" and the voltage at which this occurs is known as punch through voltage, Vp.

Such a transistor would not exhibit avalanche phenomenon. Thus, the transistor has to be chosen so that it operates in the region displayed in fig. (5.1.b.), where $V_A < V_P$.

Thus, with a transistor biased for avalanche operation, if carriers are injected into the base region, a very fast multiplication occurs and the voltage drops down at the collector extremely rapidly, causing M to fall down to unity. But the amount of minority carriers stored in the base region keeps the current rising for some time even after the value of M has decreased to unity. The rise of the current pulse is

approximately linear.

Fig. (5.1.d.) illustrates the basic avalanche switching circuit along with the static and dynamic load lines usually found in this type of circuits, (Bell,1964). The resistor R_C is used to bias the collector by allowing a controlled current through it. This is necessary because V_A varies quite a lot from one transistor to another so that there is a considerable fear of damaging transistor by putting too high a value of V_C. On the other hand, R_C automatically allows to take V_C upto very near V_A for almost any transistor. The static load line is so chosen that it does not cross the low voltage breakdown point. Avalanching occurs between points 4,0 when the transistors operating point is pushed beyond its normal-region ratings. Capacitor C_1 supplies the large rush of current for the avalanching region 0-1, The cycle is completed between 1-2-3 and 4, provided C_1 is recharged between 3 and 4. After C_1 has been recharged through R_C, the circuit is ready for the next transient.

For faster circuits, silicon NPN transistors are better suited than the germanium PNP types because, in the former, electrons are the minority carriers and hence faster in their transit from base to collector than their counterpart (holes) in a PNP transistor. Also, silicon transistors are stabler in operation because of greater temperature stability.

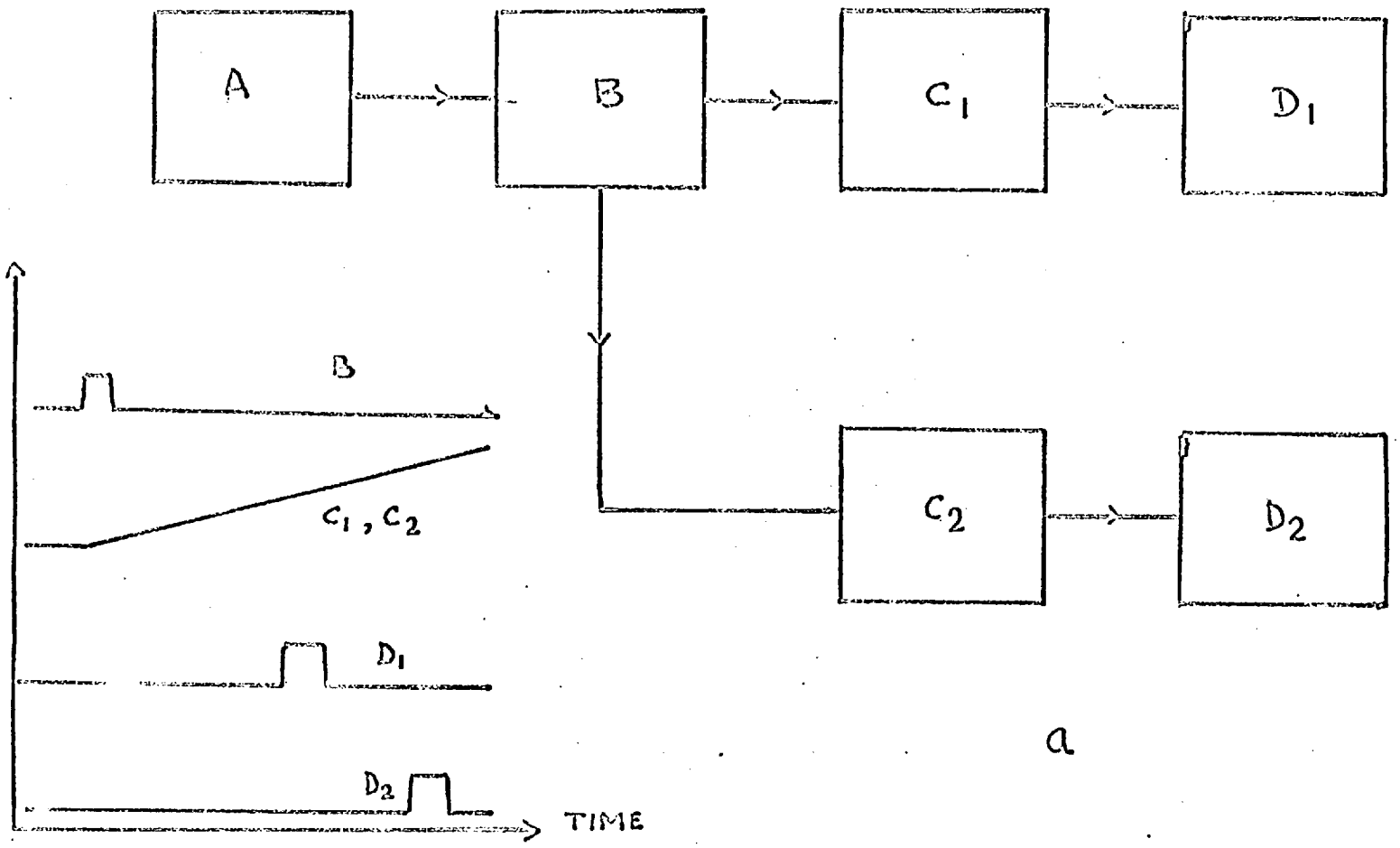


Fig 5.2

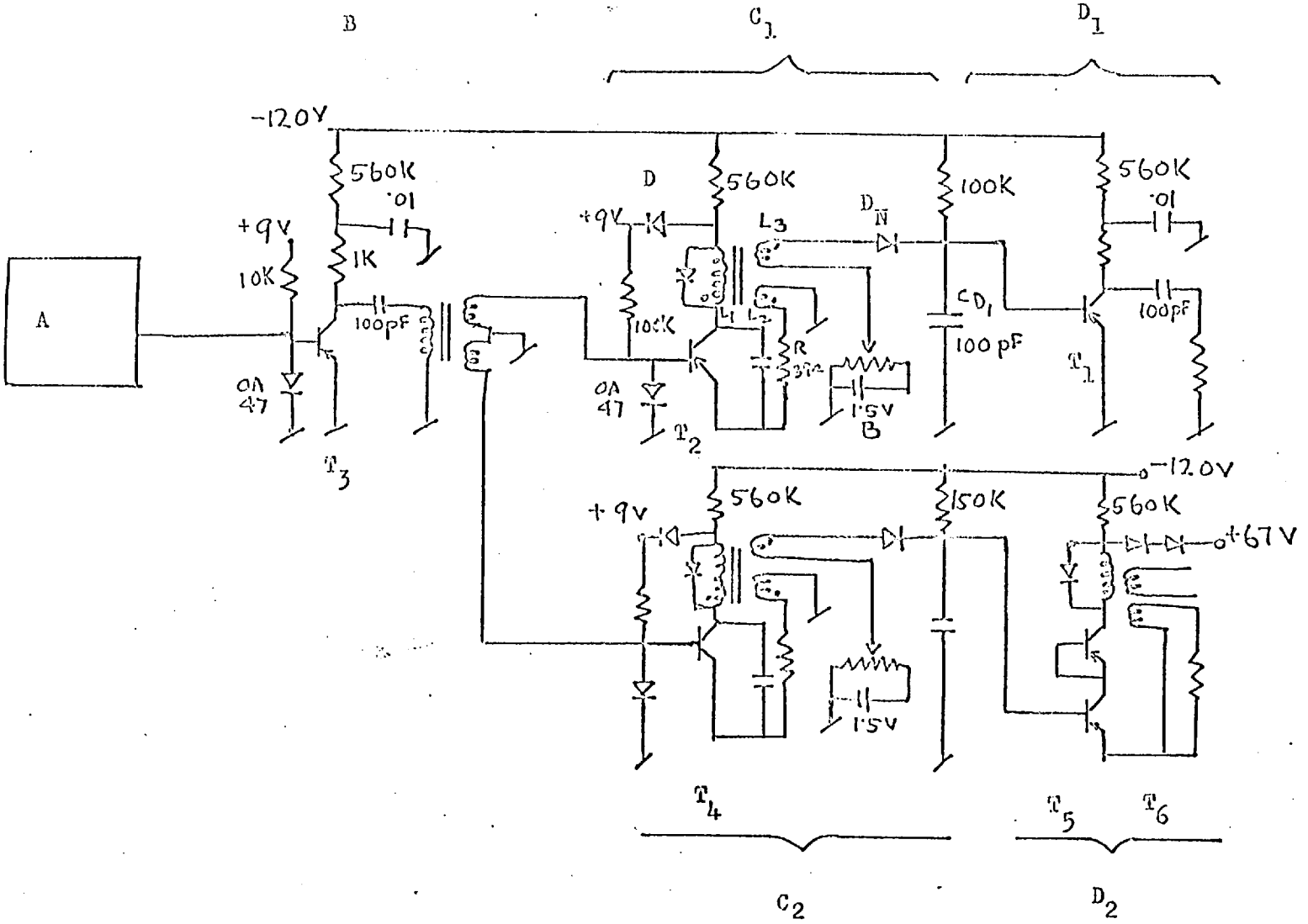

B
C1
D1
-12.0V
560K
.01
+9V
10K
1K
100pF
A
0A 47
T3
D
560K
+9V
L3
DN
100K
560K
.01
10K
L1
L2
R
CD1
100 pF
100pF
T1
T2
1.5V
B
-12.0V
+9V
560K
150K
560K
+67V
1.5V
T4
T5
T6
C2
D2

Fig 5.3

The trigger pulse generator.

The multivibrator feeds in a negetive pulse to the base of transistor T which is biased for working in avalanche mode. T triggers and the sharp output pulse is differentiated to produce two 5 volt pulses of 10 n.sec. diviation, which are fed into the two delayed output pulse generators that follow.

The delayed M grating pulse:-

One of the two avalanche pulses generated in B is now fed to the base of the avalanche transistor T working as a wide pulse generator (Chaplin 1959). As this transistor avalanches, the collector voltage rises rapidly. As soon as it reaches -12 volts, diode D starts to conduct. After that a voltage is developed across the primary winding L_1 of the transformer as the collector continues to rise. The secondary turns L_2 in the emitter circuit of the transformer now provides positive feedback and as a result the transistor is held at the highly conducting state for time determined by L_1 and R , like an ordinary blocking oscillator. Pulses more than $\frac{1}{2}$ .sec wide and about 12 volt amplitude could be obtained from this circuit. Rise time of about 5 nanoseconds could be achieved.

The transistor T is biased to a voltage V_B beyond cut off with the help of the battery B through a IK potentiometer, the secondary turn L_3 of T_1 and the diode D , which also charges capacitor C_{D_1} tc V_B. When a wide pulse is conveyed to the diode D through L_3, it ceases to conduct, and consequently C_{D_1} starts to charge towards V_{bb} . But as soon as it reaches the triggering level of T , the latter starts to

conduct producing a sharp output pulse the duration of which was controlled by a differentiating circuit. Since $V_{bb} \gg V_B$, the portion of the ramp between $+V_B$ and 0 V is linear, the time duration being $\frac{V_B C_{D1}}{I}$ where I, the charging current can be taken as constant for small V_B. By varying the potentiometer the bias on T_3 and hence the delay could be varied.

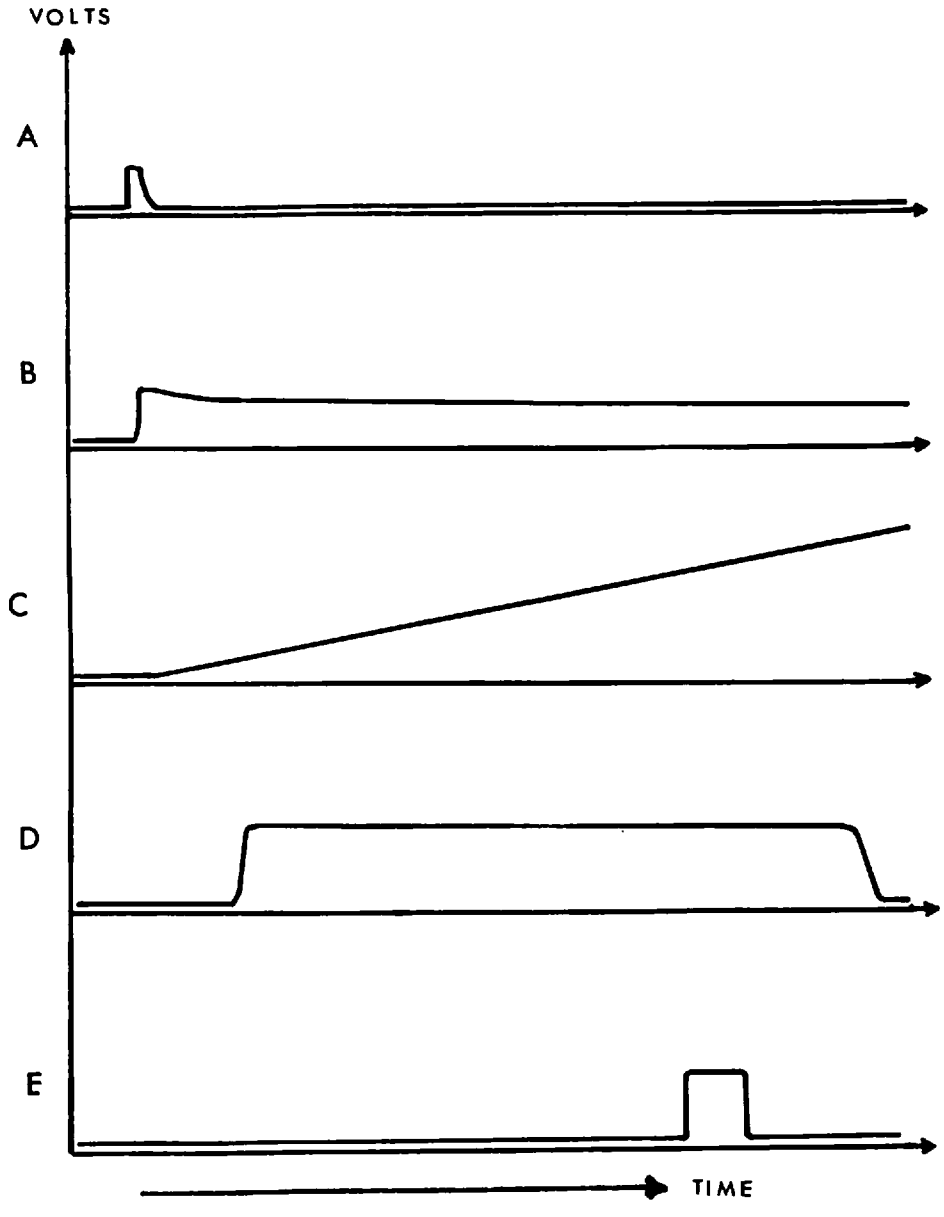
Delay and Aperture Gate:

The width of the aperture gate needs to be fairly long - equal to the duration of the event to be time resolved. Thus, a differentiated output pulse is inadequate. Besides, the aperture was expected to need a higher voltage trip to turn it from off to on stage and vice versa. Hence, a wide pulse was generated using the technique described in previous section, with two avalanche transistors connected in cascade. Because of the higher output volts required, two diodes had to be used in series to define the voltage trip.

Pulses at different points in the circuit are shown in fig.(5.4.). The rise times as well as shape of the pulses were not ideal, although good enough to test the general validity of the principle and design of the system.

Impidance matching was found fairly critical, and it appeared that the use of the avalanche transistors as blocking oscillators tended to increase the rise time. This may be due to the use of transformers in the circuit.

Although variable delays were acheived in this circuit, variable width of the output pulses could only be obtained by changing circuit parameters, or employing new circuits altogether.


VOLTS
A
B
C
D
E
TIME

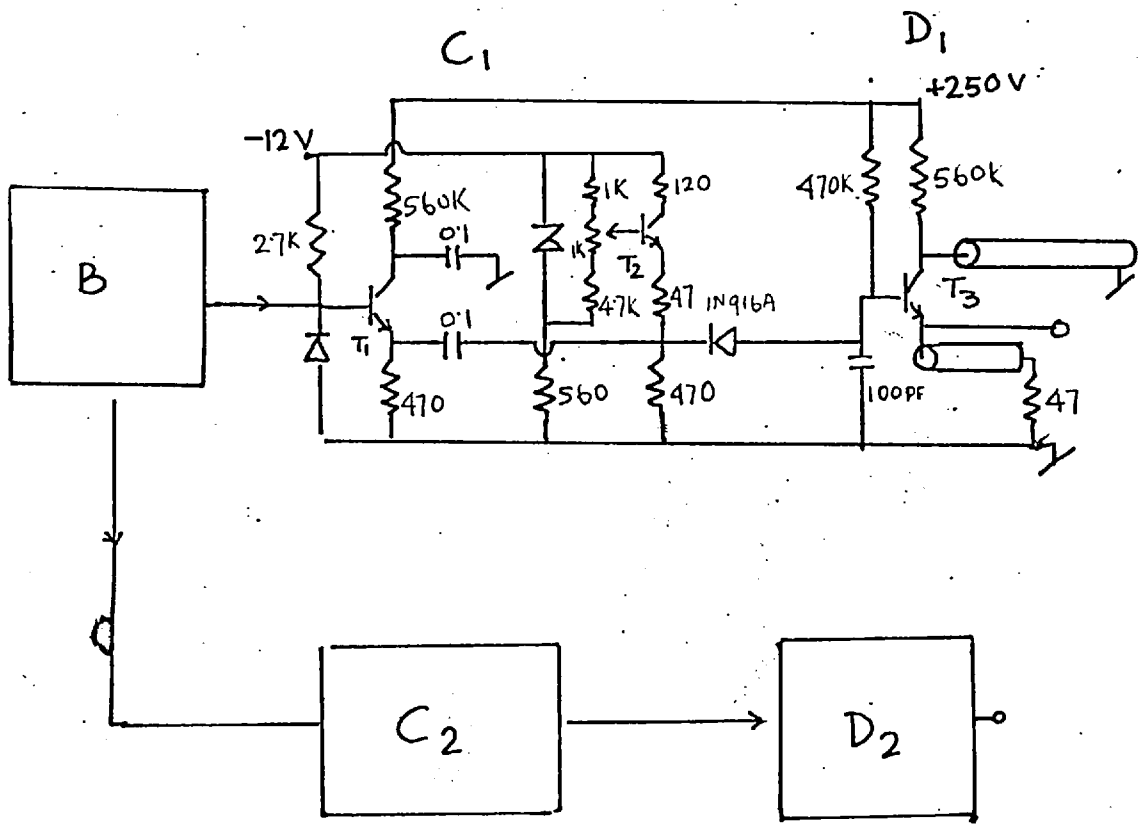

C1
D1
+250 V
-12 V
560K
27K
0·1
1K
120
1K
T2
47K
47
IN916A
T1
0·1
T3
470K
560k
B
470
560
470
100PF
47
C2
D2

Fig 5.5

5.4. Improvement of Electronic Circuits.

It was clear that pulses of better shape and rise and fall times along with better calibration of time delay would be required for quantitative evaluation of the tube performance.

Improved electronic system was used to test the last two tubes. In these circuits, there were four basic differences:-

i) Only silicon transistors and diodes were used, because they seemed to produce better stability and performance at higher frequencies.

ii) No transformers were used.

iii) Wide pulses were generated with the help of charging lines, which were easily replaceable for variation of pulse width

iv) Stabilised power supplies were used instead of batteries.

The basic sequence of pulses were the same, as were the basic scheme of circuit layout.

The multivibrator was replaced by a commercial pulse generator of slow risetime. Rest of the circuit is shown in (Fig.5.5.) In this layout, 2N708 transistors supplied by Hughes International were used to work in the avalanche mode. Same brand of transistor, made by STC did not avalanche. Section B in this circuit is essentially the same as section B of Fig.(5.3.), the only difference being that the circuit is now an N.P.N. circuit with silicon active components. Positive output pulses of less than 10 nanoseconds duration and 6 volt output voltage are applied to the inputs of C_1 and C_2 which are the two delayed pulse generators, of almost identical design. Only one of these two circuits is explained here. The principle of operation was the same as that

explained in the previous section. But here, the capacitor C at the collector of T_1 controls the width of the wide pulse which initiates the delay. Section 2 of this circuit is used to supply a controlled steady current through a bias resistor R which determines the bias voltage V_B at the base of the output transistor T_3. Current through R has two components: The major part of this current is supplied by the collector of T_2 whose bias voltage is supplied from a helical potentiometer forming part of a bleeder chain voltage across which is controlled by a zener diode D_Z. The potentiometer could be used to vary the bias on the base of T_2 thus varying this controlled current through R . The other portion of current, which is about a tenth of the above controlled current, passes through R_1 , D and R .

When T_1 is triggered, wide pulse at its output is impressed on R , which biases D off. C_D starts to charge towards V_{CC}. As soon as C_D charges up to the triggering level of T_3, the latter starts to conduct producing a delayed output pulse. The amount of delay is given again by $V_B = CR/I$ as in Section (3).

The output pulse, so delayed, appears across the emitter and the earth. The short coaxial line connected between the emitter and the 47 Ω emitter resistor was used for proper matching. The length of the charging line at the collector of this transistor determined the length of the output pulse.

Fig.(5.7.) shows the type of output pulse obtained from this circuit as displayed in a type 585A Tektronix oscilloscope with a type N sampling plug-in unit. This showed that pulses of about one nanosecond duration

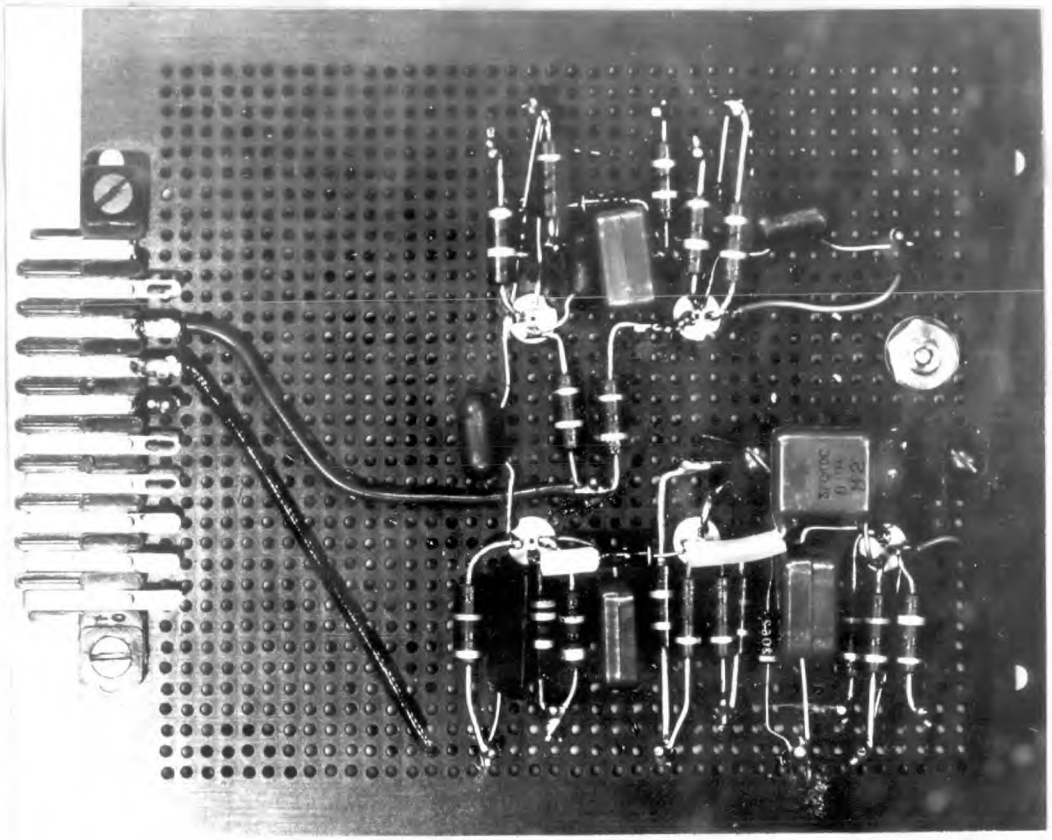


Fig 5.6

was possible to obtain from such a circuit.

A further improvement of the electronics was made recently which produced pulses with variable delay as well as width, Another circuit with cascarded transistors for high voltage pulses was also designed and constructed, to produce pulses heights in excess of 100 volts, with a view to using for streak operation of the tube. These are described in Chapter(7) Section ( ).

5.5. Spurious Triggering and Shielding:

Since the triggering voltage required in these circuits is always very low (one or two volts maximum), spurious triggering was anticipated to be a problem specially when the tube was to be used in plasma or laser diagnostics, where very high voltage transients are used to create the event.

This was actually found to be the case while the tube was being tested for 45 nanosecond exposures from a spark gap (Ref.Chapter 7). The following special precautions had to be taken to ensure no spurious triggering -

1) The box containing the electronic circuits was double screened, the outer one being earthed.

2) The cable which leads the trigger from the photodetector to the input of the trigger circuit was also double screened.

3) The power supply which generated the spark had its earth isolated from the rest of the circuits.

Fig 5.7

5.6. General Layout of the Electronic and other Variable Electrical Outputs:

Variation of many potentials are required in order to test and optimise the performance of the tube. These include:-

1) The mesh bias - Variable, negetive as well as positive.
2) Aperture bias, variable, negetive.
3) Potential on 1st accelerating electrode.
4) Potential of the drift space.
5) Deflecting field.
6) Magnetic field.

Power units supplying all the d.c. potentials except the last item were boxed inside one casing which also contained power units for the electronics. The potentials 1 to 5 could be controlled by knobs and switches on the front panel, which also contained meters for direct read out of potentials. The electronic circuits for gating the tube were housed in a seperate box which could either be fitted into the other housing, or, if required, could be taken outside and kept nearer the tube. This helped to keep the cables which transferred the gating pulses to the tube to a minimum. Fig.(5.8.) whows the photograph of this control unit.

Power supply for the photodetector, the Brandenburg E.H.T. unit for supplying high tension to the image tube, the stabilised coil current supply, as well as the tube control unit were mounted in a 19" rack, and is shown in fig.(5.9.). This was the set up used to test the last two tubes. In previous tubes, many of the tube potentials were supplied from batteries.

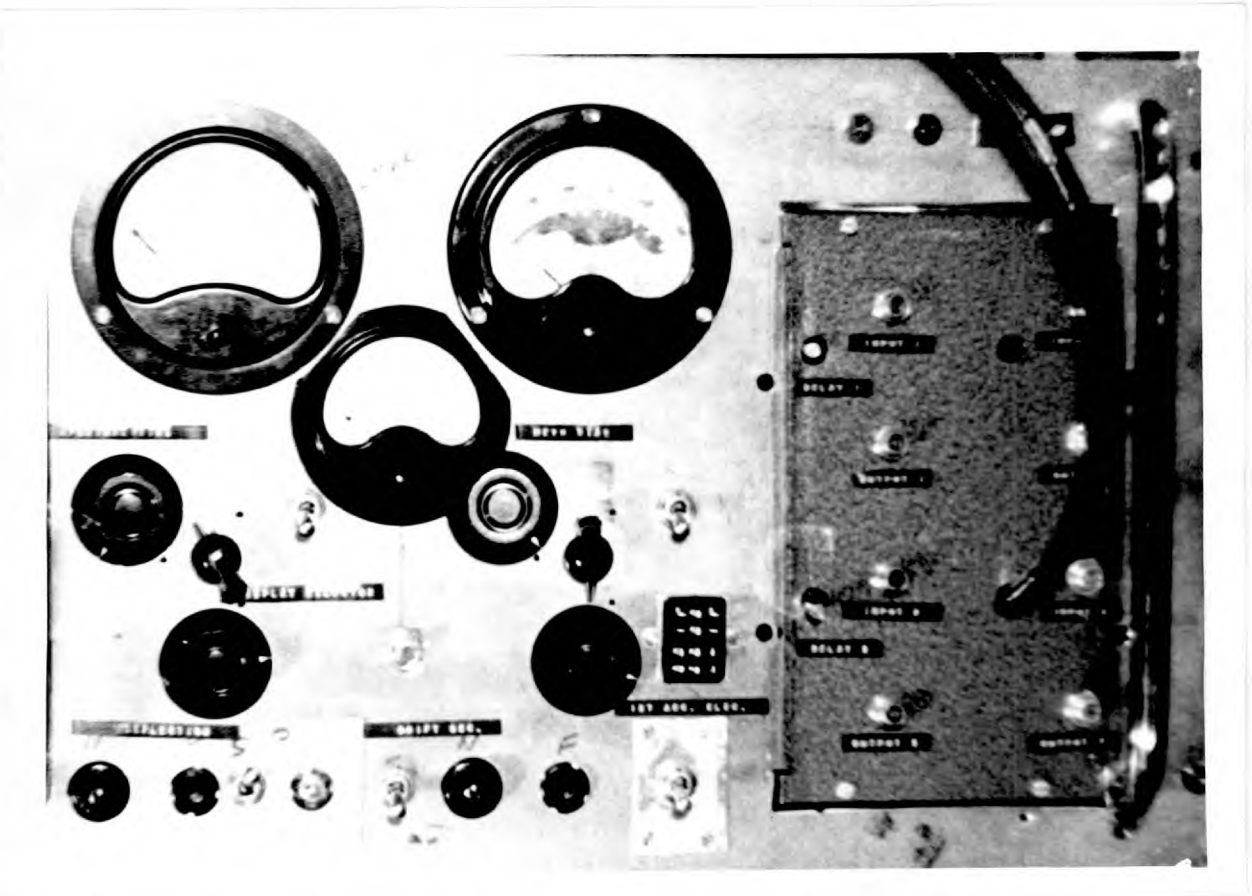


Fig 58.

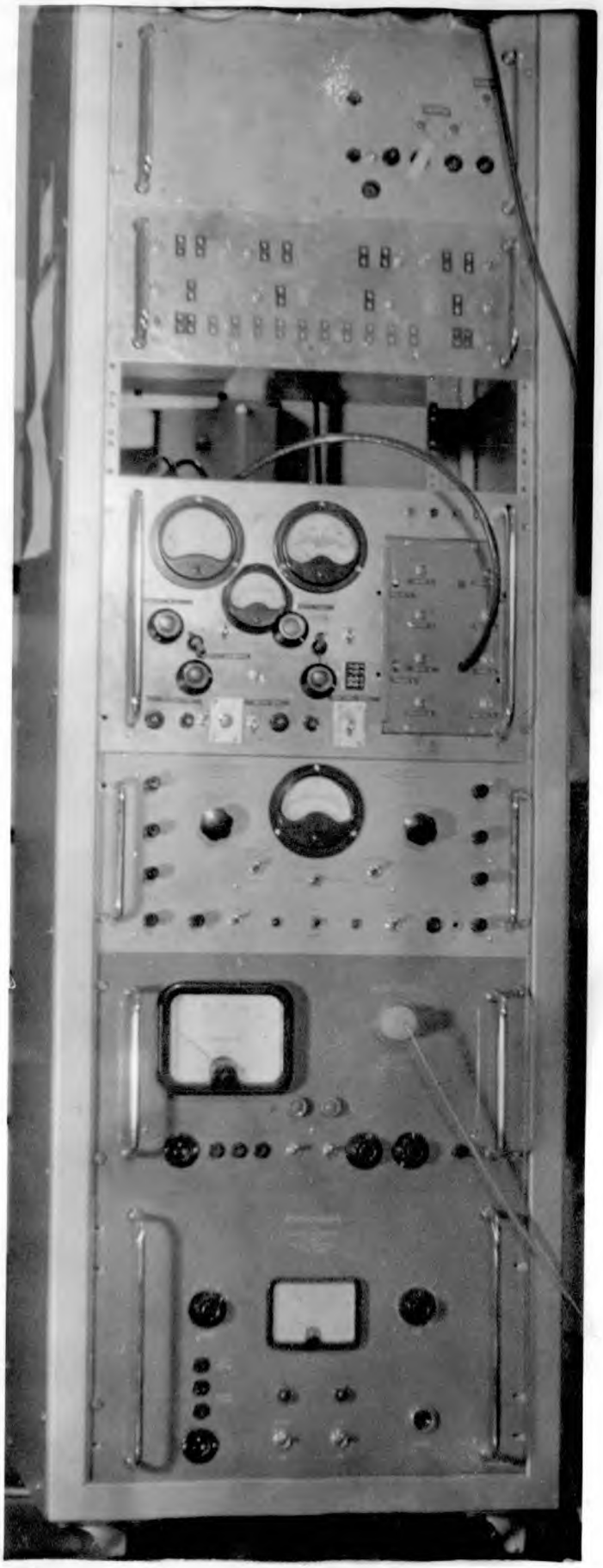


Fig 5.9

CHAPTER 6

DESIGN AND PRODUCTION OF HIGH-SPEED TUBES.

6.1. Electrode Assembly for the First Tube Design.

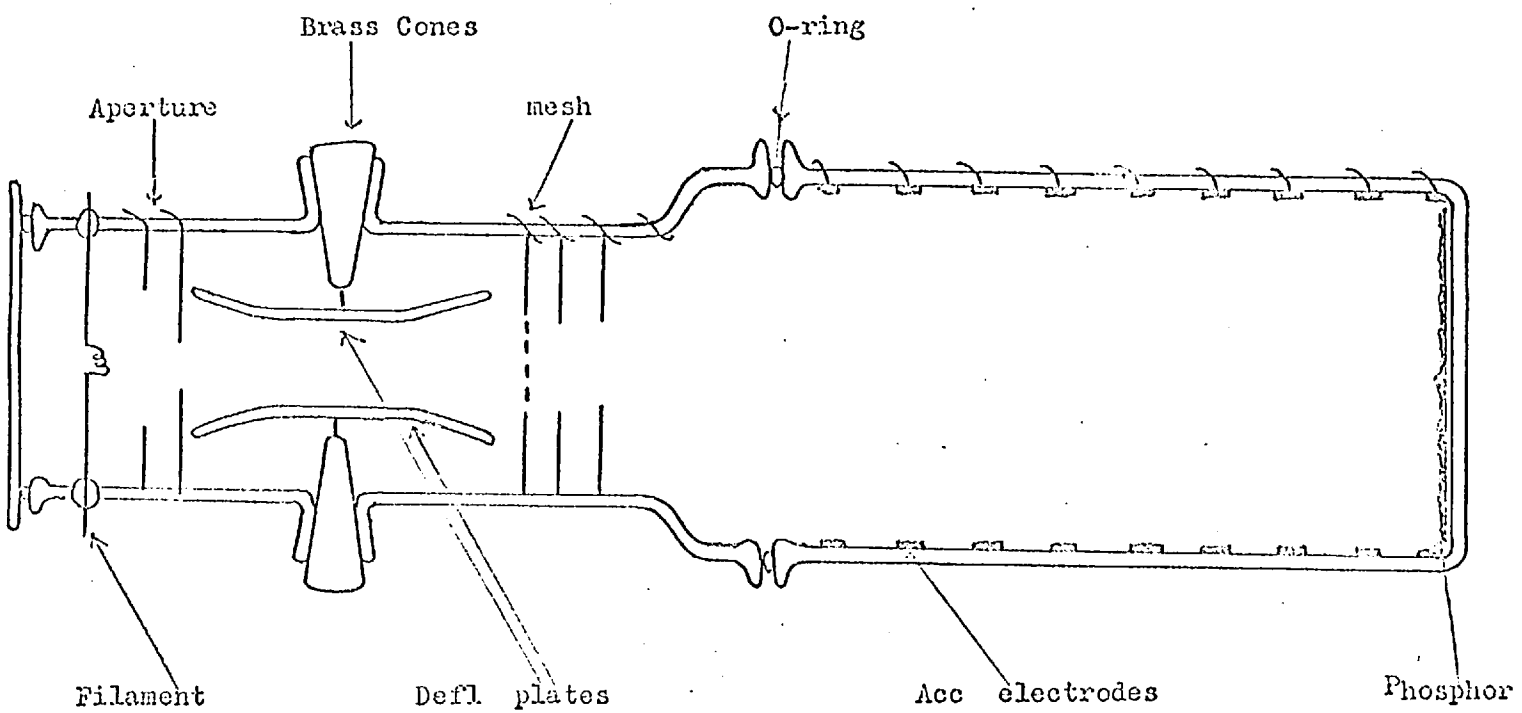
It was decided that the preliminary test of the tube design and evaluation of its feasibility as a high speed camera would be performed on demountable tubes for two main reasons, viz.

i) Assembly of parts could be changed more easily.

ii) For the purpose of testing the general idea roughly, imaging of a thermionic cathode would be just as good as a photocathode, with the added advantage that problem of a dying photocathode due to a leak in the tube or poisoning was eliminated.

The schematic diagram of the first demountable tube is shown in Fig.(6.1). An O-ring was used to combine the storage part of the tube with the intensifying section.

In this tube, a tungsten wire (.004″) was used as a filament. All the electrodes except the deflecting plates were fixed into slots in the inner wall of the tube. The deflecting plates were curved to follow the equipotentials in the deflecting field so that there may not be any abrupt change in the field along the path of the electrons. These deflecting plates were too heavy to be fixed inside the tube with tungsten pins since the mismatch of tungsten pin and pyrex tube limits the diameter of tungsten pins to about 1mm. or 2 mm. Besides, proper alignment of these plates parallel to the axis of the tube and with



THE FIRST DEMOUNTABLE TUBE

Fig 6.1

precise seperation between them was almost an impossible job with tungsten pins. Hence, these plates were suspended inside by means of tapered brass cones through ground glass taps attached to the side of the tube. A coarse tungsten mesh (50 t.p.1.) was mounted on an annular ring electrode and fixed by springs into slots made in the tube body. There was no stainless steel annular electrodes in the high voltage intensifying section of the tube - acceleration was produced by platinum ring electrodes fixed onto the glass wall as described in Chapter (3) Section (3). A settled p-11 phosphor with a floated aluminium backing was fixed into slots at the E.H.T. end of the tube, also in the usual way. An O-ring union was used to connect the tube to a high vacuum system.

The set up was found grossly unsatisfactory primarily because the brass cones holding the deflecting plates proved a constant source of air leak. It was obvious that in a tube with a photo-electric cathode anything like this type of mounting was useless. Besides, the conventional way of holding the electrodes by cutting slots in the glass wall of the tube as described in Chapter(3) was far from stable. Also, precise alignment of photocathode, aperture and deflecting electrodes in a tube would be extremely difficult, if not impossible. It was therefore clear that the assembling of this tube in the way described in Chapter (3) was not practicable.

6.2. <u>New Assembling System using Ceramic Rods.</u>

A new system of assembly was therefore to be devised where no slotting would be required for fixing the metal electrodes. The most obvious answer to this problem was the employment of the techniques used in

making cathode-ray tubes. i.e. mounting the metal parts on ceramic rods. The main objection to assembling an imaging device on ceramic rods was that these rods might charge up and hence cause distortion of the electric field in the tube. But Twidy and Mende(1964) have shown that by proper designing of the electrodes the ceramic rods could be screened from the useful tube space.

A design of such an assembly of metal parts was made, as shown in fig.(6.2.), for all the metal parts beginning from the cathode upto the gating mesh. The rest of the tube did not have any metal parts except the phosphor mount. This part had a corregated tube wall as described in chapter (3) section(9) which were to act as baffles to cut down background.

Ferry clips were used to fix the electrodes to the ceramic rods while tubular ceramic spacers with internal diameter slightly larger than the diameter of the ceramic rods were used between different electrodes. Around the central hole of the annular electrodes and inside the ceramic rods were placed short cylinders of pyrex tubing between different electrodes. These pyrex cylinders kept the circular symmetry of the electric field in the useful space of the tube by shielding the ceramic rods from the electrons.

All the electrodes except the aperture and the mesh had .015" dia ferry wires spot welded to them for external connection via tungsten pins. External connections for the aperture and mesh electrodes were done with the help of springs spot welded on them which pressed against platinum electrodes pasted and fired on the glass-wall and connected

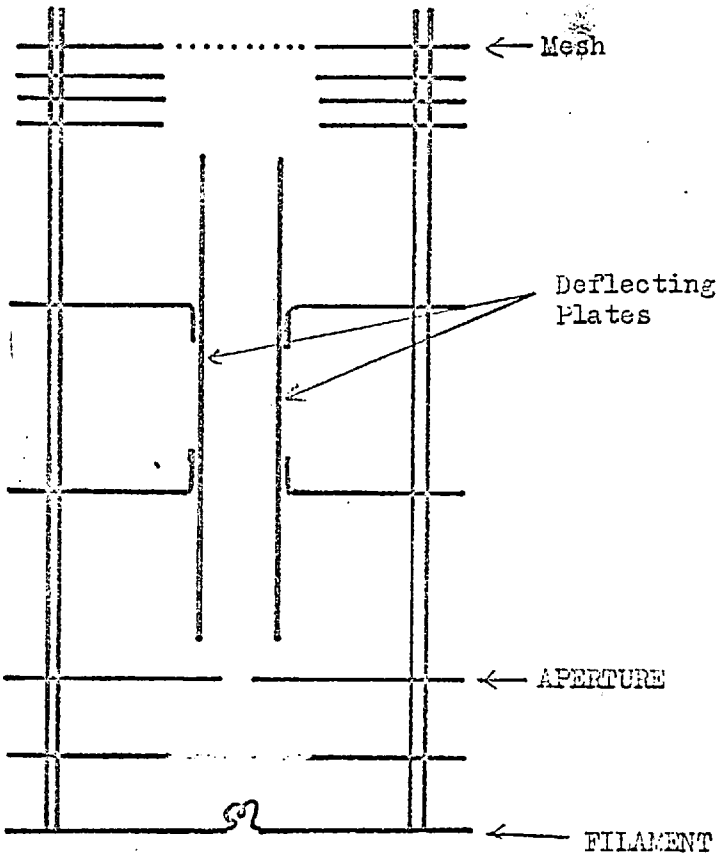


Fig. 6.2.

to the outside by a platinum tape passing through the pyrex tube body (Chapter 3). This was done to keep the length of the leads conveying the gating pulses to minimum.

Fig.6.2. shows the actual photograph of the electrode assembly. It is seen that the deflecting plates were not curved as was done in the previous design. This was done in order to find out whether the curving of the deflecting electrodes was really necessary. In fact tubes were made with and without curved deflecting plates in this new system of assembling and the results are discussed in Chapter 7.

Variation of Design for Thermionic and Photoelectric Cathodes.

The same basic design was used both for a demountable tube with thermionic cathode for preliminary tests and tubes with photocathodes. For the demountable tube, a short straight tungsten filament (.004" dia) was placed in the plane of the 1st electrode which would otherwise hold the photocathode. Fig. 6.4.a, show the mounting of the filament and Fig. 6.4.b. shows the system used for holding the externally processed photocathode. Fig.6.4.b. shows the cathode shelf in two planes. The cathode plate had a dimension of 10 mm. x 8 mm. x 1 mm. The shelf was made by spotwelding two stainless steel discs, one with a slot just clearing the cathode plate, the other slightly smaller (9 mm. x 7 mm.). The cathode plate was held in the slot of the first disc, supported at the bottom by the second one. The first disc was made of 0.040" thick stainless steel sheet and the second one of 0.008" thick sheet. Two retractable and springloaded stainless steel flaps were used to hold the cathode in position once it had dropped into its place in the shelf.

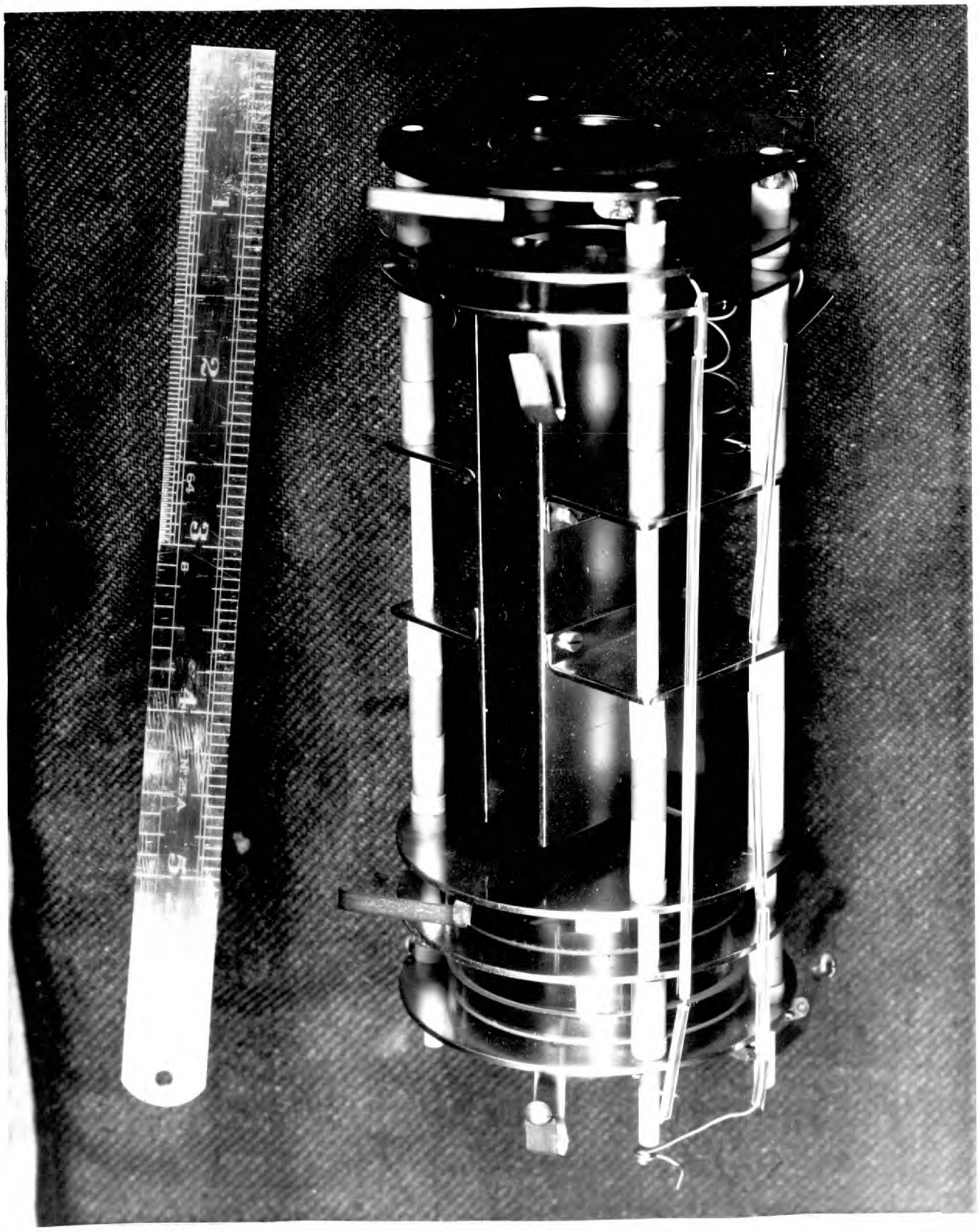
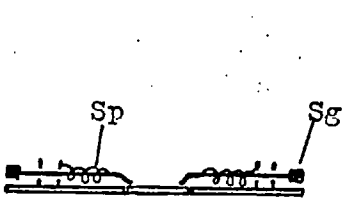
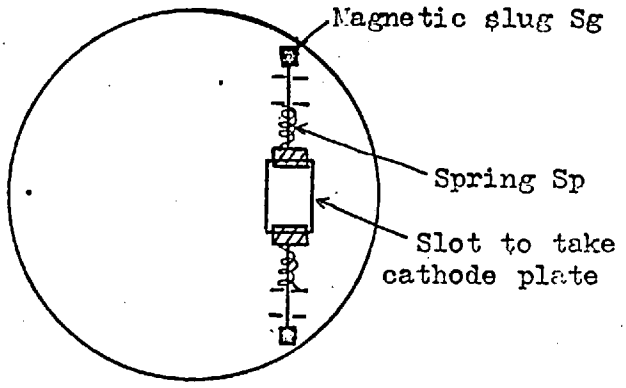
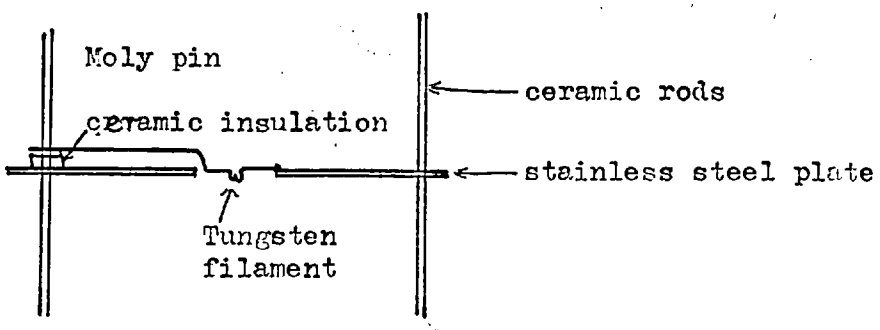


Fig 6.3


Sp
Sg


Magnetic slug Sg
Spring Sp
Slot to take cathode plate

b


Moly pin
ceramic insulation
Tungsten filament
ceramic rods
stainless steel plate

a

Fig 6.4.

The magnetic slugs on these springs were far enough from the cathode to aviod magnetic distortion, arising from them, in the electron image. The metal parts assembled as described, but before putting any springs for fixing or electrical connection and without the pyrex cylindical spacers was degassed in a vacuum stove at 1000°C. for 6 hours. The final pressure obtained in the vacuum stove while at 1000°C was around 10^{-5} mm. of Hg. The parts were taken out of the stove when it was cold and springs were spot welded on. Pyrex spacers were fitted in and the ferry connecting wires were sleeved with pyrex capillary tubes. The metal electrode system, thus finally assembled, was degassed again in the vacuum stove at 600°C for four hours. The whole tube was assembled within a few hours of taking the metal assemply out of the vacuum stove and connected to the high vacuum system without delay. Dry argon was let into the vacuum stove every time vacuum was broken for taking the metal parts out, so that diffusion of moisture into the metal parts could be kept to a minimum.

6.4. Fixing of the Metal Assembly inside the Pyrex Carcase and Assembly of the Whole Tube.

The pyrex tube carcase was divided into three sections (fig.6.5.a.)

1) The storage section containing the first portion of the tube upto the gating mesh. This part of the tube also contains the tungsten pins used for connecting the metal electrodes to the outside with the help of ferry wires.

Rings of platinum paste were applied to the portion of the tube

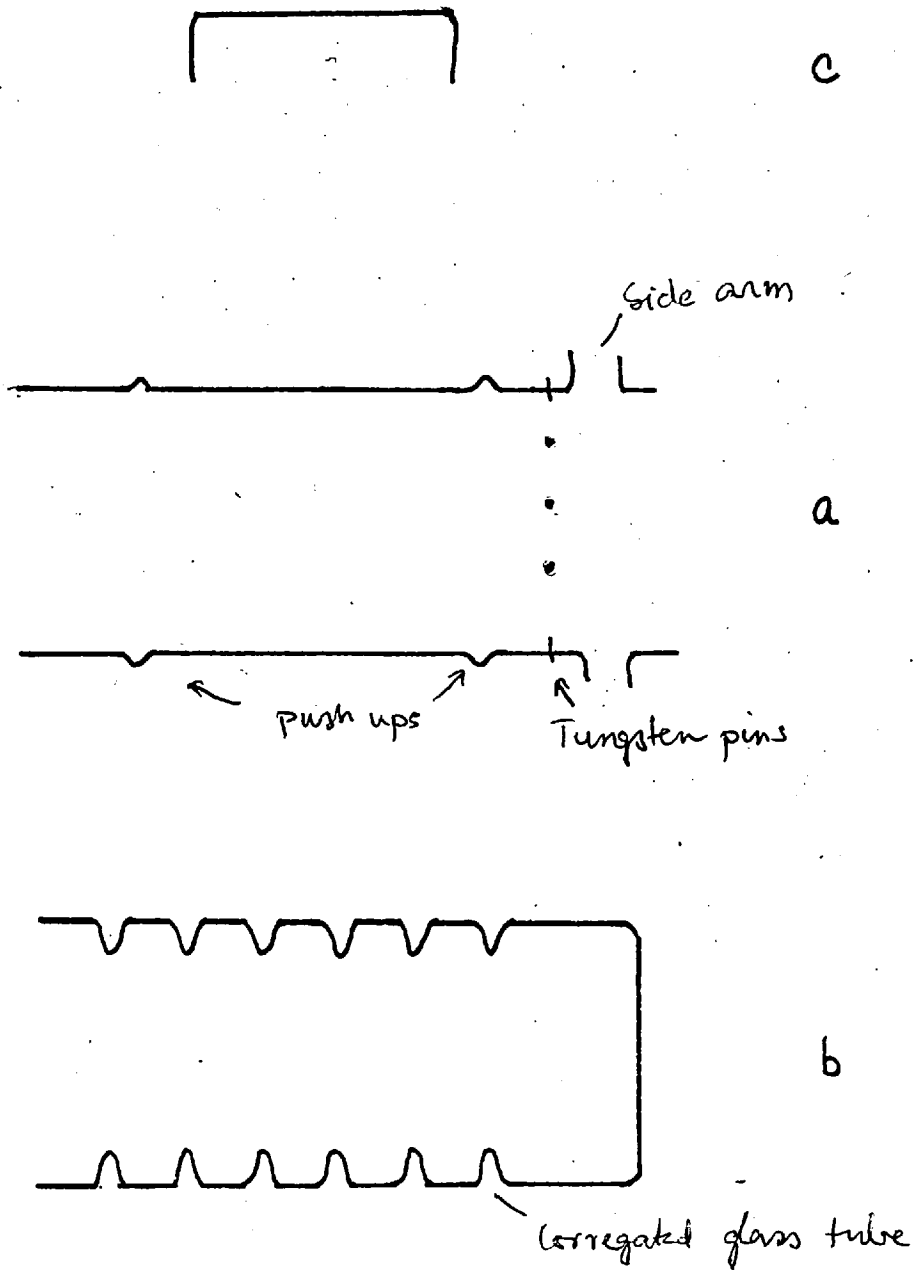


Fig. 6.5.

where the aperture and the mesh electrodes were to be positioned. The portion of the inside wall of the tube which covered the drift section i.e. from the aperture electrode to the first annular electrode after the deflecting plates, was painted with liquid platinum paint, and connected to the outside of the tube by a platinum tape as usual (Chapter 3). Two rings of platinum paste were applied to the two boundaries of this painted portion in order to prevent discontinuity in the painted tube wall which could be caused by the scratches produced in it when the metal assembly with protruding springs were to be inserted inside the tube. On the Cathode electrode and the first electrode after the deflecting plates were spotwelded three fixing springs, at 120^{o} from each other. Push ups were made on the proper portions of the tube body to fix these springs, thus locating the metal electrode assembly with precission and rigidity.

Three cms. further from the cathode electrode and away from all other electrodes, ten tungsten pins were sealed into the tube body along a circumference for external connection of the internal electrodes via the ferry connecting wires,

The two ends of this section of the tube were ground and polished, in a plane at right angle to the tube axis and platinum paint was applied to them for sealing it with other postions of the tube by silver chloride.

2) The second portion of the tube corregated wall on which platinum electrodes were painted as described in Chapter 3. The P-11 phosphor deposited on a glass substrate and backed by an aluminium film and mounted on a metal frame was fixed at the end of this section in the way described

in Chapter 3 section (9). The other end of the tube was ground, polished and painted with platinum for sealing it to the mesh end of the previous section by silver chloride.

3) The third section of the tube was just a short "monax dish" type portion with a window used to seal to the cathode end of the tube.

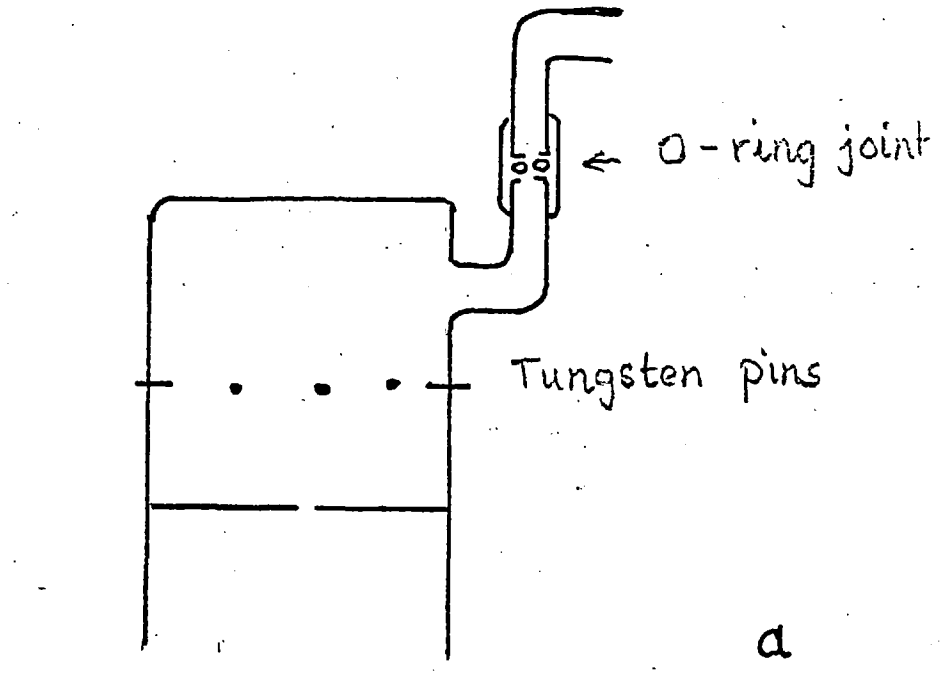
Variations in design for demountable and photoelectric tubes:

In the demountable set up, the tube had a side arm at the end of which was an O-ring union for connecting the tube to a high vacuum system (Fig.6.7.a.) In the tube with an externally processed photo-electric cathode, the 1st section of the tube had a side arm positioned in such an angle just below the cathode electrode that the photocathode in its carrier (as explained in Chapter 3 section (7)) could be moved to align it just against its place in the cathode electrode, ready to be dropped in position (Fig. 6.7.b.). It also had another side arm fitted with a barium getter and an ion pump, as safety measures against a rise in pressure inside the tube.

Sealing of the three parts of the tube together.

After fixing the metal parts and phosphor mount into the respective sections of the tube, the different parts were sealed together in the way described in Chapter 3 section (9), and the whole tube was connected to the pumping system without delay.

The demountable tube was mounted inside the solenoid before connecting it to a vacuum system and, it was ready for testing once the pressure had come down.



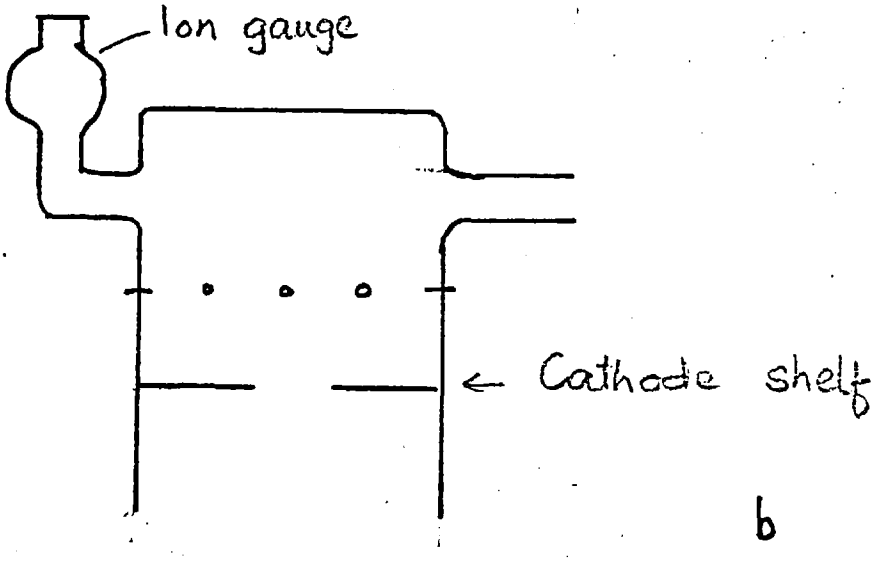


Fig. 6.7.

6.5. Introduction of the Photocathode inside the Tube.

Fig. (6.8.) shows the set up of the tube connected to a high vacuum system. The side arm for introducing the photocathode was also used for connecting the system to a high vacuum pump. The ampoule containing the photocathode had a breaking slug as described in Chapter (3). Section (7) The whole system was evacuated, tested for leaks, baked at 320°C for about 15 hours, cooled down tested for leaks again, and finally the high vacuum seal gevac was applied to all probable points where a leak might appear. Now the system was baked at 200°C. for one hour to curve the leak sealing compound. This procedure has been described in detail in Chapter 3. When the system was found to be satisfactory in all respects, and the pressure was better than 10^{-7} mm. of Hg, the thin glass wall of the cathode ampoule was broken by hammering it with the breaking slug. The cathode was now carried into the tube just above its house in the cathode shelf and was dropped into place by releasing the springs of the carrier with the help of magnets. The springs on the cathode shelf in the tube were held open to allow the cathode to drop into position and released to hold it in place subsequently. The tube was now sealed off from the pump.

6.6. Loss in Photocathode Sensitivity after Seal off.

The seal off point was degassed by a soft non numinous flame before the ampoule was broken so that there may not be too much of seal off gas. This was the proceedure employed for sealing the ampoule off after the cathode was processed, as explained in Chapter 3, and proved successful in retaining

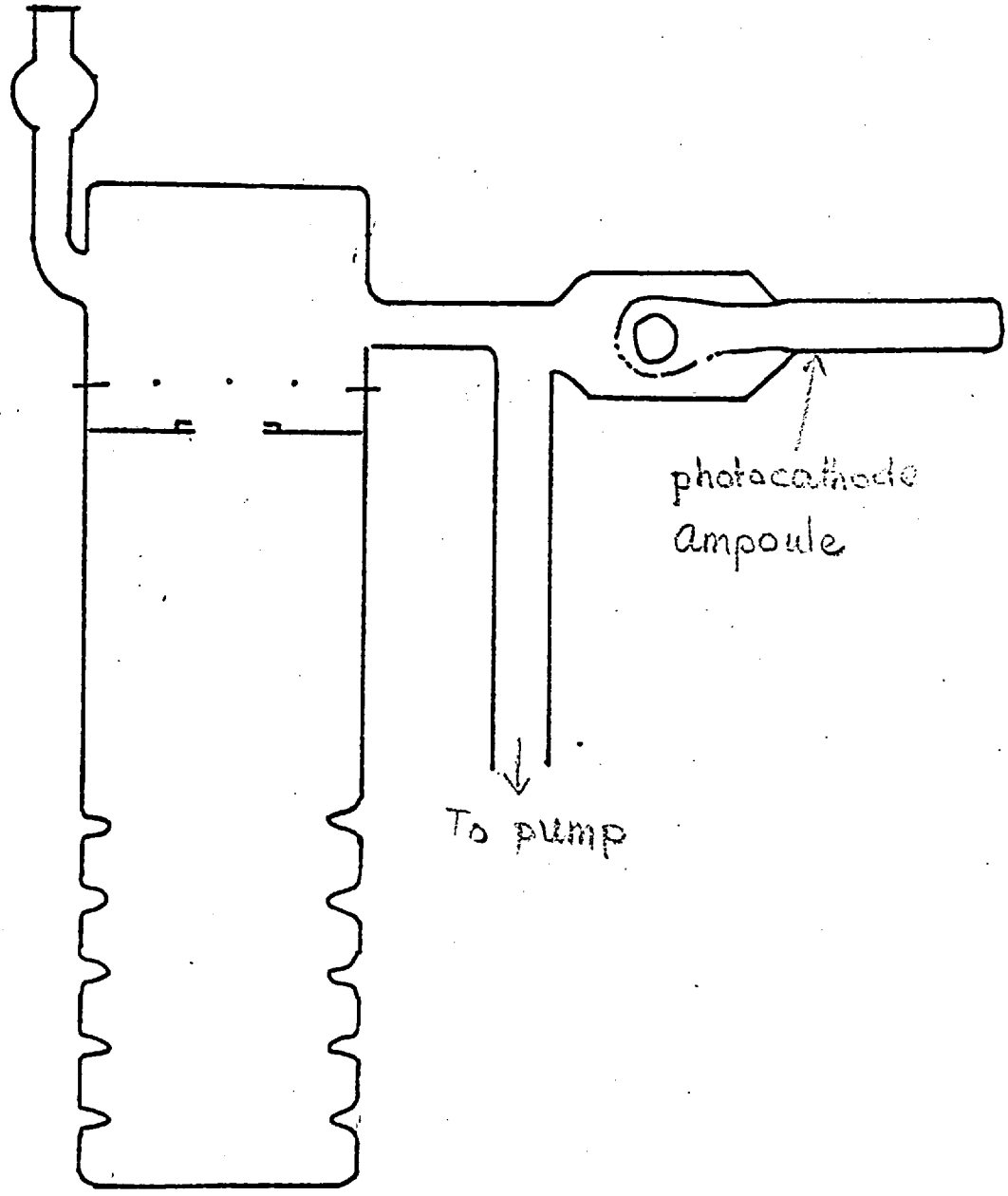


Fig 6.8.

the cathode sensitivity, and hence was thought to be enough precaution when introducing the photocathode into the image tube.

But the cathode died almost immediately after seal off, even though the pressure of the system at seal off was 3×10^{-7} mm of Hg and it never rose higher than 5×10^{-6} mm of Hg when the side arm was being softened by the flame.

Others had similar experience in dealing with $SbCo_3$ and Trialkali Cathodes (Davis 1962, McGee 1966, Theodorou 1966, Huston 1965, Kron 1960). McGee and Davis claims that this was (at least in $SbCs_3$ cathodes) primarily due to poisoning of the photocathode and they could protect the cathode by proper precautions against poisoning. Theodorou endorses this while working with trialkali photocathodes. Kron and Huston found that, for antimony cesium photocathode, their photocathode would die as though of cesium starvation. Thus, Huston could stop his cathodes from dying by letting in cesium into the image tube and then baking them out before introducing the cathode so as to saturate any reactive material inside the tube, which would otherwise take up cesium from the photocathode. Kron could bring back sensitivity by recesiating the photocathode.

6.7. Recesiation inside the Tube.

Although these results were obtained for a different type of photocathode, a cesium channel was incorporated in the next tube, which was of identical design as the tube just described, hoping that the cathode might be recesiated back to life if the same thing happened again.

When a 15 μA/Lumen Bi-Ag-Is-O cathode was introduced into this tube, its sensetivity dropped to about 0.1 μA/Lumen after seal off. Pressure inside the tube after seal off, as measured from the ion pump, was about 7×10^{-7} mm of Hg.

The whole of the tube was now heated up to a 250°C while the cathode part was kept at 150°C, and Cs was generated. Because of the glass spacers in the metal assembly system, cesium could not reach the photocathode surface without going deep inside the tube. Thus, the cesiation of the Cathode was not very efficent, and also the rest of the tube was getting some cesium.

It was in fact possible to increase the photocathode sensitivity to 2.4 μA/Lumen in this way. But unfortunately, it's phosphor connection was broken before the performance of the tube could be tested.

Another tube was made in the same way but its sensitivity could not be increased beyong 0.5 μA/Lumen because of lack of cesium during the process of resuscitation. But this tube could be used for demonstrating the principle of the method (Bradley and Majumdar, 1966).

6.8. Redesign of the Tube for an Internally Processed Photocathode.

It was now clear that unless proper precautions could be taken to protect the photocathode sensitivity after it has been sealed off, the virtue of such an externally prepared photocathode is diminished as the whole of the tube would otherwise get a large does of eesium which this particular design was aimed to obviate. It was therefore decided that tubes with internally processed photocathodes would be produced. Fig.(6.9.)

shows the modifications in the tube design in order to incorporate a turnover photocathode shelf and processing components for a BiAgO Cs photocathode. Fig.(6.9.a.) shows the design of the new cathode shelf. During the period of processing the photocathode faced the input window of the tube, and, could be turned to face the image tube side by tilting the tube when the weight of the bent tungsten rod B swang it through 180 degrees.

Fig.(6.9.b.) shows the new arrangement for processing the tube. Two side arms on opposite sides in the section of the tube containing the input window carried the two coaxial evaporators for evaporating Bi and Ag. Analar potassium chlorate was placed in a tube connected to the side arms for Ag evaporation to generate oxygen. An annular stainless steel shield S was fixed between the evaporators and the tungsten pins for connection to the tube electrode so that no metal could be deposited at the base of the tungsten pins causing an electrical leak. Two eesium channels were fixed between three tungsten pins for generating eesium by electrical heating of the nickel channels.

This tube did not have any ion pump. There were two slight modifications in it from the last tube. This tube had straight deflecting plates whereas the previous tube had curved ones. This was to compare the performance of the two photo-electric tubes in regard to the effect of curvature of the deflecting plates. Also, there was only one decelerating electrode before the gating mesh. This was to shorten the distance through which photoelectrons pass as they slow down, thus cutting down a little the total transit time of electrons in the storage section.

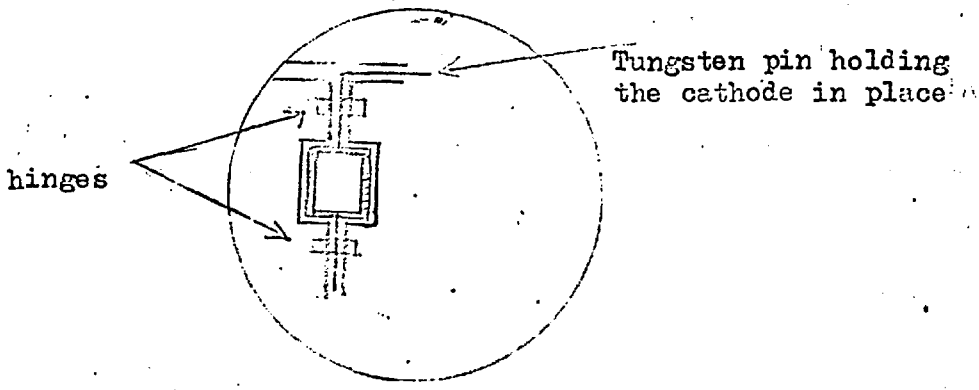


Fig 6.9.a

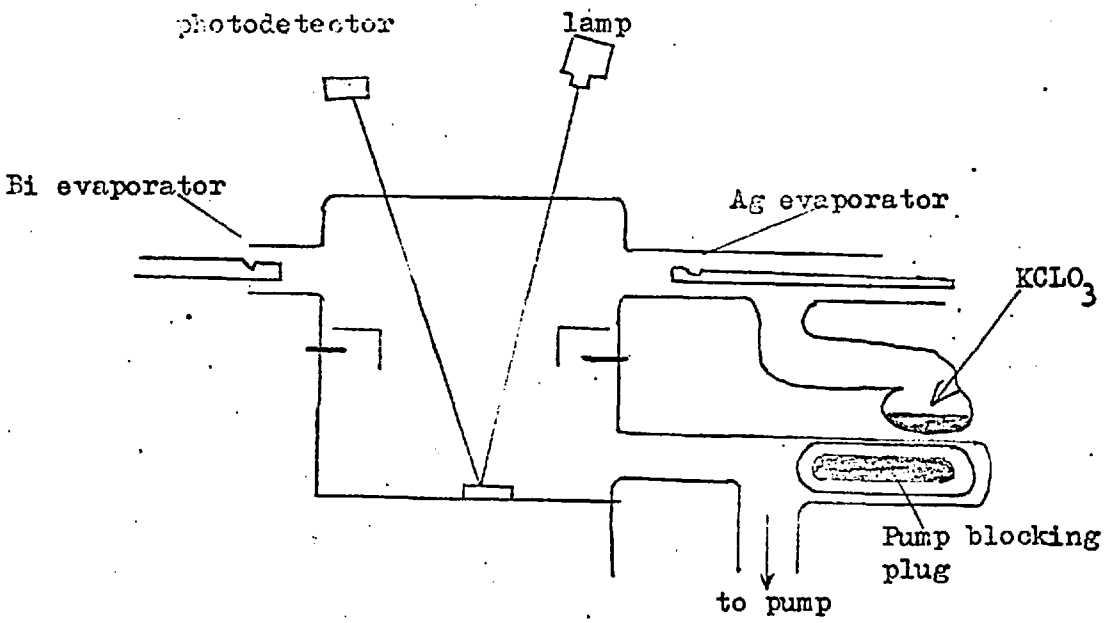


Fig 6.9.b

Set up for processing with reflection monitoring

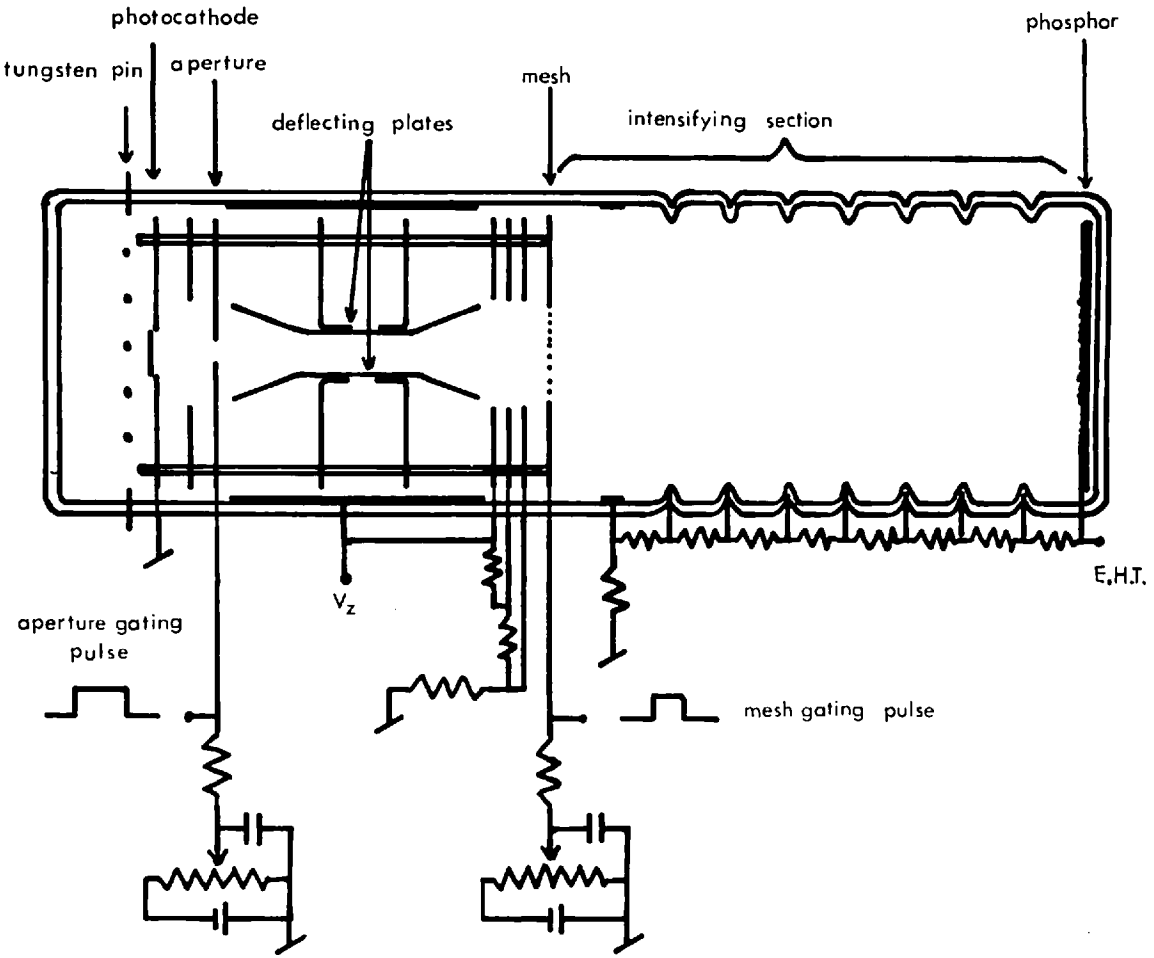

photocathode
tungsten pin
aperture
deflecting plates
mesh
intensifying section
phosphor
E.H.T.
V_z
aperture gating pulse
mesh gating pulse

Fig 7.1

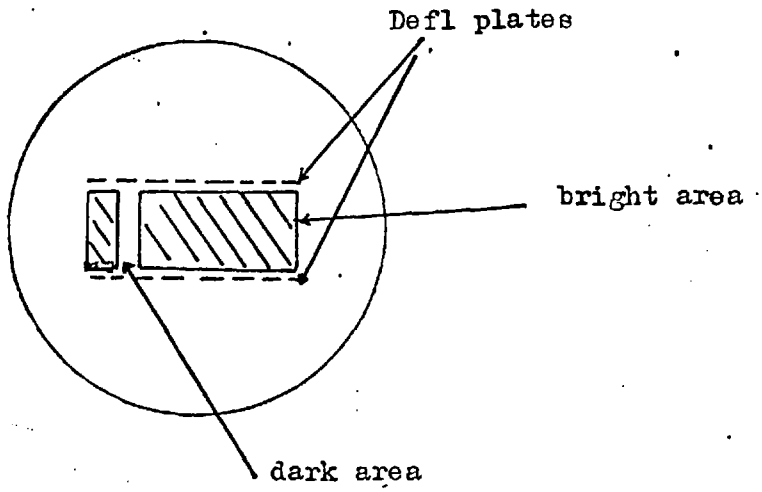
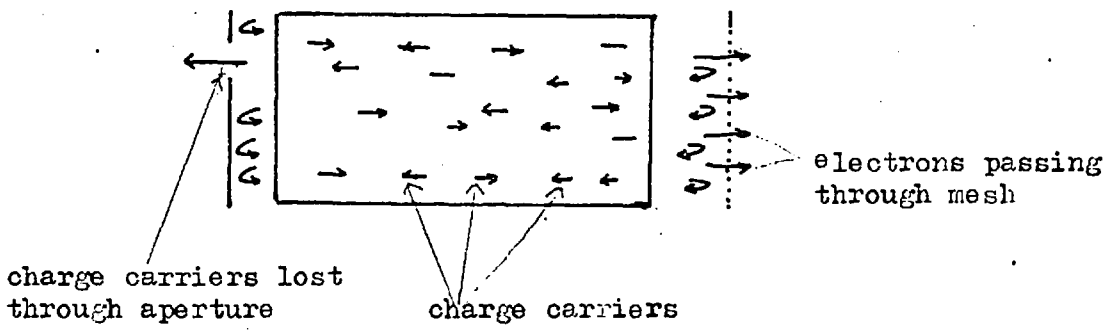


Image on phosphor screen



The mechanism of ionisation

Fig 7.2.

6.9. Monitoring the Evaporation and Processing in Reflection.

It was not possible in this system to monitor thickness of the evaporated layers or cathode sensitivity during processing in transmission, as was done in previous tubes described in Chapter 3. Thus, it was necessary to try out processing with reflection monitoring seperately and standardise the system with control set ups for transmission monitoring. This was done in a set up schematically showin in fig.(6.9b.). Here, simultaneous reflection and transmission monitoring were were done during the whole processing schedule. While the processing was done by the transmission system as described in Chapter 3.10 , simultaneous readings on the reflection system were recorded. Monitoring was done with a narrow band of green light obtained by using a filter and a tungsten lamp. The experiment was repeated in the same system with reflection monitoring only and a photocathode sensitivity of 10 μA/Lumen was obtained.

6.10. Processing of the Image Tube.

After the usual baking procedure and fixing of the getters, the tube was processed with reflection monitoring as described in the previous section. At the end of processing a sensitivity of 7 μA/Lumen was obtained, which dropped down to 4.5 μA/Lumen after seal off. This sensitivity remained steady over a period of two months.

CHAPTER 7

EVALUATION OF THE PERFORMANCE OF MULTIPLE-BEAM TUBE.

7.1. The Demountable Tube with Thermionic Cathode.

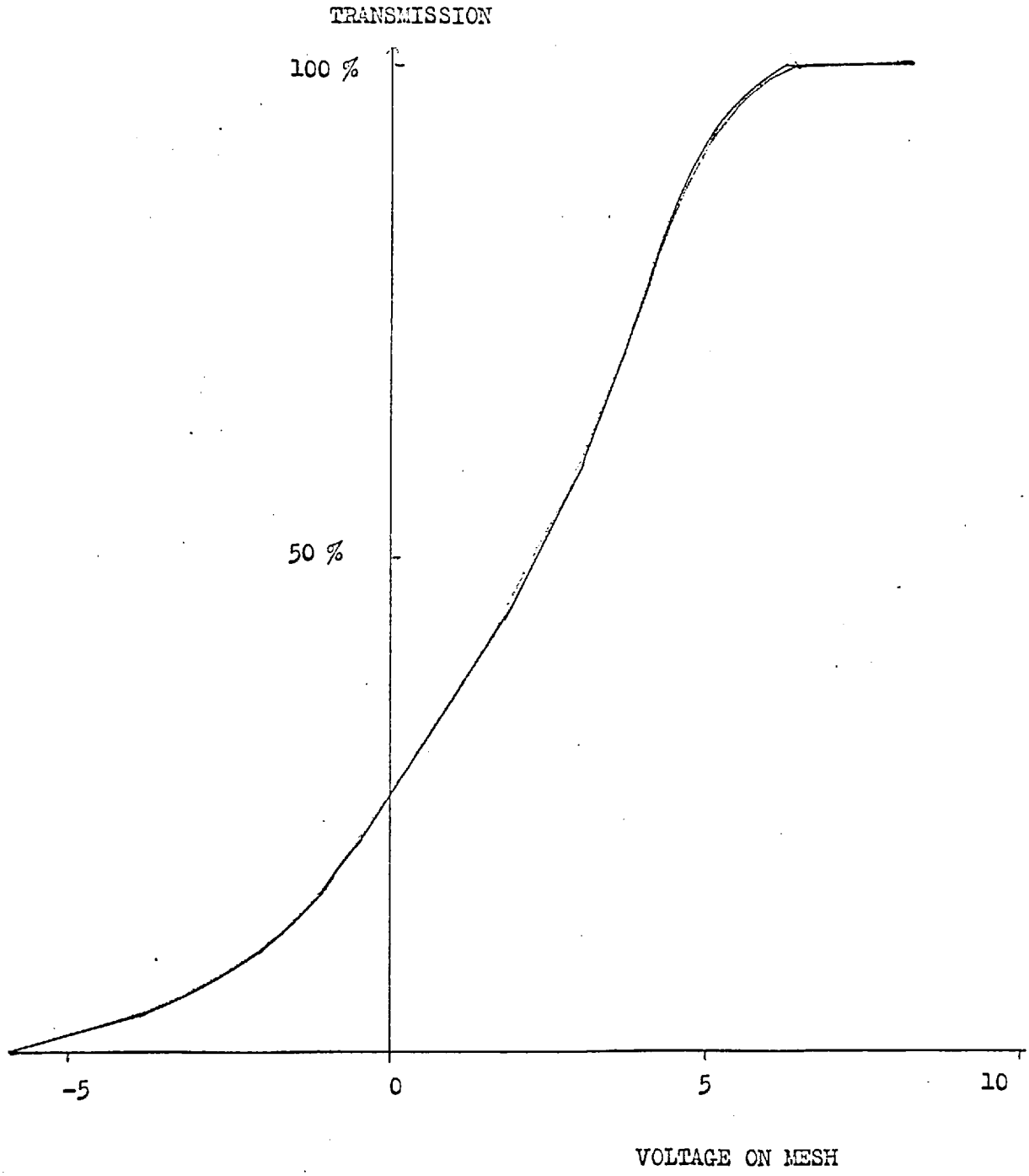
The first demountable tube described in Chapter (6.1.) was not satisfactory because of poor pressure inside and bad alignment of the metal electrodes. The second demountable tube, whose design and construction has been described in Chapter 6 was tested for general behaviour and "multiple-beam" operation.

Fig. (7.1.) shows this tube with electrical connections used for testing it. The deflecting plates of this tube were straight, one of the subsequent tubes with photo-electric cathodes had different shapes of deflecting plates - they were bent to follow the equipotentials they would create (Rose and Iams, 1935). The idea of this variation was to find out whether bending of the deflecting plates was really necessary. No appreciable variation of image quality could be found from this variation; distortions due to chromatic aberration and time dispersion were more serious (discussed later).

General Behaviour as an Image Tube:

Electrode assembly and a few other things in this tube were different from the conventional designs used previously. The performance of the tube was therefore tested in order to find out whether these variations had any undesirable effects.

The corregation of the pyrex tube body worked satisfactorily in this tube for suppressing the background due to electron-bombardment on the tube wall. This helped to minimise the amount of metal which had to be



ELECTRON TRANSMISSION VS VOLTAGE ON GATING MESH

Fig 7.3

used inside the tube.

The ceramic rods used in this tube to support and position electrodes in the storage section of the tube were found to have no effect on the image quality. This proved that the screening by glass spacers and positioning of the electrodes were efficient enough to protect the useful portion of the storage section from electrostatic distortions due to the charging of the ceramic rods.

The connecting wires(with glass sleeving) used to connect different electrodes in the ceramic assembly to the tungsten pins also did not affect the image quality.

A large amount of background was created inside the storage section if the pressure inside the tube was worse than 5×10^{-5} mm of Hg. This background appeared as a rectangular patch of uniformly bright area on the phosphor corresponding to the section of the tube between the deflecting plates. The area corresponding to the rectangular slot in the input aperture electrode appeared dark against this background. This could easily be explained in the following way (Fig. 7.2.)

Pressure inside the tube was high enough to cause ionisation of the gas molecules inside the drift section where they moved to and fro for a long time. These were partially transmitted through the mesh when it was biased midway between the 'shut' and 'open' positions. Electrons and ions moving inside this storage section also escaped out of the section toward the photocathode through the aperture. Thus, no electrons or ions could be reflected back towards the mesh from this area, Consequently, this section appeared on the fluorescent screen as a dark

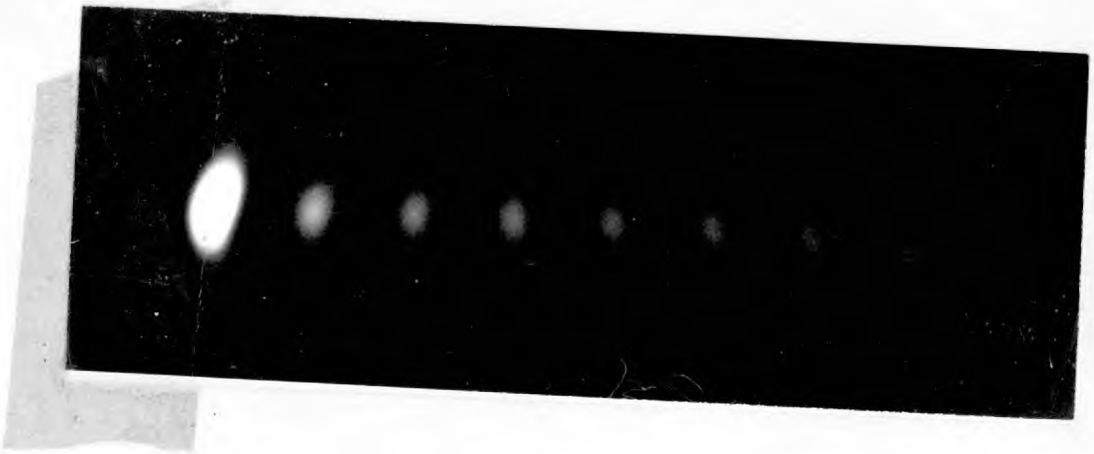


Fig 7.4

rectangular patch against a light surrounding. All this background was cut off when the mesh was biased off. At this p r. only 6Kv overall p could be applied to the tube.

With a better pressure inside the tube (5×10^{-6}), the drift voltage could be increased to 600 volts without practically any background and to 800 volts with slight background appearing on the phosphor(when the mesh was not biased off).

With an overall potential of 20Kv on the tube and no emission from the thermionic cathode, there was no background observable on the phosphor. But when the thermionic cathode was emitting, a certain amount of background appeared on the phosphor. This was most probably due to the same process of ionisation inside the drift section as it could be cut off by biasing the mesh sufficiently negative.

The emission from the cathode was 8 μA at a temperature of 1300°C. as measured with a pyrometer. This could be increased substantially by increasing the current through the tungsten filament.

Biasing of the Aperture:-

The negative voltage which could be applied to the aperture varied with the voltage in the drift section and that of the first accelerating electrode. When these voltages were high, a fairly large negative potential had to be applied to it in order to cut off the beam from entering the storage section. But for normal operation using only the biasing of the gating mesh, the aperture is kept at a slightly negative potential (-IV), enoughto reflect the elctrons from its surface as explained in Chapter (4.2.).

3) Biasing of the gating mesh:

Transmission of the gating mesh as a function of mesh potential is shown in Fig.(7.3.). A tungsten mesh with 50 t.p.i. was used and because of this 'coarseness' of the mesh a relatively large voltage swing was required to switch it from off to on position and vice versa. Such a coarse mesh allowed some of the electrons to pass through while reflected the others over a relatively large voltage swing. In other-words, it acted like an aggregate of a number of apertures with spaces inbetween them which were reflecting. When the bias on the mesh was enough positive, all the electrons were dragged through the aperture causing a full transmission. Thus, the mesh had three states, reflecting, 'semitransparent' and transparent. Both for better resolution and efficient gating, a fine mesh could be an advantage, since the gating could be performed with a very small voltage swing.

4. Gating property of the mesh and the aperture:

The minimum voltage swing required to gate the mesh from 'off' to 'on' position was 13 volts. It was observed that the image quality did not detoriate if the mesh was made to swing 10 or 20 volts higher than required. Hence, for ensuring proper switching from a stable 'off' to a stable 'on' position, the mesh was kept at - 25 volts and a 32 volt pulse obtained from a cascaded avalanche circuit using germanium 2 G103 transistors was used to gate the mesh open. (Chapter 5).

The emission from the thermionic cathode was not enough to produce a bright enough image on the phosphor for photographic recording when the mesh was gated for once. Hence, to show the gating to be operative, the

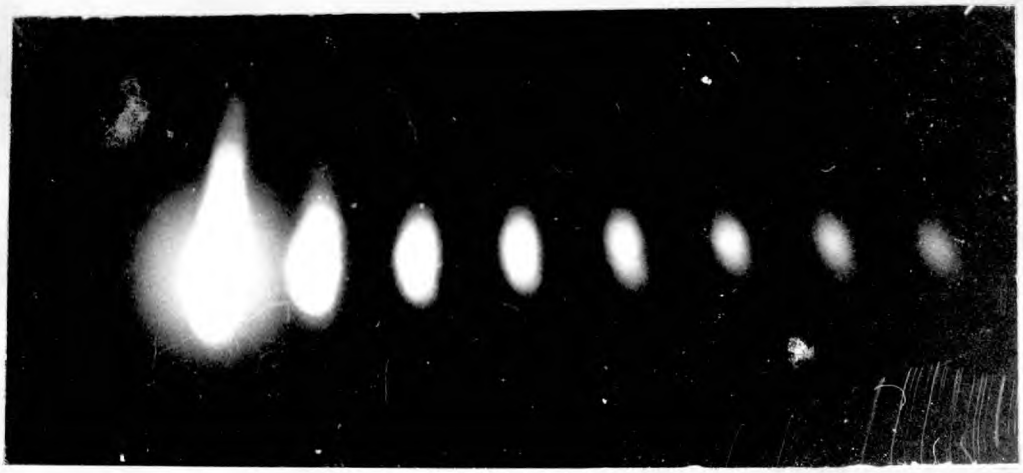


Fig 7.5

gate pulse had to be used repetitively about 2000 times a second, while the electrons were continuously entering the storage section. These electrons were undergoing deflection and reflections in the storage section in the way explained in Chapter (4.2.) until they 'walked' out of the useful area. Every time a gating pulse was applied to the mesh, a set of frames was extracted and imaged on the phosphor screen. Repetitive operation produced a persistant image at the phosphor which could be recorded (Fig.7.4.). The first image was brighter than others because the gating mesh was kept open for 50 nsecs while the calculated framing time was 16 nanoseconds (using eqn.4.4.).

The 'framing' of the image was also visible when the gating mesh was "semitransparent", without any gating pulse on the mesh. This was the type of operation which was somewhat analogous to a Febry-Perot system in optics — electrons were partially transmitted at each transit. Result is again a number of frames as shown in Fig.(7.5.). The rotation of the image as greater number of transits were made seemed to be caused by (1) The magnetic field and (2) Time dispersion. These are discussed later.

Gating of the aperture, as discussed, depended on the potentials applied to both sides of it. It was not tried on this particular tube, although it was obvious that a rapidly rising pulse of relatively high voltage would be needed.

This tube thus showed that framing was possible to achieve simultaneously while the image was being stored. The gating of the aperture could be a useful additional advantage, although not always necessary, because

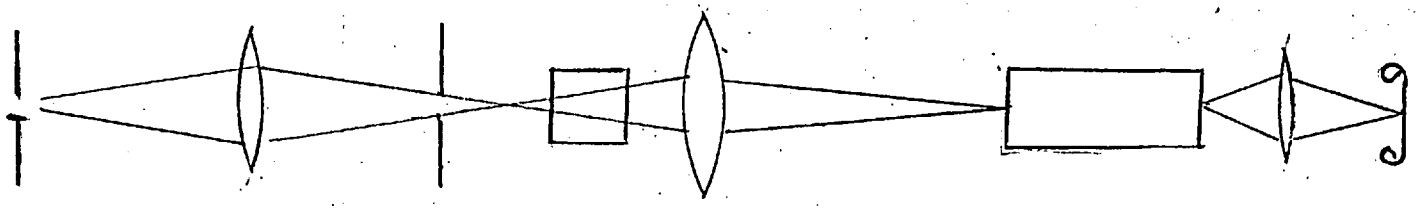
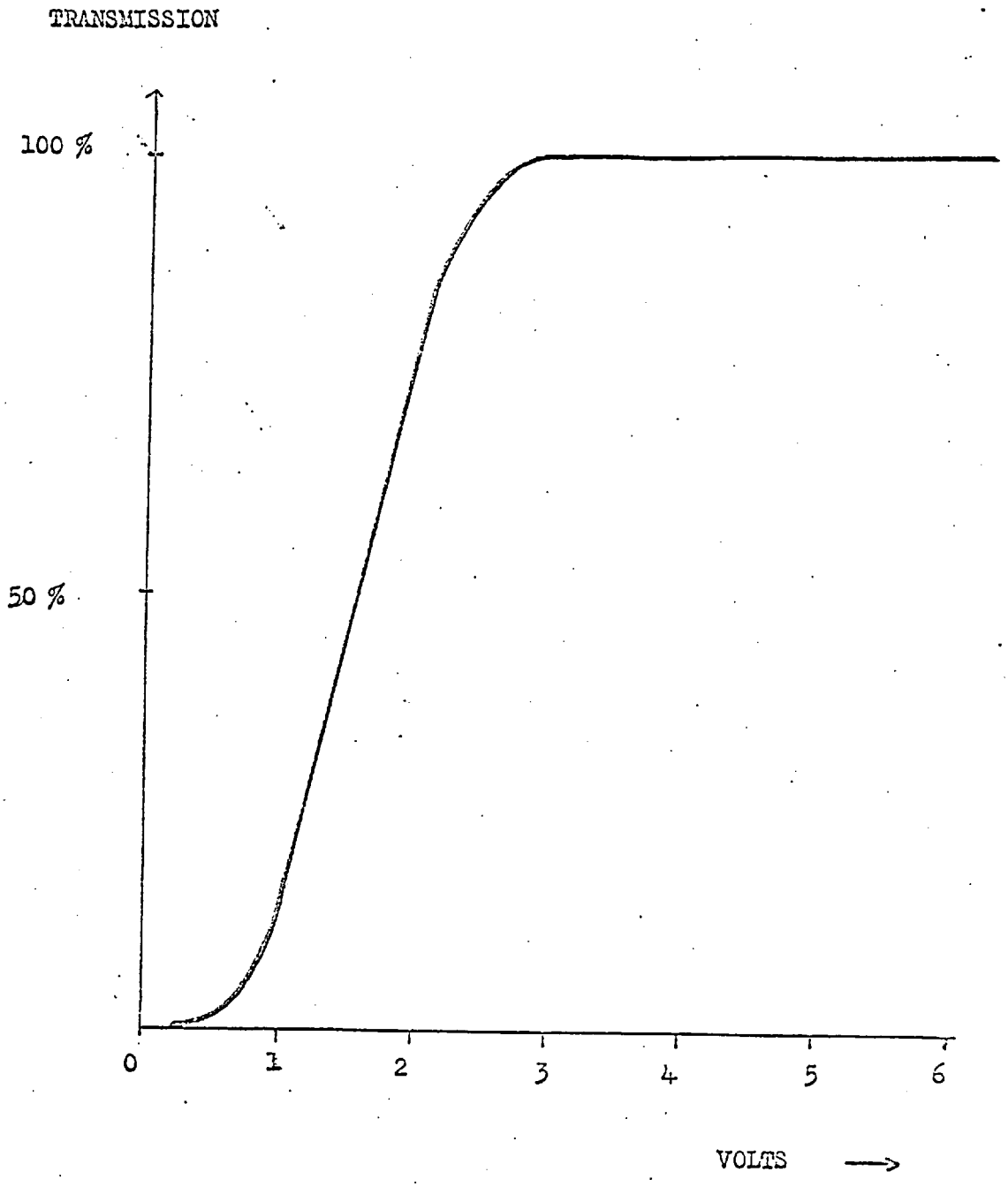


Fig 7.6



TRANSMISSION VS MESH POTENTIAL IN PHOTOELECTRIC TUBES

Fig 7.7

a calibrated delay system for the gating mesh would be sufficient for selecting the event required to be recorded. It also showed that with possible improvement of the gating mesh by using much finer meshes, such a tube with a photocathode in place of the thermionic cathode should work as a highspeed camera.

7.2. Tube With a Photocathode. (Bradley, Majumder, 1965).

Two tubes were made as described in Chapter 6.5. . As explained before, only one of these with a very poor cathode sensitivity (0.5μA/L) could be used, the electrical contact of the phosphor being broken in the other tube. The pressure inside the tube was 10^{-7} mm of Hg when sealed off, but must have gone up by about an order of magnitude during the process of recesiation.

Sensistivity of this tube was so low that proper testing with single shots and tests on time calibration or time dispersion could not be performed. Still, framing of a Fabry-Perot type fringe pattern by repetitive framing could be obtained, and certain assesment on tube resolution and overall performance could be done. A mercury arc lamp was used to test the tube. To protect the photocathode from drying due to heat from the lamp a cell containing $CuSO_4$ soln was used as a heat filter (Fig.7. 6.)

Since the tube was filled with cesium vapour during recesiation, background was expected to be poor. But on the contrary, the tube seemed to behave very well from this point of view. It could be operated at an overall voltage of 20 Kv without any appreciable background. The

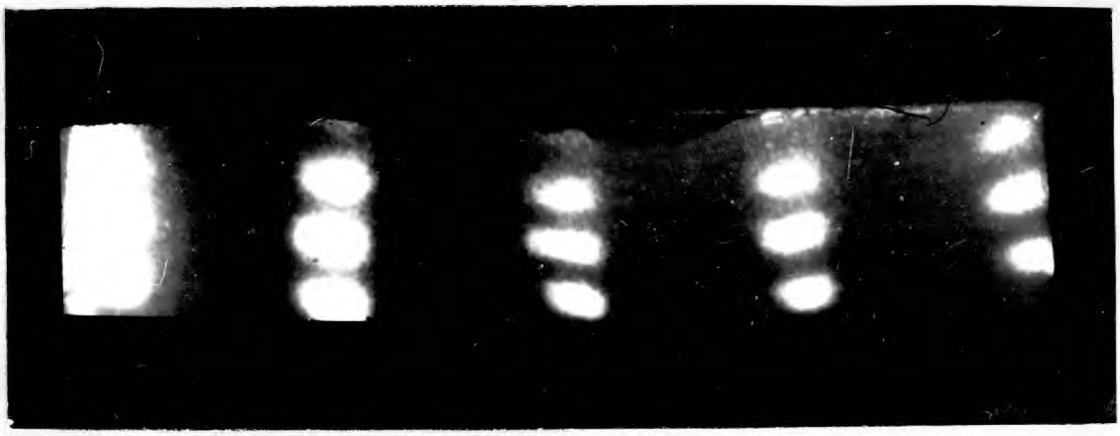


Fig 7.8.

tube was generally operated with an axial magnetic field of 300 gaus. A resolution of about 8 line pairs/mm could be achieved. This resolution did not seem to deteriorate due to gating neither did it show any fall with the number of transits in the storage section.

Biasing and gating properties of the mesh and the aperture were studied. The characteristics of the aperture biasing remained the same while the biasing of the mesh and consequently its gating properties improved with the introduction of a 500 t.p.i. copper mesh. Fig.(7.7.) shows the transmission of electrons through the mesh as a function of mesh potential. It is shown that a 2 volt swing of potential can now switch the mesh from off to on position. In this tube, the "semitransparent" region of biasing is reduced to about 2 volts. Hence the indeterminacy in gating the mesh with a sharp rising pulse is reduced as well. The pulses used to gate the mesh have rise times of just less than a nanosecond for a 13 volt swing. Hence the indeterminacy in gating is $\frac{1}{6}$ nanosecond, which was, negligible.

The electronic circuits made up for testing this tube were all constructed with silicon transistors and diodes rather than the germanium system used before for primarily two reasons (a) faster transistors and diodes are available for prices equivalent to slower germanium devices, (b) higher temperature stability resulting in less time jitter.

The general scheme of distribution of voltages and electrical connections in this tube were the same as that in the previous tube with thermionic cathode.(Fig. 7.1.).

Five frames with repetitive pulsing of the mesh (2000 times a sec) were photographed, (Fig. 7.8.), the framing time being 35 nanoseconds, as calculated from the drift potential (Eqn.4.Ch.4.)

Frames obtained by biasing the mesh "semitransparent" are shown in (Fig. 7.9.). Here the non uniformity of illumination in the middle due to wrinkles in the gating mesh because of slightly imperfect mounting. This of course did not matter while the tube was used for proper pulsing.

Experiments in time dispersion and calibration could not be done with this tube because of its extremely low cathode sensitivity.

7.3. Tube with Photocathode Processed Inside.

This tube, whose construction was detailed in Chapter 6 (Section 6.8., 6.9. and 6.10.) was the most useful multiple beam tube constructed yet. It was used to test general behavior of the tube, as well to record a transient event, described later. Electrical connections and general voltage distribution is shown in Fig.(7.1).

Although the sensitivity of this tube was not high, it was enough to carry out experiments to test the behaviour of the tube in single shot, time dispersion in the frames, effect of magnetic field on framing, spatial resolution and limits of time resolution. Although for most of the experiments the previous electronic set was sufficient, there was scope to test the tube more thoroughly with slightly different delay

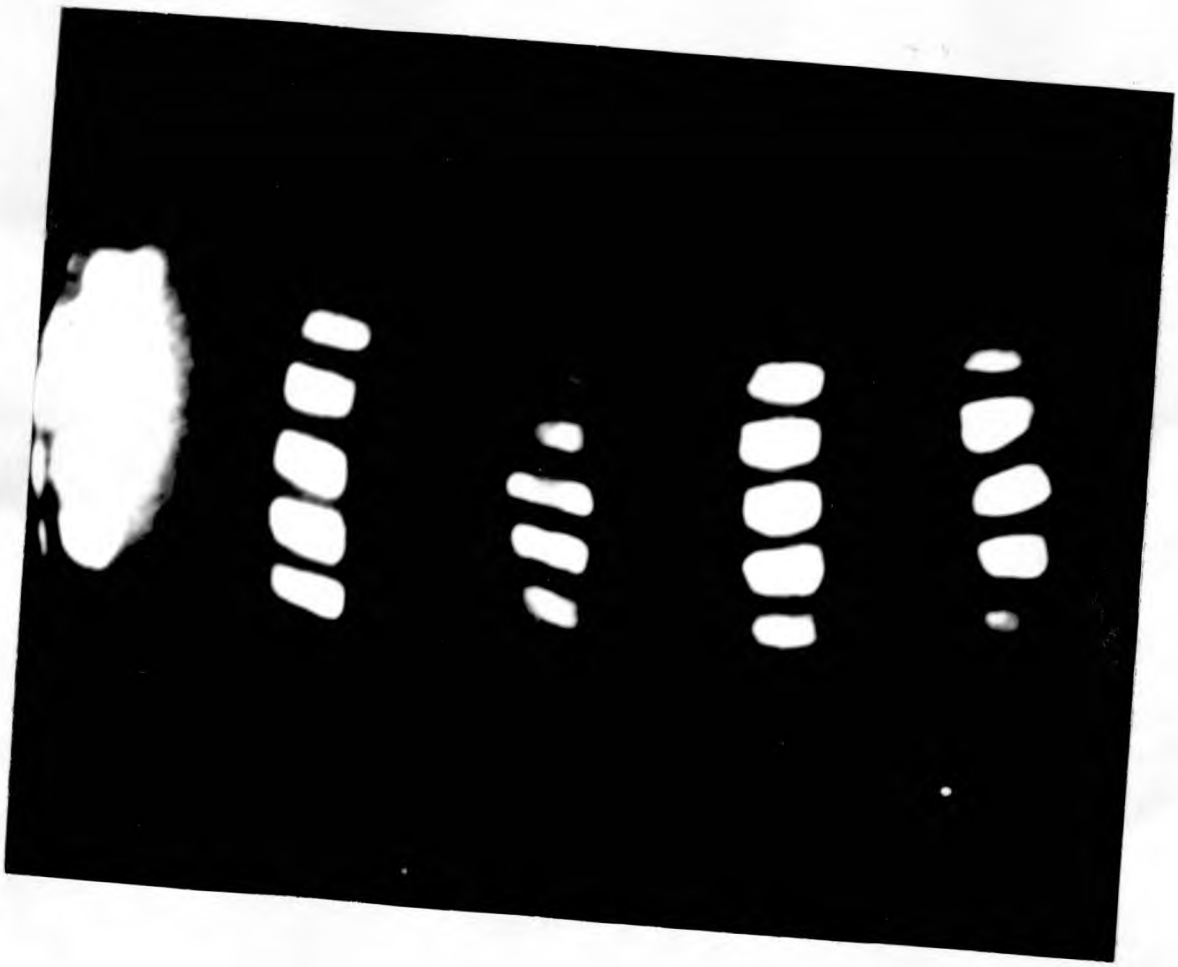


Fig 7.9

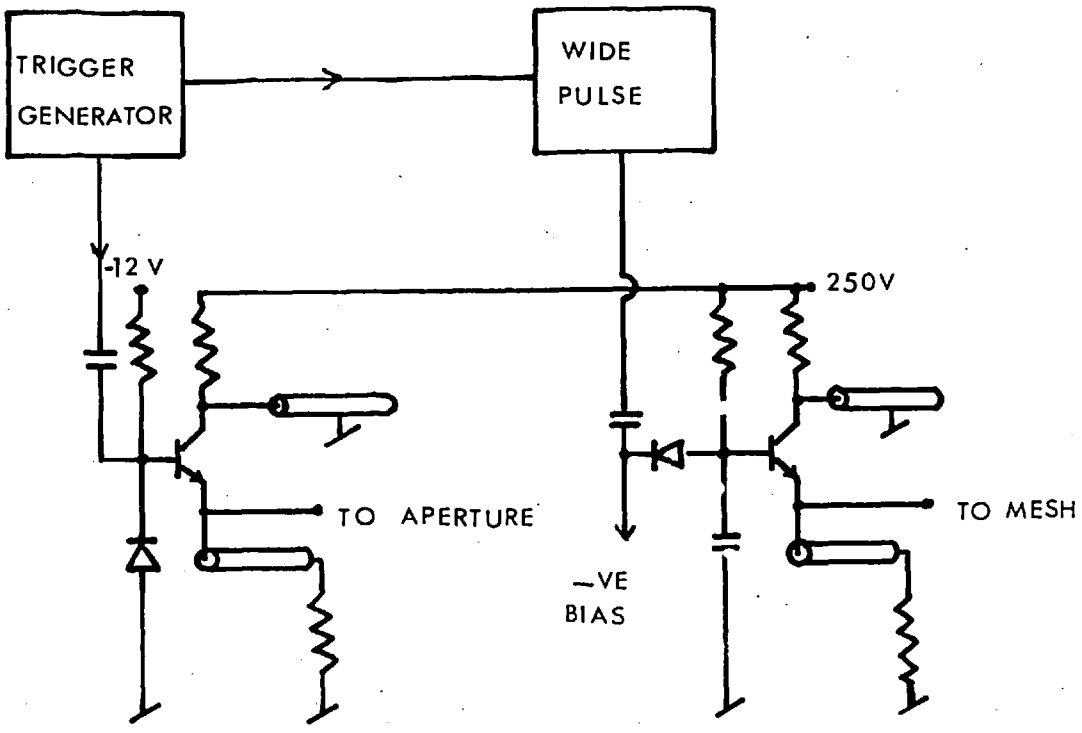

TRIGGER
GENERATOR
WIDE
PULSE
-12 V
250V
TO APERTURE
TO MESH
-VE
BIAS

Fig 5.10

and pulse width control systems. Once such modification was constructing and avalanche pulse generator with continuously variable width without changing charging lines and retaining sharpners of rise and fall times. The other modification was, building a cascaded avalanche system to produce square pulses of larger amplitude. The first circuit was useful for precise evaluation of time dispersion and calibration, while the second circuit was used to test the potentiality of the system as a streak camera.

One great problem with a high speed camera like this with transistorised electronics was to avoid sparious triggering when one wanted to study the most common type of event - spark or plasma discharge. Since the tube worked on gating circuits operating and triggering at voltages lower than 3 or 4 volts, spurious trigger from such noisy and radiative sources like a spark a plasma discharge could produce unreliable and misleading results.

In fact this posed a serious problem when the tube was tried as a framing camera to photograph the expansion of spark discharge at the latter stages of the discharge. This problem was overcome by taking a number of steps in isolating and shielding the electronic circuits. The electronic circuitry was encased into a small box which was kept enclosed in another large chasis. The earth of the sparking system was isolated from the earth of the tube control system. Double screened weve was used to carry the triggering signal from the photodetector to the pulse circuits.

Fig.(7.10) shows schematically the gating system used for this tube,

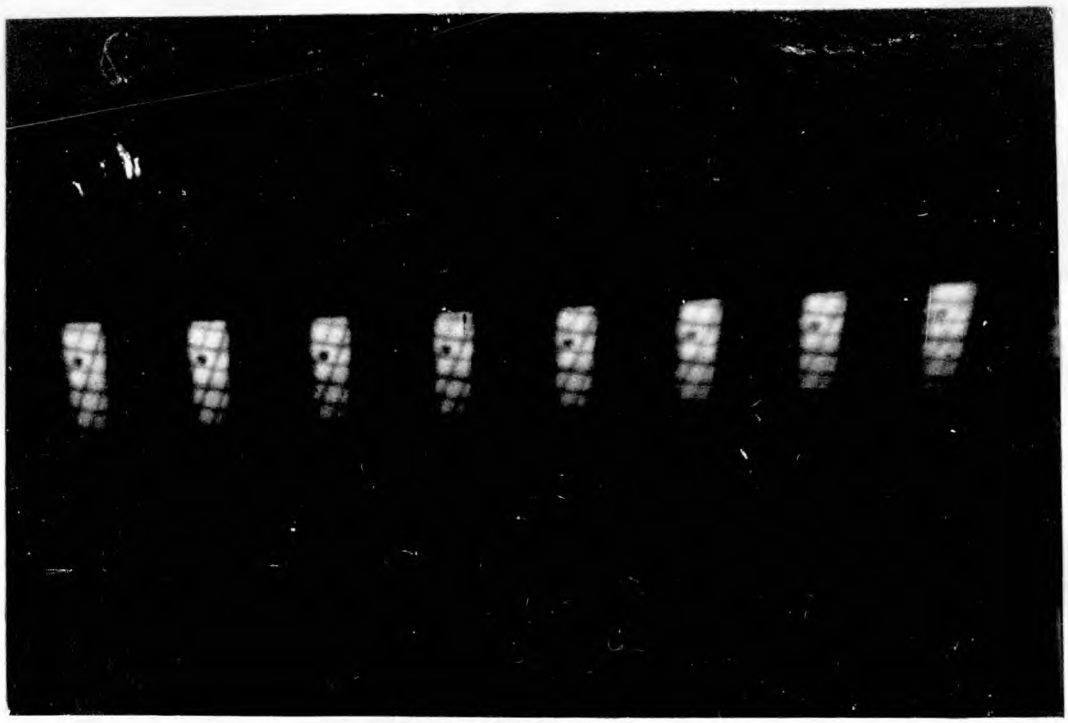


Fig 7.11

where only the new additions are laid down with full circuit details.

The behavior of the image converter in its different modes of operation are described below:

Background: It showed very little background when operated at 21 Kv overal potential. Spatial resolution while on d.c. operation was better than 10 line pairs/mm. The first accelerating electrode reached its maximum collection efficiency at 40 volts positive with respect to the cathode. The D.C. biasing of the aperture was exactly similar to the two previous tubes. The transmission of the mesh as a function of mesh bias is shown in Fig.(7.7.) which was the same as that of the previous tube with a photocathode.

Framing with an Ordinary Projection Lamp with Repetitive pulsing:

It was observed that at a fixed magnetic field, a fixed number of frames could be obtained without any great tilt on either side. Two parameters take part in tilting the image progressively from frame to frame. One of this is the tilting due to variation in the time of fleight of the electrons at the top and bottom and as a result, the lower portion gets more deflected than the faster part. This is related to time dispersion and is governed by eqn.(9.) Chapter (4). The other is the tilting of straight image due to different amount of rotation at different parts of the image due to their different energies. This effect depends on the presence of the magnetic field alone. It may be called chromatic aberration and had been used previously for β-ray spectrometry using a line sonice (Siday 1942, Geargisco 1949, Batt 1949). It has been shown by Siday that rotation inside a poleroid

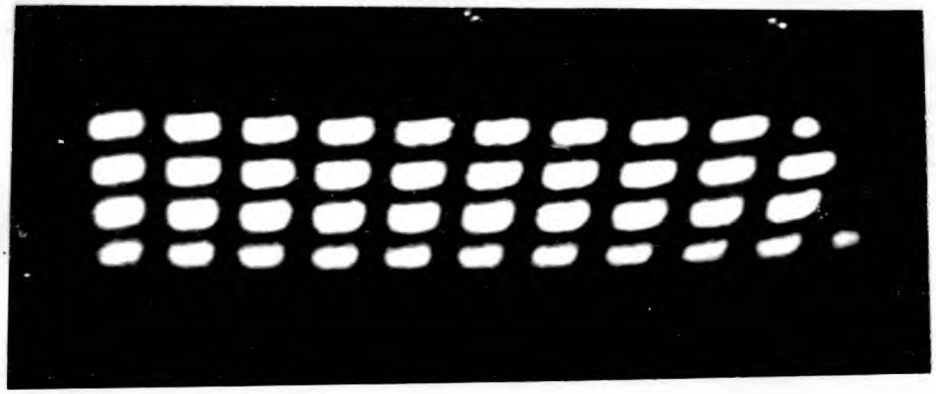
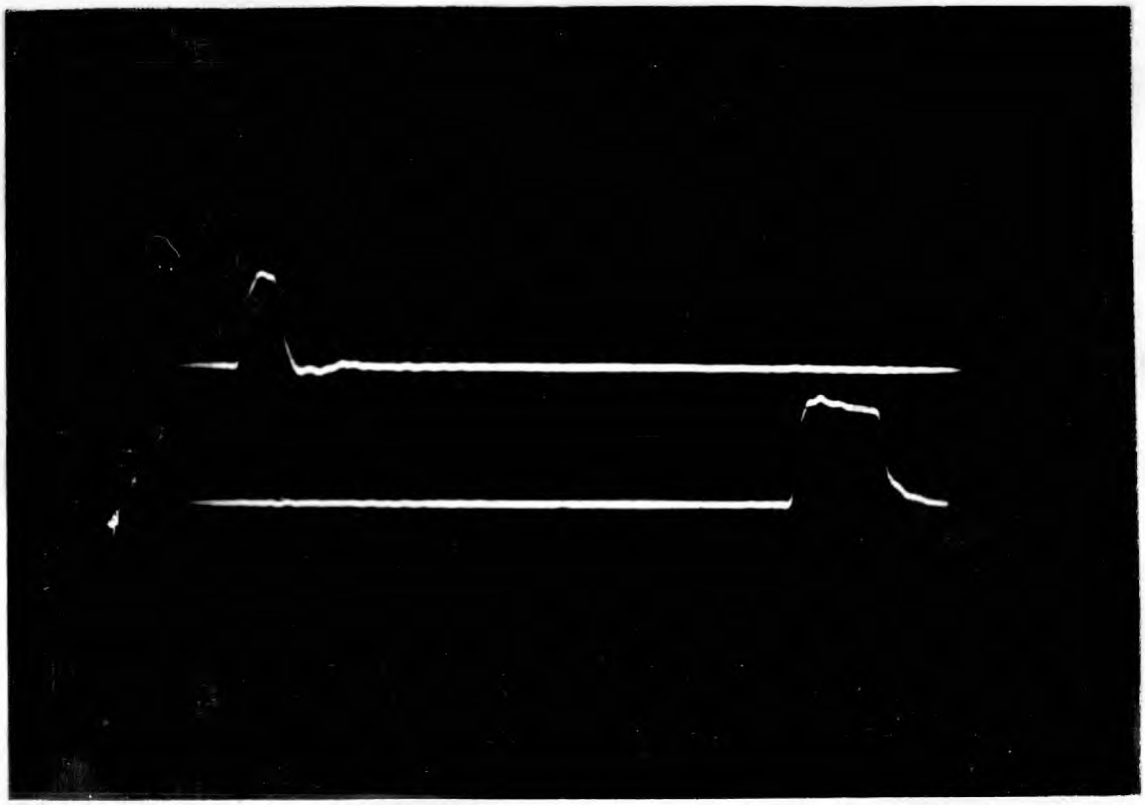


Fig 7.11.a.



Pulse height 13 volts, calibrated delay.

Fig 7.12

of length 1 and magnetic field H, can be expressed as

$$\frac{1}{2}\ \frac{e}{m}\ \ \frac{Hl}{v} = \theta \text{ in radians.}$$

Where θ is the angle between the image and object axis, both perpendicular to the axis of the soleroid. Relative rotation of different parts would be dependant on their velocities, and will be be different. The net effect will be a tilt of the image which could be approximated to be linear for a small length of object. This rotation could be used to cancel the image tilting due to time dispersion by proper choice of H. In such a case, the time dispersion can be present even though there may not be any appreciable image tilting over a number of frames.

In Fig.(7.11) a photograph is shown with 9 frames with a framing time of approximately 46 nanoseconds each. The calculated time dispersion of 5 nanoseconds between the top and bottom segments could have caused an image seperation at the top (higher velocity side) 6 mm less than that at the bottom. But the tilting due to the chromatic aberration has reduced this to .1 mm. Fig.(7.11a) shows similar correction over 10 frames in a condition where time dispersion between the top and the bottom segments is selected to be as much as 23%. These two photographs were taken with an image of a slit projected on the photocathode by a lamp. The mesh was biased beyond cut off and gating pulses with a repetition frequency of 1.5 Kc/sec. were applied to it. Repetitive operation of this gating mesh produced a persistant image on the phosphor bright enough to be visible. In this way the general property of the image tube and the quality of the image when gating was performed could



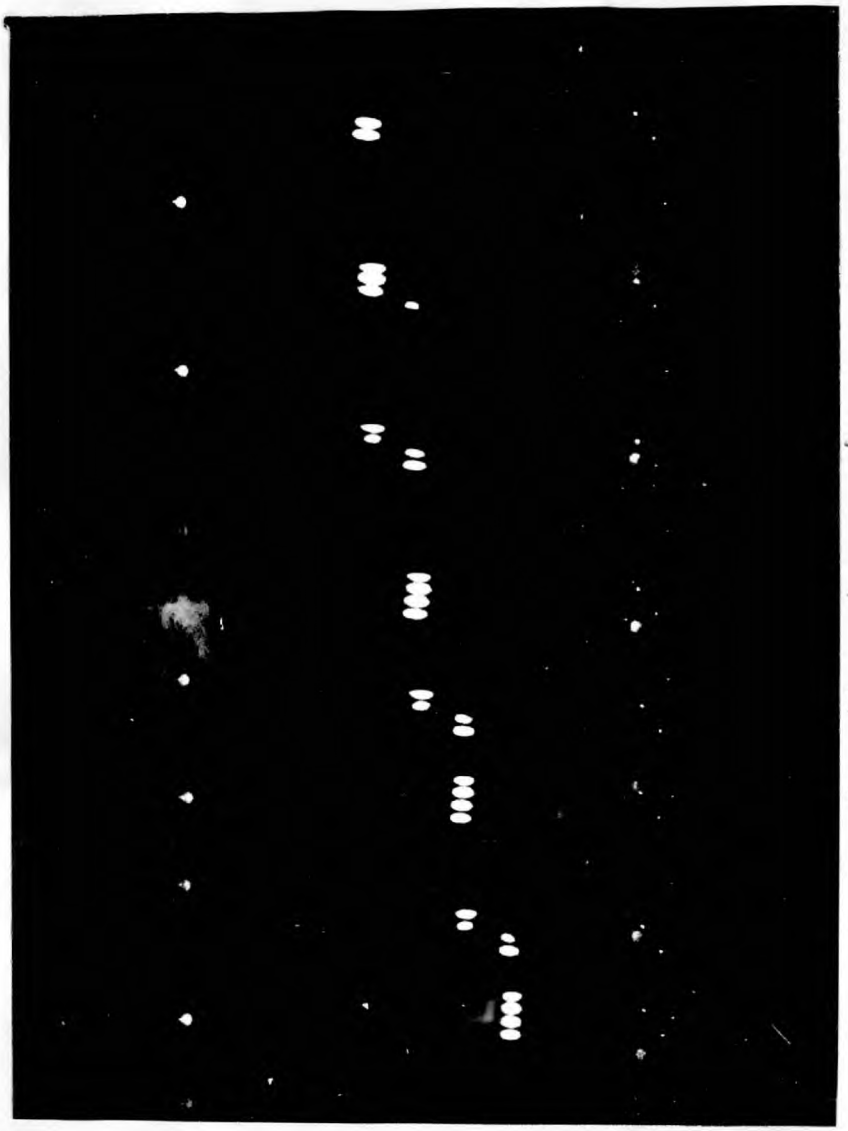
Fig 7.13.

be tested and different voltages on the tube could be optimised.. Spatial resolution of the tube was better than the previous tube. Fig.(7.11) shows the photograph of a number of frames of a grid pattern obtained by repetitive gating. Resolution was better than 10 line pairs/mm with about 450 gauss axial magnetic field. This figure shows now change in resolution between the first and the last frame. So, this could be taken as the dynamic spatial resolution when the multiple beam tube was used as a fast framing camera.

Calibration of the framing time could not be attained in this mode of operation of the tube, for which the following set up was used, still using the thermal source of light for projection of a slit image on the photocathode.

The aperture as well as the mesh were biased off so that they could both be gated open at prefixed times, with calibrated delays between them. The set up of electronic circuits and the sequence of pulses produced there is shown in Fig.(7.12.). Both the aperture gating and the mesh gating circuit had variable delays in them. The width of the aperture gating pulse was kept less than the framing time as well as the width of the mesh gating pulse. By varying the delay between the mesh gating pulse and the aperture gating pulse, the amount of information let in through the aperture could be allowed to pass into any of the frames obtainable on the output phosphor.

If we assume that there is no time dispersion along the length of the image, framing time for the whole length of the image would be the same. Then for a delay T_D between the initiation of the aperture gate



Time dispersion. Variation of delay moves different parts of image to different frames

Fig 7.14

and the mesh gate, we would have

$$T_d = C\ T + \tau$$

Where C is an integer, giving the number of frames the front edge of the photoelectrons would have completed and T = framing time: and τ denotes the time the front edge would have stayed in the (C + 1)th frame at the time of opening the mesh gate ([redacted]). If the widths of the aperture and mesh gating pulses are such that $T > T_A > \tau$ and $T_M = T$, a fraction $T_A - \tau$ of information would be displayed in Cth frame while the information during the first secs would be displayed in (C + 1)th frame. For $\tau = 0$ in eqn.(1),

$$T_d = C\ T \text{ or } T = T_d/C \qquad (2)$$

This could be done in practice by varying T_d in such a way that the image in (C + 1) th frame just disappears and the whole of the image is displayed in Cth frame.

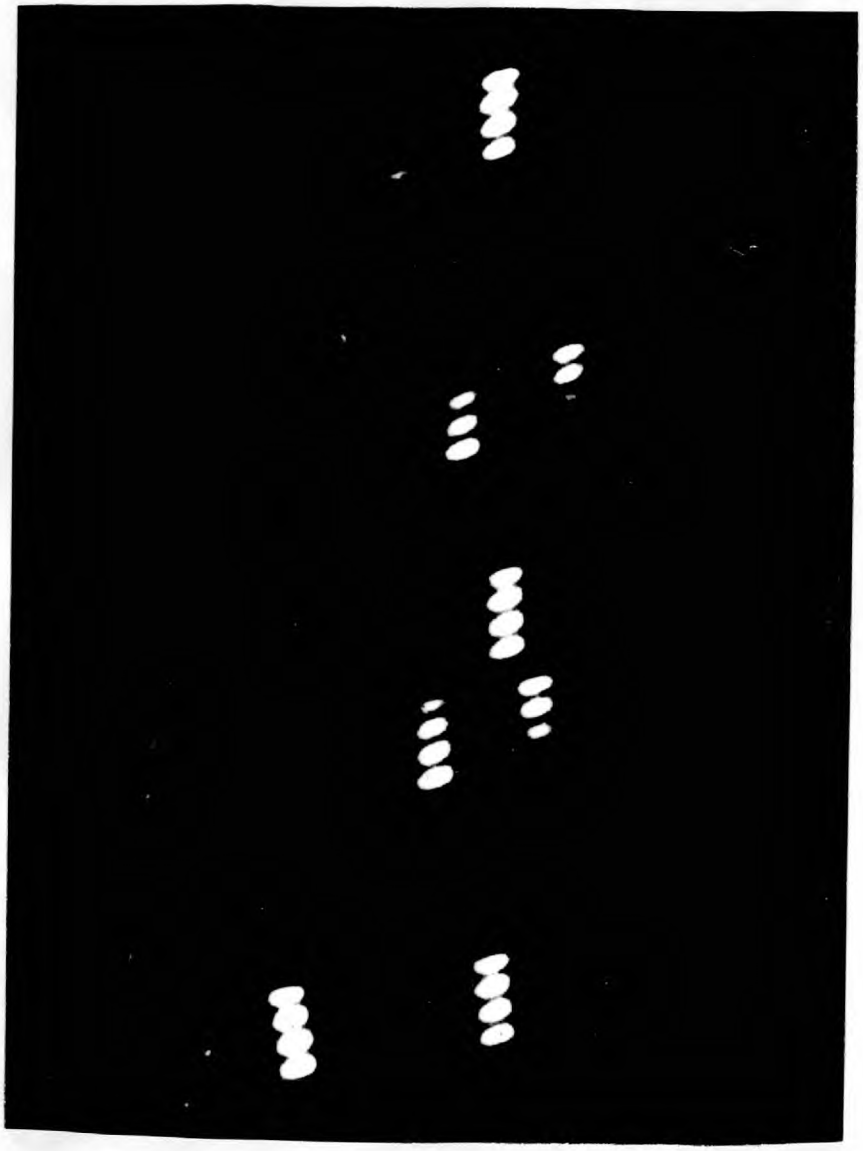
Eqns. (1) and (2) are valid only for the imaginary case of no time dispersion along the length of the image. Consider the image being divided into n segments so that time dispersion in one such segment is negligible compared to the framing time. Now, let for the mth segment of such a frame, eqn. (1) can be written as

$$T_d = C_m\ T_m + \tau_m \qquad (3)$$

which only represents a part of the whole image. This equation is valid and the portion τ_m would be displayed in the $(C_m + 1)$th frame if

$$T_M > T_m > T_A > \tau \qquad (3a)$$

where T_M width of mesh gating pulse. If ΔT is the time difference in framing time between mth and m + 1th segment, we can write,



Time dispersion.

Fig 7.15

$$(C_{m+1} + q) = \frac{T_d}{T_{m+1}} = \frac{T_d}{T_m + \Delta T} = \frac{T_d}{T_m}\left(1 + \frac{\Delta T}{T_m}\right)^{-1}$$

$$= \left(C_m + \frac{\tau}{T_m}\right)\left(1 + \frac{\Delta T}{T_m}\right)^{-1}$$

Therefore $(C_{m+1} + q1)\left(1 + \frac{\Delta T}{T_m}\right) = C_m + \frac{\tau}{T_m}$ (4)

where q' is a fraction. If $q = 0$

and $C_{m+1} = C_m$, eqn (4) becomes.

$$C_m \cdot \Delta T = \tau \qquad (5)$$

Eqn.(5) is valid only if condition (3a) is maintained, i.e. among other things

$$T_A > C_m \cdot \Delta T \qquad (5a)$$

Generalising eqn.(4) for any segment $C_m + p$,

$$(C_{m+p} + q_p)\left(1 + \frac{p\Delta T}{T_m}\right) = C_m + \frac{\tau}{T_m} \quad . \qquad (4a)$$

(where $m + p < n$)

Again, if the delay is such that $C_{m+p} = C_m$ and $q_p = 0$

$$C_m p \cdot \Delta T = = T_d - C_m T_m \qquad (6)$$

Which gives the total time dispersion between the mth and pth segment in the Cmth frame.

For $C_{m+p} = C_m$ q_p could be calculated from (4a):

$$q_p = \frac{\tau - p. C_m \Delta T}{T_m + p \Delta T} \qquad (7)$$

By making = 0 in eqn.(3) and counting C_m, T could be obtained for the mth segment of the frame.

Knowing T_m, total time dispersion between mth and pth segment and hence the time dispersion per frame could be obtained from eqn. (6).

Experiments were done with various framing time and deflecting potentials and the true framing times were obtained at the different points on the image axis, along with the time dispersions. This was done by setting the delay at first to satisfy condition.

$$C_m = \frac{T_d}{T_m}$$

from which T_m was obtained, T_d and C_m being known from observations. Then the delay was changed to satisfy eqn.(6), for the (m +p)th segment, i.e. the front edge of the (m + p)th segment is allowed just to reach the gating mesh in the C_m th frame by adjusting the dealy, when the mesh is gated open.

The results so obtained are found to agree broadly with the theoretical prediction that with higher electron energies, the time dispersion is relatively smaller. Fig.(7. 14) shows a photograph of a series of shots taken with different delays between the aperture and mesh gating pulses for very long framing times. The specifications are shown under the photograph. The mesh gating pulse was shorter than the framing time. Time dispersion was high. As a result, all the electrons which were midway in their journey from one frame to the next were not extracted at the mesh. Thus, at certain delays between the aperture and mesh, the top and bottom parts of the image appeared at two seperate frames. The photograph clearly demonstrates the existence of time dispersion (which was as high as 23% per frame) without the accompanying tilt. It was assumed that the chromatic aberration of the electrons in the magnetic field corrected the tilt. This correction needs further investigation.

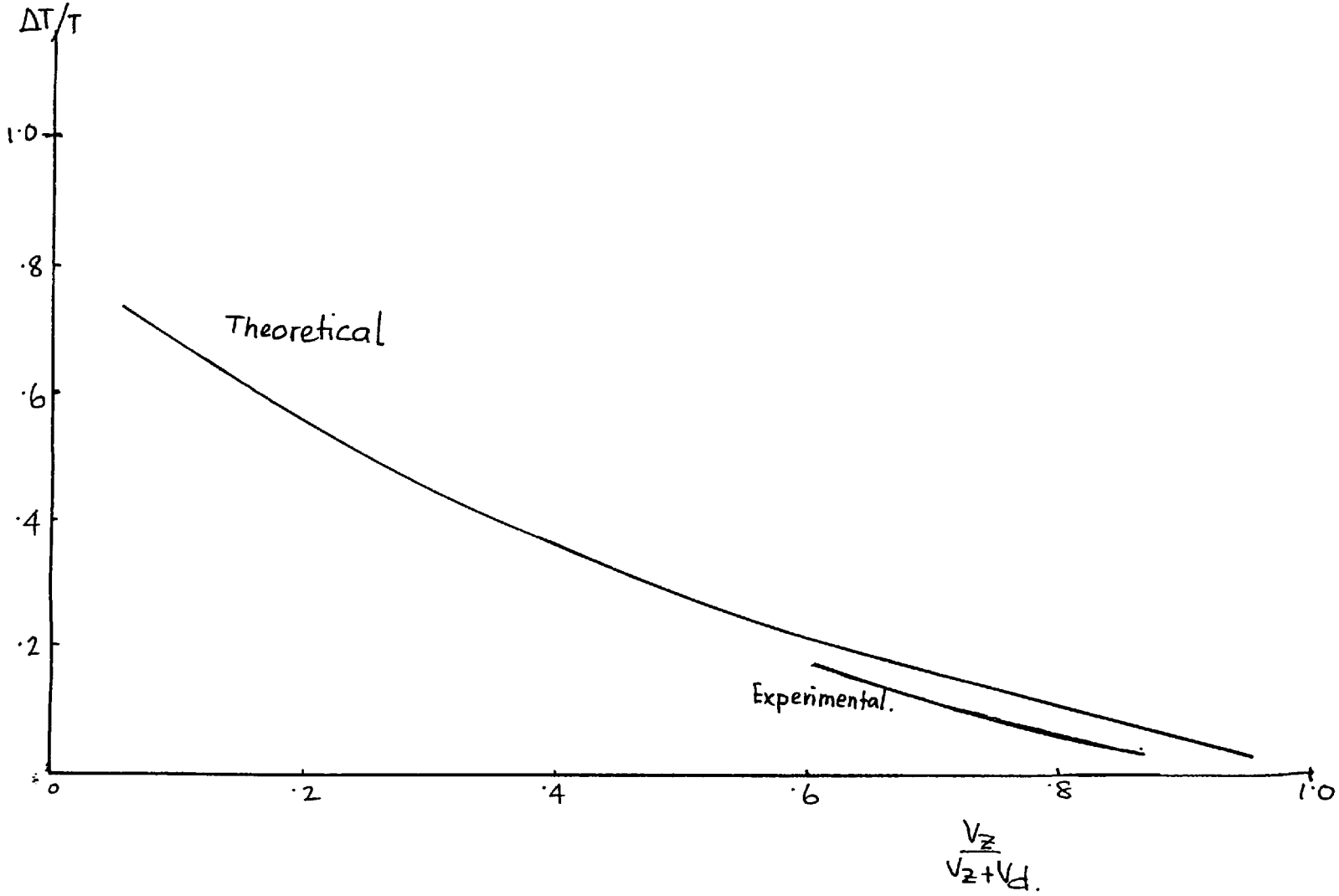


Fig 7.16.

Fig. (7.15) shows another photograph similar to Fig.(7.14) except that the framing time was shorter than the width of the mesh gating pulse. This was a case similar to that explained in Chapter (4.8.). The information of 20 ns. duration had been spread out in different amounts at different segments, into two frames. The variation of $\frac{\Delta T}{T}$ for a variation of $\frac{V_z}{V_z + V_d}$ between the top and bottom of a frame was plotted from theoretical consideration and was compared with the experimental results, as shown in Fig.(7.16). It was observed that the measured time dispersion was less than the calculated value. This could be qualitatively explained by considering the field distribution due to the deflecting plates in the storage section as illustrated in Fig. (7.16A) where the equipotentials towards the high velocity side are pushed towards the mesh compared to those at the low velocity side because of a higher potential gradient. As a result, the electrons with higher velocity move an extra distance towards the mesh before returning back. This would happen at both ends of the storage section, resulting in elongation of d_1 and d_2 to $d_1 + \delta d_1$ and $d_2 + \delta d_2$ for the higher velocity electron compared to d_1 and d_2 for its lower velocity counterpart.

If the fields were plotted for the tube storage section to determine d_1 and d_2 and δd_1 and δd_2, quantitative evaluation of the effect could be made by substituting $d_1 + \delta d_1$ and $d_2 + \delta d_2$ for d_1 and d_2 respectively in eqn.(5) chapter (4) which now becomes

$$T_2 = \frac{2(d_1 + d_2 + \delta d_1 + \delta d_2) + 1}{v_z}$$

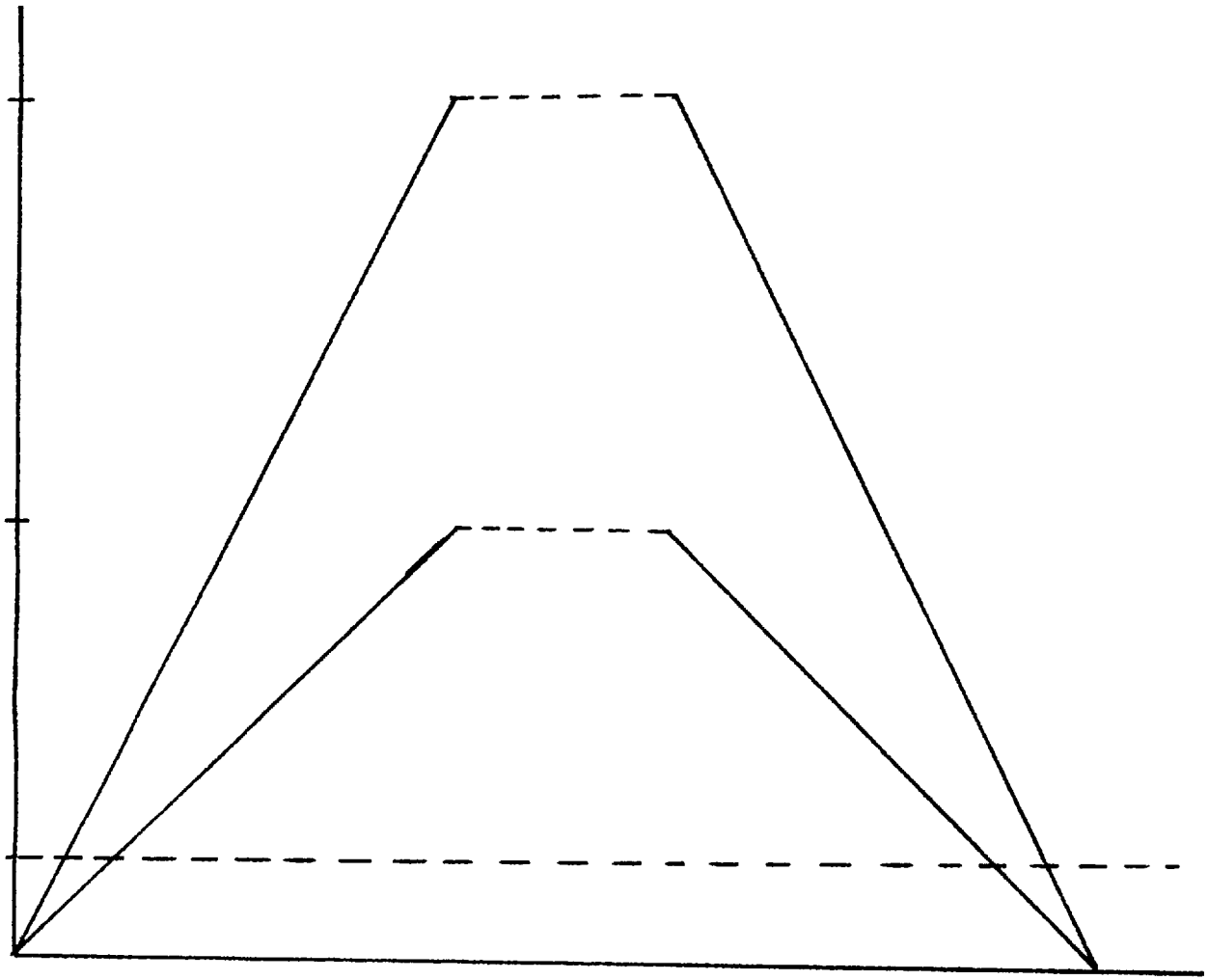


Fig 7.16 a.



Fig 7.18

This field plotting is expected to done with future tubes in order to evaluate this effect.

7.4. Recording of a Luminous Transient Phenomenon

The photocathode sensitivity was rather low, and hence comparatively long daviation shots were tried for recording luminous transient phenomena. At first a straight xenon flash tube was tried for this purpose. But it was not found intense enough for recording 50 nanosecond frames. Besides, since the whole tube was cesiated during the processing of the photocathode, as well as secondary emitter because of lowered work function. This caused rather high background on the fluorescent screen as diffused flash light of about $\frac{1}{2}$ millisecond duration continued to fall on the mesh, emitting electrons, which were falling on the phosphor screen. To overcome this difficulty, an argon spark was used which produced high power light pulses of about 5 μsec. duration. Fig.(7.17) shows the optical system used in this experiment. The framing time was 48 nanoseconds while the mesh gating pulse was 50 nanoseconds.

With a 2.5. μsec delay between the initiation of the spark and gating of the mesh the expansion of the spark over 250 nanoseconds was recorded in five frames of 50 nanosecond duration. Fig.(7.18) shows the photograph, taken on a polaroid film. A mullard 90 CV photodiode, followed by a cathode follower supplied the trigger pulse, which was delayed by 2 μsec using delay cable type [illegible] prior to application to the input of the transistorised gating pulse generator. The aperture electrode was kept open all the time, and time selection was done entirely

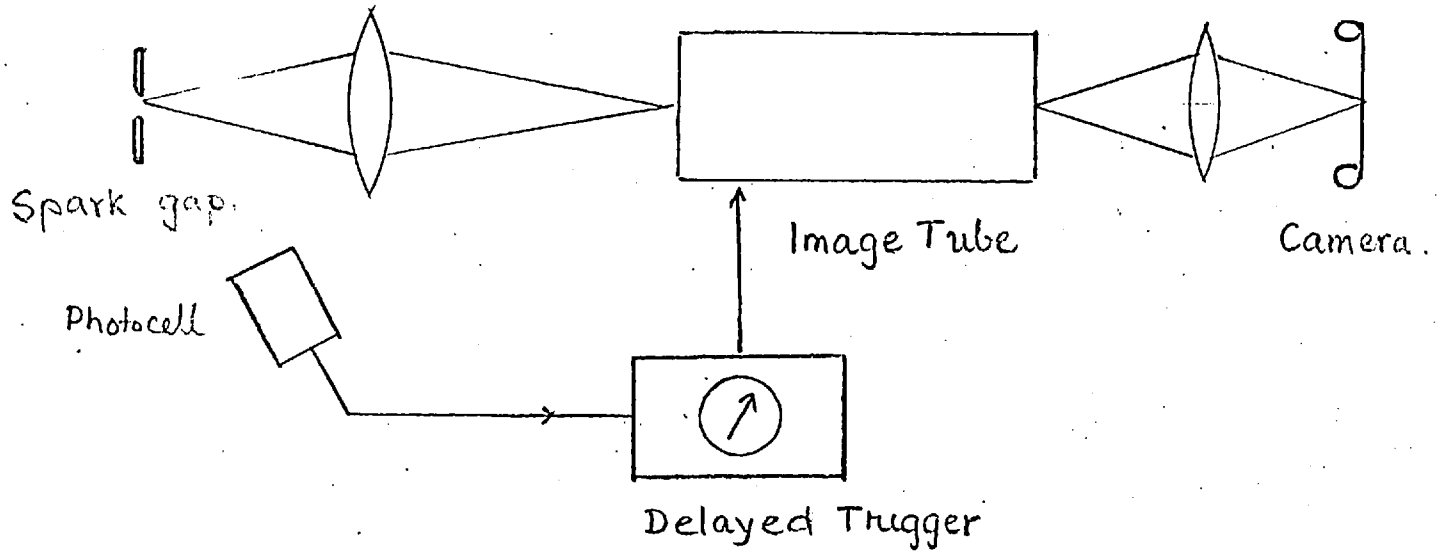


Fig 7.17.

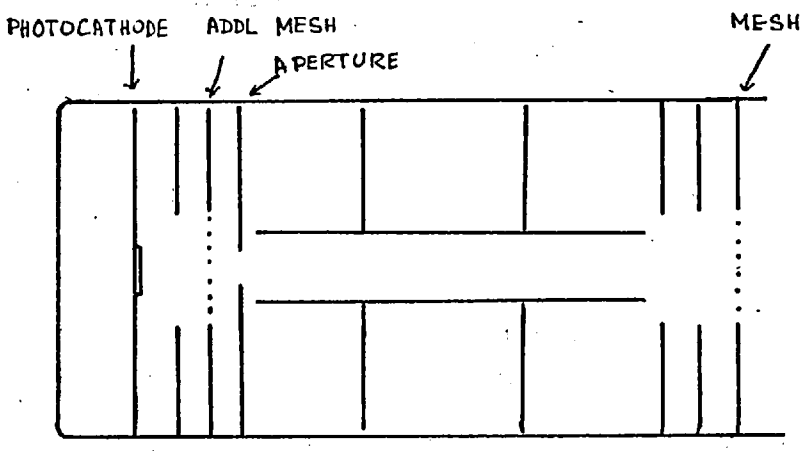


Fig. 8.1.

with the help of delays in the mesh gating pulse. The time dispersion between the top and bottom of the frame was calculated to be 2.6. nanoseconds.

A framing time of about 15 nanoseconds should be possible with this tube by using 1 Kv at the drift section, provided a light source of sufficient intensity were available. In the chopped mode of operation, there is no reason why framing with 10 ns. or less exposure should not be possible, A time interval would then occur between two consecutive frames, as discussed in chapter (4.6.)

Shorter time exposures will be tried with sparks generated by focussing a Q spoilt laser pulse shortly. Streak operation would also be tried with the laser spark with streak lengths between 50 and 100 nanoseconds. The linearity of the streak could then be compared with those obtained by other types of image converter tubes (e.g. the A.W.R.E. tube).

CHAPTER 8.

DISCUSSIONS AND FUTURE DEVELOPMENTS.

8.1. Limit of Time Resolution Achievable with the Multiple-Beam Tube.

The results described in the last chapter demonstrated the possible applications of the multiple beam tube to ultra high speed photography in general and time resolved spectroscopy in particular.

In general ultra high speed photographic work like obtaining a number of frames each with several nanosecond duration, the use of the system is essentially limited to framing images of small dimensions. For example, if the last tube described in Chapter (7) section (3) is set for five frames each of 14 nanosecond duration, with a seperation of 3 mms between frames, the following values of V_d and V_z will have to be employed at a magnetic field strength of 500 gauss.

$$V_z = 1 \text{ kV}$$

$$V_d = 137 \text{ V.}$$

as calculated from equations (2) and (4) of Chapter 4, using dimensions of the said tube:

$$d_1 = \tfrac{1}{2} \text{ cm} \qquad d_2 = 1.5 \text{ cm.}$$

$$S = 1 \text{ cm.} \qquad L = 8.6 \text{ cm.}$$

If the length of the image is 1 cm, time dispersion between top and bottom of the image per transit is, according to equation(8)Chapter 4,

$$\Delta t = \frac{t_1 \times V_d}{2 V_z} = \frac{14 \times 137}{2000} \text{ nanoseconds.}$$

= 0.91 nanoseconds.

Hence time dispersion per frame will be 1.82 nanoseconds, and for five frames 9.1 nanoseconds.

This is just about tolerable for a framing time of 14 nanoseconds. But no shorter time per frame could be usefully achieved by using the tube in the chopped mode (Chapter 4.6.).

But if the image was only 3 mm high, the time dispersion per frame, would be

$$2\Delta t = 2.\ \frac{t_1\ \frac{1}{3}\ V_d}{2\ V_z}$$

= 0.6 nanoseconds

in which case the number of frames that could be achieved without being very much affected by time dispersion could easily be ten. Also, framing times as small as 5 nanoseconds could easily be employed when used in the chopped mode. Thus the limiting speed at which the device could be used for framing will depend on the size of the image. It is also clear that the device is more useful at higher framing speeds. For example, if a drift potential of 5 kilovolts is employed instead of 1 Kv in the previous example, V_d has to be increased by a factor of $\sqrt{5}$ to get the same deflection i.e. the modified V_d will be 306 volts and time dispersions in the two examples would be 0.38 nanoseconds and 0.13 nanoseconds respectively per frame, with a framing time of 6.26 nanoseconds. The technique of making a tube which will stand such high voltage in close proximity to a slightly negative aperture electrode is of course quite involved. But this problem can be avoided if the

spacing between the aperture electrode and the drift section is slightly increased. Thus frame rates in excess of 10^8 frames could be obtained in such a multiple beam tube with continuous recording of an event into a number of frames. Framing times approaching one nanosecond should be achieved when the tube is operated in the chopped mode, without much error due to time dispersion. Thus, with an image of small dimensions framing rates approaching 2×10^8 frames/sec and to framing times approaching 10^{-9} seconds should be practicable.

When the system is used for time-resolved spectroscopic work with Fabry-Perot fringes crossed with a slit image, framing times should be possible to achieve in the way discussed in Chapter 4, section 8. Here each element of a fringe can be taken as a seperate frame, and the time resolution will eventually be limited by the width of the fringes. If for example, the camera is set in the same way as the first example, for 0.5 mm fringe width the time dispersion inside the fringe would be 0.09 nanoseconds, or 90 picoseconds per frame. Thus, time resolution that could be achieved with such fringe systems would require this time dispersion to be negligible compared to the framing time. If the maximum tolerable error is assumed to be 20%, minimum framing time obtainable would be 450 picoseconds. In the second example this value becomes about 100 picoseconds. Electronic control circuits of course become more vulnerable to producing an error at these speeds, although 10 volt pulses with 200 picoseconds rise timeare nowadays within practical limits (Transitron data Sheet, 1964). Designs of such tubes are now being considered.

8.2. Improvements in Tube Design:

An Input Gating Mesh.

When a high drift potential and a moderate accelerating potential are applied to the drift section and the first accelerating electrode before the aperture, aperture cut off voltage becomes large. Gating of the aperture effectively was found difficult in these cases, and also the image quality became worse because of crowding of equipotentials near the aperture, imparting radial velocity to the electrons. A fine copper mesh close to the photocathode used as an input gate (Fig.8.1.) would solve this problem. The aperture potential can then be fixed at a slightly negative potential. This gating mesh need only be used in special modes of operation like chopping and in cases discussed in Chapter (4.8.).

Addition of a Gain Stage It was obvious from the experiments performed, a stage of gain after the first stage would be a very useful addition to overcome limitations due to scarcity of photons. In fact, this was going to be one of the uses of the two stage cascacaded image intensifier discussed in Chapter 3. Optical coupling between the two tubes will be required in such a system. A built-in stage of gain after the multiple beam tube with proximity focussing (McGee, 1947), (but keeping the whole tube inside the same axial magnetic field) would seem to be the simplest way of achieving this (Fig.8.2.). More sophisticated types of gain stages will only be required if higher spatial resolution can be achieved in the multiple beam tube.

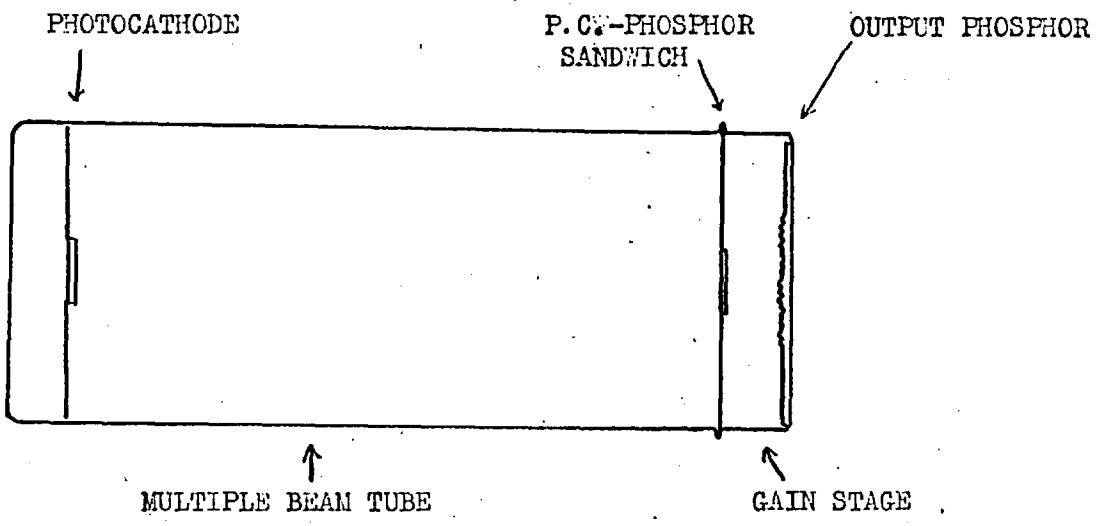

PHOTOCATHODE
P.C.-PHOSPHOR SANDWICH
OUTPUT PHOSPHOR
MULTIPLE BEAM TUBE
GAIN STAGE

Fig. 8.2.

Wide Spectral Range Tube:

A multiple beam tube with a gain stage, a spectrosil input window, and photocathode substrate is now under plan for production. Such a tube with an S-10 input photocathode would be of invaluable use for spectroscopic work with 2nd and 4th harmonic of a ruby laser emission. It will also be very useful for plasma diagnostic spectroscopy in the ultraviolet.

Improvement of Spatial Resolution:

So far, 'brute force' focussing of the photo-electrons by a strong axial magnetic field was employed to retain the image in the storage section. It is proposed to explore the possibilities of employing proper magnetic focussing by allowing the photo-electrons to complete an integral number of loops in the deflecting field. The main problem to be tackled will be the difference in lengths of the loops for electrons with different velocities.

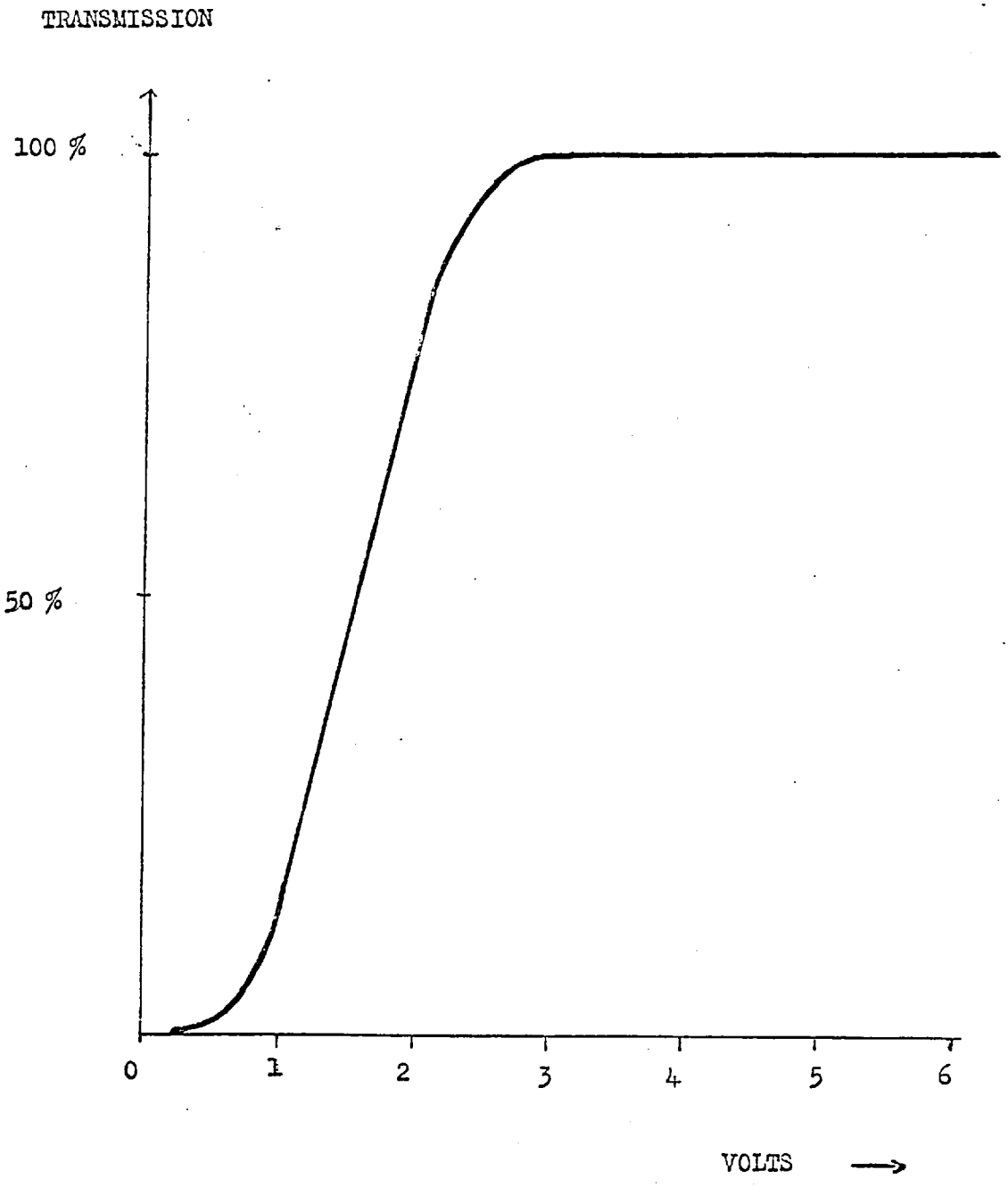
8,4. Use of the Multiple-Beam Principle for Wideband and Sensitive Oscilloscope:

Wide band oscilloscopes with a band width in excess of 100 mc/sec are generally of two types - the travelling wave type like the Tektronix oscilloscope type 519 (with a 1000 mc/sec band width or the sampling oscilloscope like the Tektronix type 661 (4000 mc/sec band width). The travelling wave type tube is highly sophisticated and has a rather low sensitivity, but it is capable of recording transients which are not repetitive. Also, it is not possible to make a double beam oscilloscope of the travelling wave type. On the other hand, a sampling oscilloscope

operates by sampling out a small portion of a wave form every time it arrives at the input and builds up the whole wave form after it has sampled it out by examining a great number ofwave forms(McQueen 1952). These oscilloscopes are very sensitive but can only operate with repetitive transients. The storage system of the multiple beam tube could be employed to make an oscilloscope with a sensitivity of a sampling oscilloscope and capability of recording a single transient phenomenon.

As has been seen in Chapter 7, a gating mesh has got an electron transmission characteristic similar to the electron transfer characteristic of a triode. The middle of this transfer characteristic (Fig 7.7.) shows a linear increase in electron transmission with the applied voltage. In this region a voltage swing of about one volt changes the electron transmission from about 15% to 90%. If this gate is biased at 0.8 volts a voltage swing of 0.5 volt either way will change the transmission of electrons through it proportionally. Thus, any impressed wave form on this mesh whose peak to peak swing does not shoot beyond one volt would produce an intensity modulated beam on the other side of the mesh. This beam is then stored and framed in a multiple beam type storage section before sampling it out at the output mesh.

Fig. 8.3. displays essential parts of such a system. G is an electron gun producing a very narrow pencil of electrons (0.1. mm) M_1 is the modulating grid A, is the aperture with a small hole .2 mm in it to let the electrons through. D_1 and D_2 are the deflecting plates, 1 cm long and 0.3 cm apart. M_3 is the field defining mesh and M_2 is the output gating mesh. The distance between A and M_2 is 2 cms. C are



TRANSMISSION VS MESH POTENTIAL IN PHOTOELECTRIC TUBES

Fig 8.2

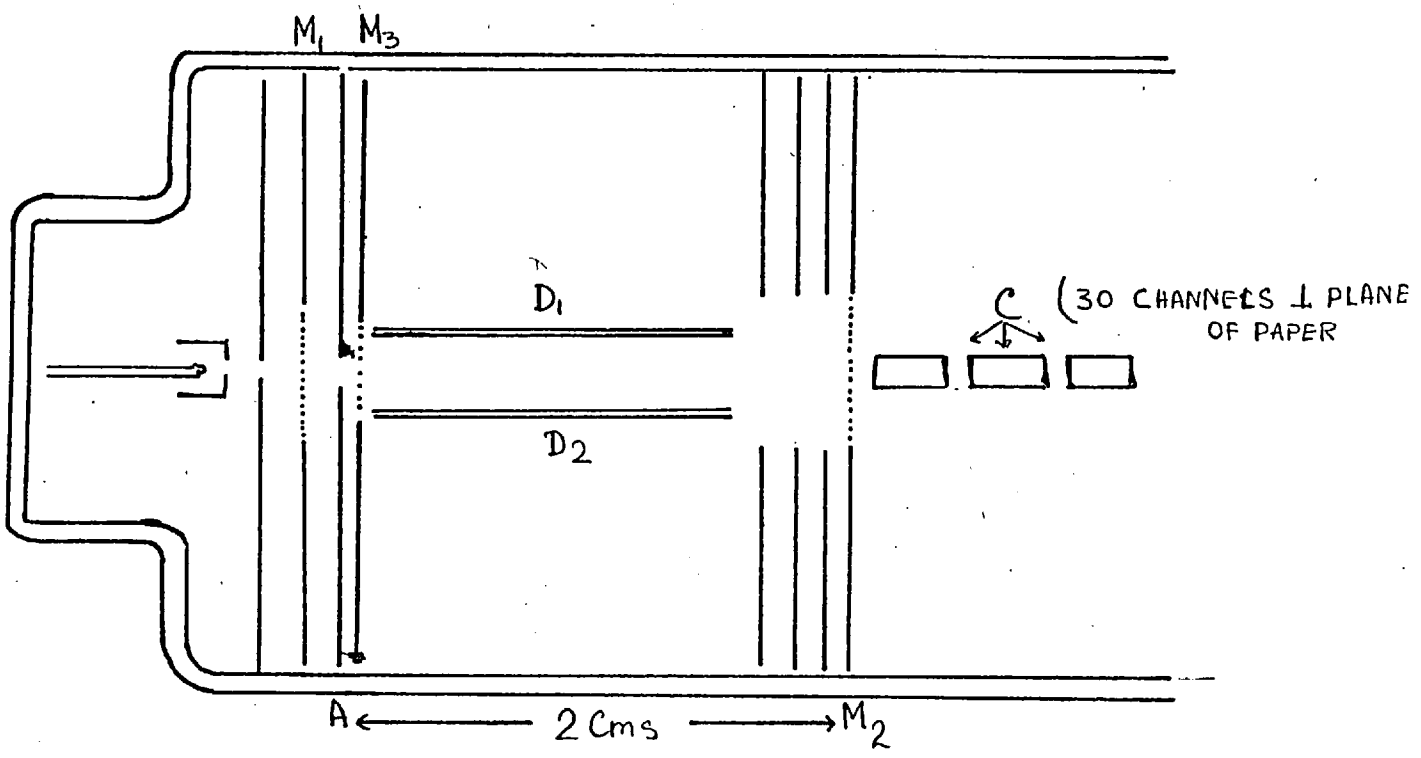


Fig. 8.3.

the channelled electron multipliers.

There are 30 channelled electron multipliers of .2 mm bore and closely packed in a row and corresponding to the 2nd to the 31st frames. The wall of the tubes has to be as thin as possible so that the deflection of the electron beam per frame may be just slightly larger than .2 mm.

In this design the electron beam is so narrow that time dispersion even in more than 60 transits is negligible. A magnetic field of 250 to 300 gauss is proposed to be used - enough to keep the electrons into tight helical paths of about .1 mm diameter. With a drift potential of 5 Kv and a deflecting voltage of about 80 volts (depending on magnetic field strength), 30 one nanosecond frames could be stored in this storage section ready to pass into the 30 channels. This system can now be used for sampling and display of a transient in two ways described below.

Simple Method to Give a Bandwidth of 300 mc/sec.

Fig. 8.4. shows the method of operation in this technique. The mesh M_1 is originally biased off at a point P beyond cut off. A pretrigger B now brings M_1 to the quiescent point (i.e. the middle of the linear portion of the transmission characteristics of M_1). The wave form C whose peak value never goes beyond the linear part of the transfer characteristic of M_1 is now impressed on M_1, whose potential therefore varies accordingly. This allows a density modulated beam of electrons to enter the drift section. Sticking to the parameters described in the last paragraph, this beam of electrons now becomes spread into 30 frames inside the storage section, each frame containing the number of electrons that entered the storage section in one nanosecond. When the electrons have taken

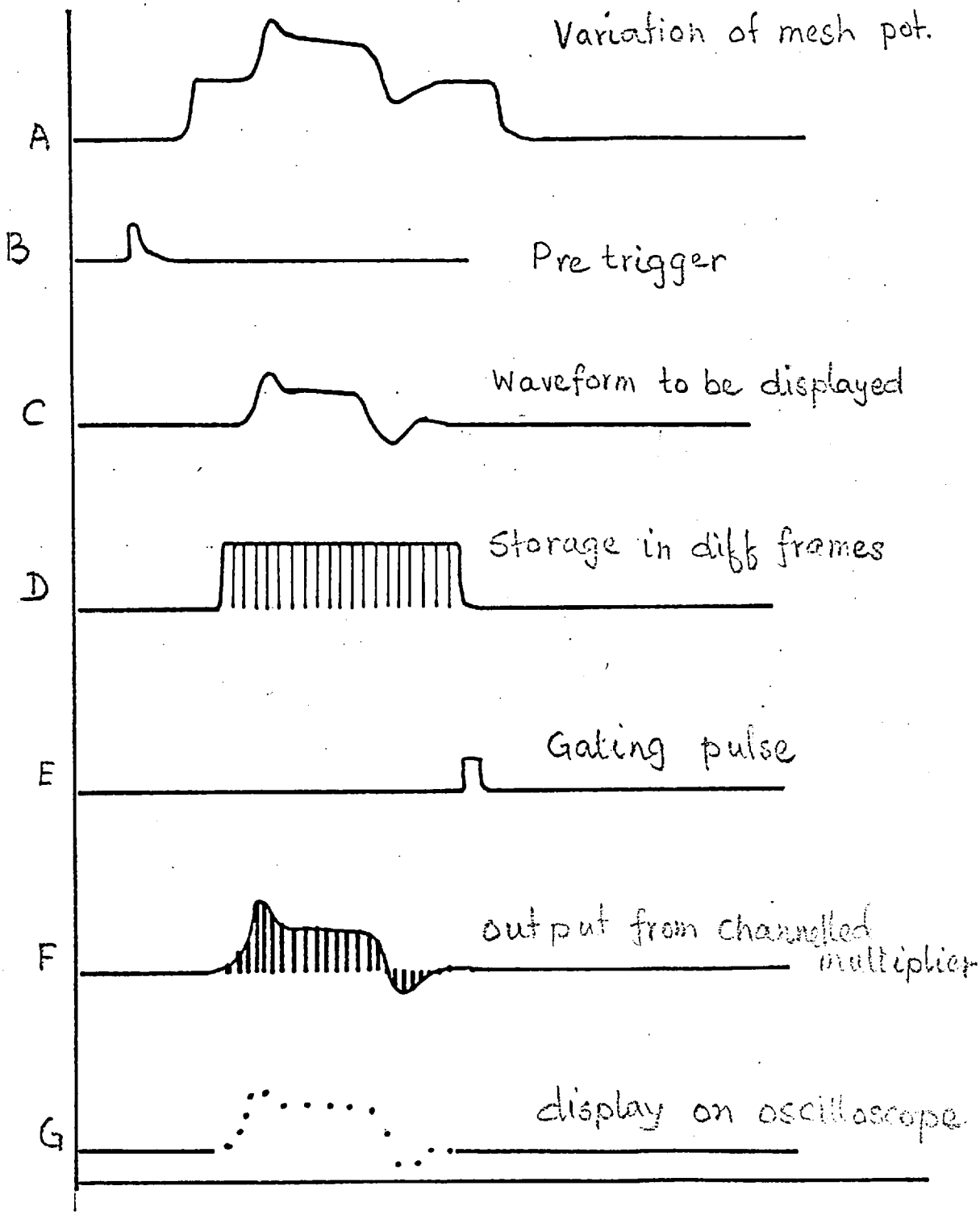

Variation of mesh pot.
A
B
Pre trigger
C
Waveform to be displayed
D
Storage in diff frames
Gating pulse
E
output from channelled multiplier
F
display on oscilloscope
G

Fig 8.4.

their places corresponding to the 30 channels of the multiplier, a sharp gating pulse E of very short duration (0.3 nsec) opens the gate M_2 and electrons enter the channels for the first 0.3 nsec of each frame and are now amplified into a number of descrete pulses at leisure to be displayed on an ordinary oscilloscope having facilities for normal sampling operation, as explained in F and G of Figure 8.4.

Operation of such a sampling system should be extremely simple and straight forward. Since one sample of information per frame is extracted for amplification, a bandwidth around 300 mc/sec should be possible.

A More Sophisticated Sampling System:

A sampling oscilloscope with a much larger bandwidth should be possible with a more sophisticated electronic control, described below (Fig.8.5.).

In this method, everything starts at the same point as before except that there is no deflecting field impressed between the deflecting plates. A pretrigger like before puts the mesh M_1 in the quiescent position and also sets a positive flat top pulse between the defleoting plates. The density modulated electron beam now enters the storage section and gets separated into all the frames in the same way. As soon as all the frames get set aligned to the channels, the deflecting voltage pulse is terminated and a sharp short pulse (0.2 ns) applied to gate open mesh M_2. Information for 0.2 nsec from each frame is thus extracted to be amplified as descrete pulses while the rest of the electrons continue to move back and forth between the mesh and aperture but without any deflection. Electrons still remain within the domains of their frames, but diffused over a larger area as shown in Fig. 8.6. The bores of the channelled

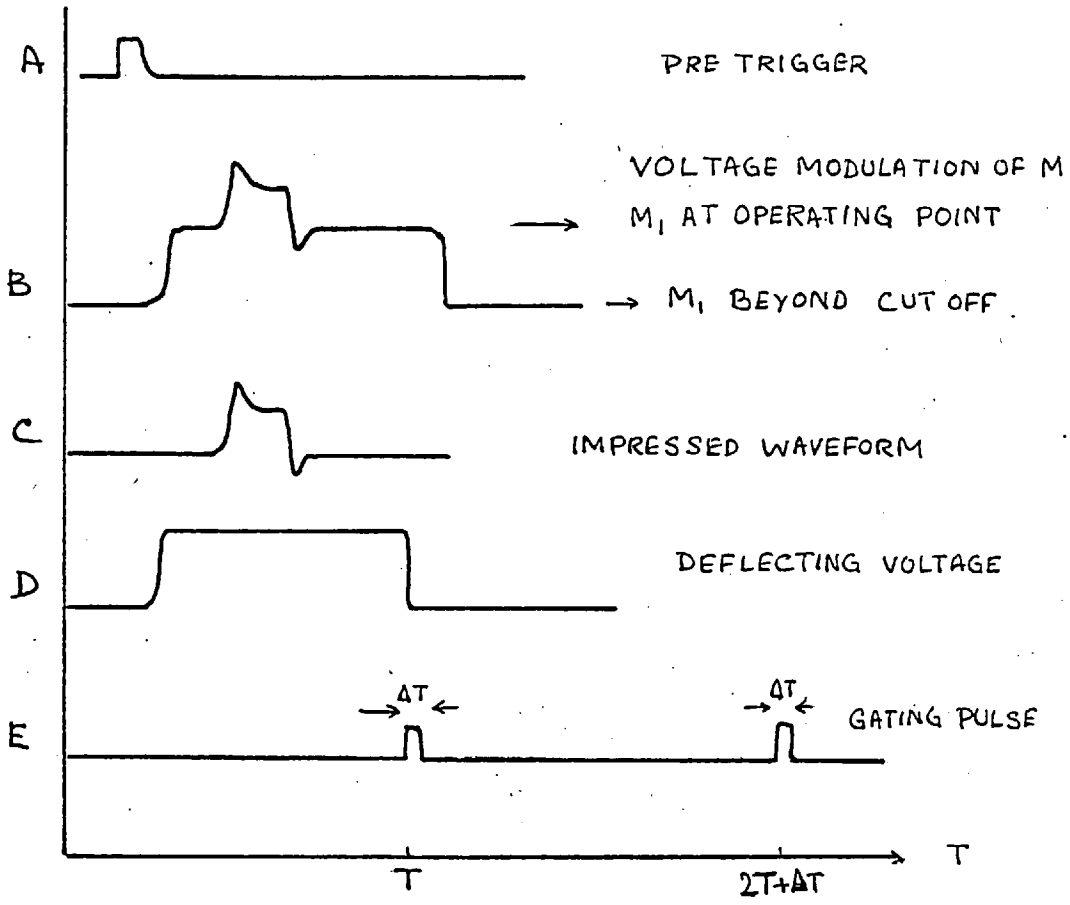

A
PRE TRIGGER
VOLTAGE MODULATION OF M1
M1 AT OPERATING POINT
B
M1 BEYOND CUT OFF
C
IMPRESSED WAVEFORM
D
DEFLECTING VOLTAGE
ΔT
ΔT
E
GATING PULSE
T
T
2T+ΔT

Fig 8.5.

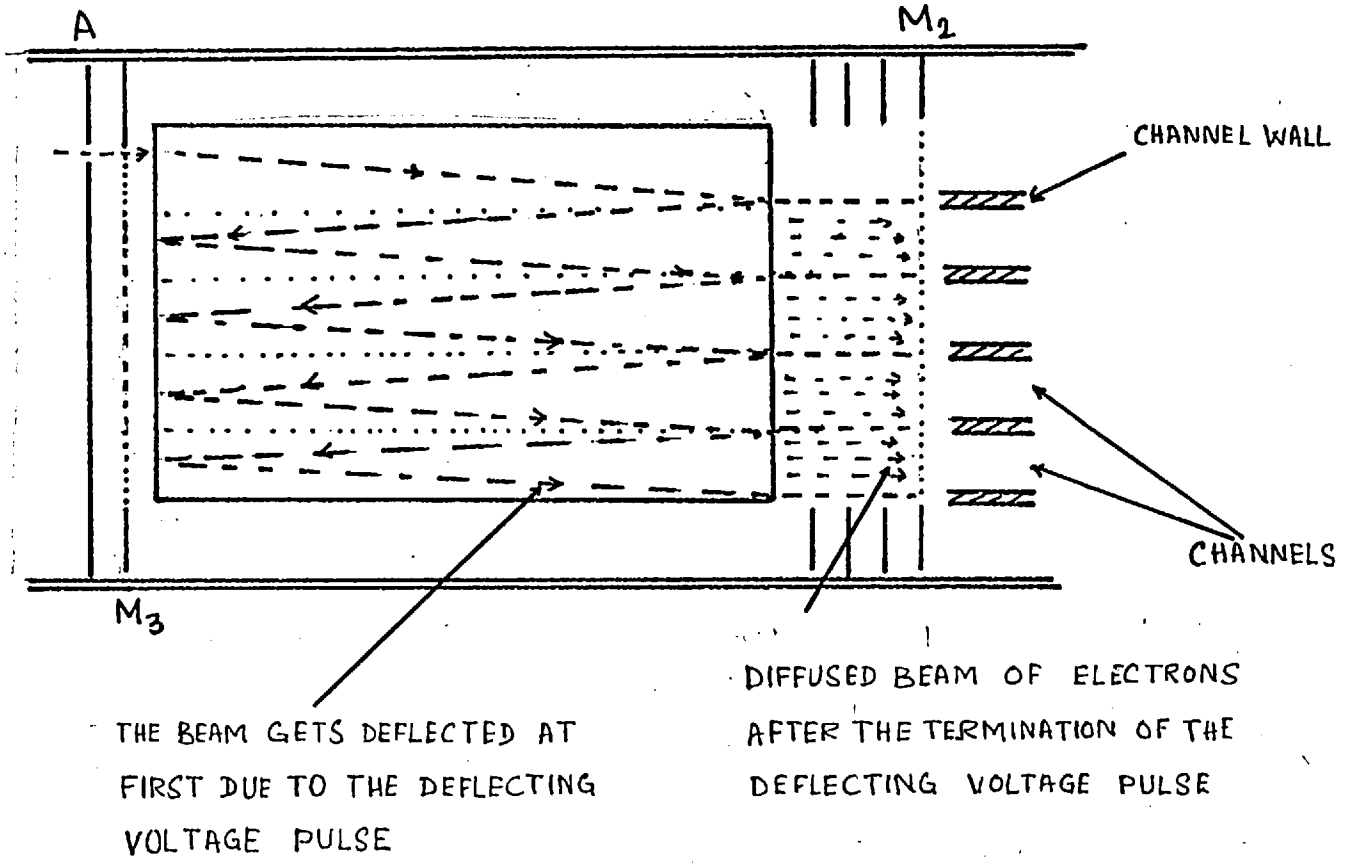

A
M_2
CHANNEL WALL
CHANNELS
M_3
THE BEAM GETS DEFLECTED AT FIRST DUE TO THE DEFLECTING VOLTAGE PULSE
DIFFUSED BEAM OF ELECTRONS AFTER THE TERMINATION OF THE DEFLECTING VOLTAGE PULSE

Fig. 8.6.

multipliers are almost equal to the total deflection per frame and hence if the mesh M_2 is gated open, almost all the electrons in each frame will still pass into the channels, Now, if T is the framing time and T the width of the sampling pulse (T = multiple of T) the mesh M_1 can be gated open at intervals of T + T from the first gating mesh to extract one discrete sample from every frame. The whole wave form can be reconstructed from these pulses in a way a television picture is reconstructed by interlacing as detailed in Fig. 8.7.

The bandwidth of such a sampling oscilloscope should only be limited by the sampling pulse until time dispersion becomes important. The time dispersion for a system like this would be negligible, about .03% i.e. for a framing time of 1 nsec, time dispersion per frame is less than one picosecond. With most advanced electronics to date sampling pulses of 0.2 nsec should be obtainable, producing a bandwidth of around 1500 mc/sec.

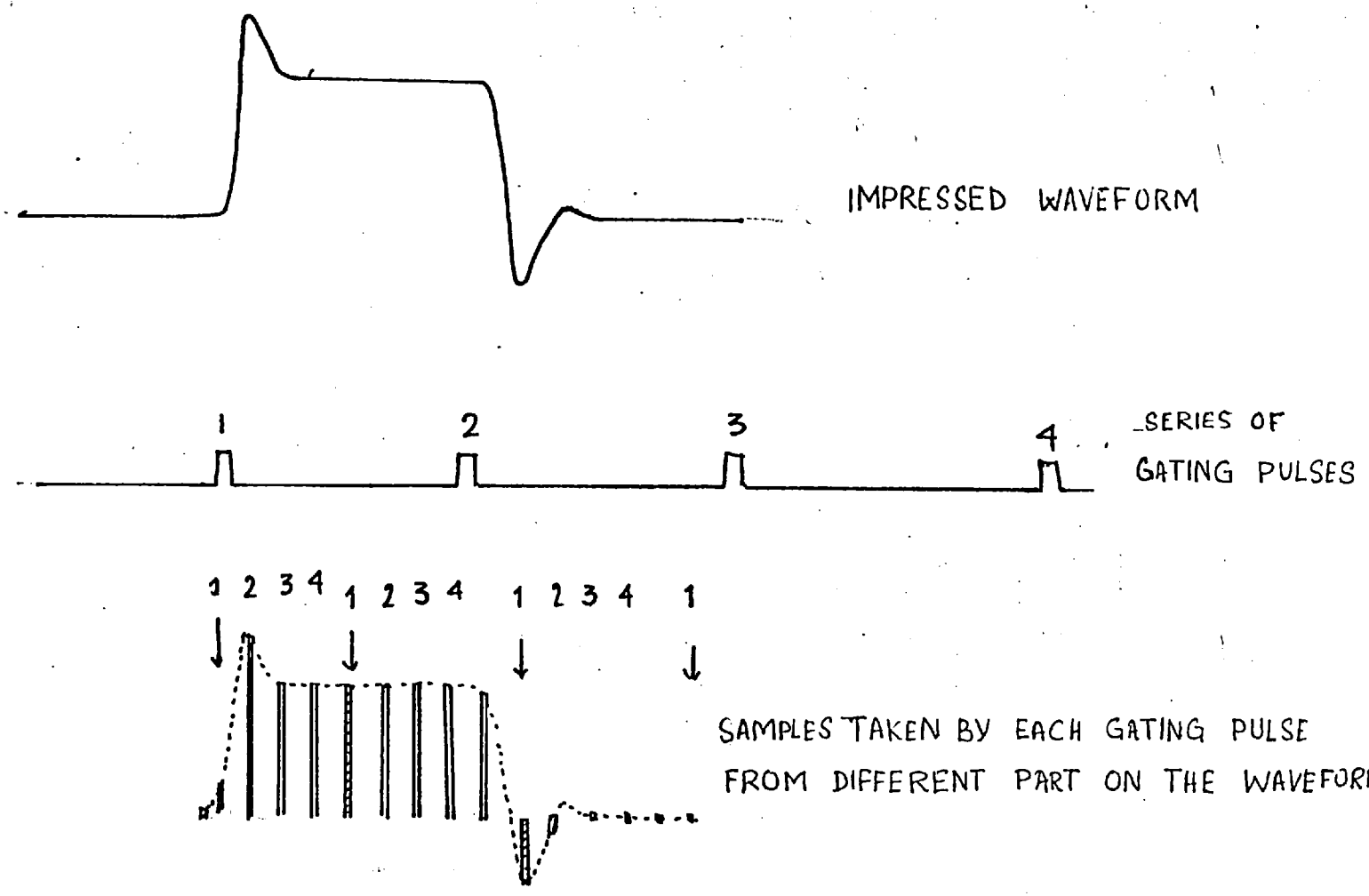

IMPRESSED WAVEFORM
1
2
3
4
SERIES OF
GATING PULSES
1 2 3 4 1 2 3 4 1 2 3 4 1
SAMPLES TAKEN BY EACH GATING PULSE
FROM DIFFERENT PART ON THE WAVEFORM.

Fig. 8.7.

CONCLUSION.

A new multiple beam image converter camera has been produced. Its capacity to store images with simultaneous framing has been demonstrated. The extreme simplicity of operation where only one single gating pulse extracts the framed images without any time seperation between consecutive frames, is shown. A simple transistorised electronic system capable of generating very accurately delayed pulses of subnanosecond rise and fall times has been constructed, and was found very satisfactory.

The experiments performed has clearly shown that the tube has the capacity of producing frames as short as one nanosecond in the chopped mode and about 15 nanoseconds if no time gap is allowed between consecutive frames.

The possibility of improving the time resolution for spectroscopic work by exploiting the time dispersion effect inherent in this tube is also demonstrated.

Five frames of an argon spark discharge, each of fifty nanosecond duration and without any time gap between frames were recorded showing the expansion of the plasma. This is a typical experiment where this tube will be of great use, besides its use in spectroscopy.

The potential use of this multiple beam technique in producing a sensitive wide band oscilloscope is also illustrated.

ACKNOWLEDGEMENT.

The author is indebted to Dr.D.J.Bradley for his constant interest, advice and encouragement throughout the work. He is grateful to Prof. J.D.McGee for his suggestion to explore the use of the used deflection system for this work.

It would not have been possible for the author to carry out this work without the technical assistance of Mr. F.E. Barlow in general photoelectronic work, Mr. A. Goodman for building electronic circuits and Messrs. R. Mason and the glass blowing workshop of Physics Dept., Imperial College, for the glass blowing work.

The author is grateful to the Pakistan Atomic Energy Commission for sponsoring him for this work with a Colombo Plan Fellowship, until Dec. 1965.

In referring to the biennial conference on High Speed Photography the abbreviation HSP will be used where:-

HSP, 3 - Third Congress 1956 London Butterworths - 1957

HSP, 4 - Fourth Congress 1958 Darmstadt Helwich 1959.

HSP, 5 - Fifth Congress 1960 New York Society of Motion Pictures and Television Engineers, 1962

HSP, 6 - Sixth Congress 1962 Haarlem Netherlands Willink 1963.

HSP, 7 - Seventh Congress 1965 Zurich Switzerland.

Airy R.W.,1964 — British Patent, application no.2060/64 16th Jan, 1964.

Airy R.W.,1965 — Proc. 3rd.Symposium on Electron tube Devices, 1965. To be published.

Ascoli-Bartoli,1965 — Proc. 7th International Congress on High Speed Photography, 1965. To be published.

Aslam M.,1965 — Ph.D. Thesis, University of London.

Barnsley D.A.,1962 — HSP 6, 340, 1962

Beale J.R.A.,Stephenson W.L., and Wolfendale E. 1957 — Proc. I.E.E. 104 B, p.394, 1957

Beckman and Whitely, 1965 — Industrial Literature

Bell, 1964 — Electronic Design, June 8th, (1964) p.394.

Bradley, D.J., 1962 — J.Opt.Soc. America, 52, 222, (1962)

Bradley, D.J., et.al. 1963 — Proc. of VI Conf. Phenomenes d'Ionization dans les Gaz, Paris (1963).

Bradley D.J., Majumdar S., 1966 J.Phot.Sc. To be published, 1966

Bradley D.J., Majumdar S., Bates B., Juulman C.O.L., 1964 Appl.opt. 3, 1461, 1964

Buck 1960 HSP 5 p 318 1960

Butslov et.al., 1958.

Chaplin G.B. and Owens A.R., 1959 I.E.E. Int.Conf. on Transistor, Part B., Suppl, 813, (1959).

Chippendale R.A., and Folbes J.R., 1960 HSP5, 104, (1960)

Coleman K.R., 1963 Rep.Pr.Phys. XXVI, 269, (1963).

Cooper J., and Creig 1962 Nature 195, 371 (1962)

Corcoran 1962 HSP 6, p 301, 1962

Courtney-Pratt J.S., 1952 Photo. Journal B92 137, (1952).

Courtney-Pratt J.S., 1957 Rep.Prog.Phys. XX, 379, (1957).

Courtney-Pratt J.S., 1964. J.S.M.P.T.E.

Drecescamp H., and Burton M., 1959 Phys.Rev.Letters 2, 45, (1959)

Edgerton H.E. and Germehausen K.J., 1961 J.S.M.P.T.E. 61

Eylon S., 1962 HSP6, 331, (1962)

Fatera D.A., 1965 J.S.M.PTE. 74, 911, (1965).

Folkes, 1962 Adv. Electronics and Electron Phy. 16, 325

Goss W., 1960 HSP5, 135, (1960)

Hargrove and Courtney-Pratt.J.S., 1965 J.S.M.P.T.E. 74, 1085 (1965)

Hill D.A., 1962 Caldwell D.D., Schluter, R.A. Adv.Electronics & Electron Physics XVI, 475, (1962)

Hogan A.W., 1951 Proc. I.R.E. 39, 268, (1951)

Hopmann, 1965 HSP7. To be published.

Huston A.E. 1964 Appl.Optics 3, 1231 (1964)

Huston A.E. 1965 HSP7 To be published.

Huston A.E. & Walters, F. 1962 Advances in Electronics 16, 249, (1962)

Jaquinot P., & Dutour C., 1948 J.Rech. C.N.R.S. (Paris) 6, 1.

Jaquinot, 1954 J.op.Soc.Am. 44, 761 1954

Jenkins J.A., and Chippendale R.A. 1951 J. Brit. I.R.E. 11 505, (1951).

Key and Stokes, 1966 Private Communication

King R.W. and Hett J.H., 1960 HSP5, 118 (1960)

Landre, J.K., 1964 Rev.Sc.Inst. 35, 796, (1964)

Leibig L. and Frungel F., 1960 HSP5, 138, (1960).

Malysher G.M., Razdobarim G.T., and Sokolova L.V., Soviet Physics - Doklady 7, 701, (1963).

Mandel L. 1960 HSP5, 110, (1960)

McGee, J.D. 1962 Proc.Symposium on Nuclear Instruments, (Harwell, 1961) Heywood 1, (1962).

McGee J.D., and Wheeler B.E. 1962 — Advances in Electronics 16, 47, (1962).

McGee J.E. Beesley J. Berg A.D., 1966 — J.Sc.Instr. 43, 153 (1966)

Ramsay J.V., 1962 — Appl. Opt. 1, 411 (1962).

Rose and Iams 1939. — Proc I.R.E. 27, 547 (1939)

Saxe R.F., and Chippendale R.A. 1955 — Brit. J. Appl. Phys. 6, 336, (1955).

Saxe R.F., and Prime H.A. 1949 — Proc.I.R.E. 96 II, 662, (1949).

Schardin H., 1956 — H.S.P.3., 316, 1956.

Simonov V.A., and Kutokov G.P. 1960 — H.S.P.5., 123, (1960).

Sommer 1960 — Optica Acta 7, 121, (1960)

Sommer 1964 — Unclassified Report, R.C.A.

Sommer 1964 — Appl.Physics Letters.

Stoudenheimer and Moor 1957 — R.C.A. Rev. 18, 322, (1957).

Tolansky S., and Bradley D.J. 1959 — N.P.L. Symposium on Interferometry, (1959), p.375.

Twiddy N.D. and Mende S., 1964 Private Communication.

Walters F. 1962 — HSP 6, 357, 1962

Weedon 1962 — HSP 6, 321, 1962

Winker 1964 — Rev.Sc.Instr. 35, 790, (1964).

Yguerabidi, 1965 — Rev.Sc.Instr. 36, 1734 (1965).

Zavoisky et.al. 1956

(*Reprinted from Nature, Vol. 202, No. 4932, pp. 579–580, May 9, 1964*)

Multiple-beam Interferometry in the Vacuum Ultra-violet

FOR orbiting astronomical telescopes and photometers, interference filters and the Fabry–Perot interferometer have considerable advantages in luminosity, speed of recording and compactness over prism and grating instruments[1–3]. Thus it is important to extend the range of multiple-beam interferometry into the vacuum ultra-violet.

The limitation so far has been in obtaining suitable reflecting coatings. Below 2400 Å there is no high-index material for dielectric multilayer films[4]. However, reported measurements[5] on the optical properties of semi-transparent aluminium films down to 2200 Å, when analysed, showed that aluminium improves in performance for multiple-beam interferometry with decreasing wave-length, provided a reflecting finesse of 20 is sufficient. It must be remembered that the defects finesse also decreases with decreasing wave-length and, even with the best-quality flats, will not greatly exceed 18 at 1800 Å, so that a higher reflecting finesse is neither required nor desirable[6]. For interference filters, the band-width decreases with decreasing wave-length and, for a given band-width, the finesse required is proportionally smaller, provided the resulting decrease in contrast can be tolerated.

This analysis and recent improvements[7] in the technique of depositing opaque aluminium films, overcoated with thin layers of magnesium fluoride to prevent oxidation and to enhance reflectivity in the vacuum ultra-violet, led us to believe that a similar improvement could be obtained in the performance of semi-transparent coatings for this spectral region. Our first results[8] indicated that thinner aluminium films, similarly overcoated, were suitable for multiple-beam interferometry down to 1900 Å. We now wish to report our results on filters with peak transmittances at ~ 1800 Å and Fabry–Perot interferograms of λ1849 of HgI.

Fig. 1 shows the transmission characteristics of two Fabry–Perot type first-order interference filters deposited on fused quartz substrates, each consisting of two aluminium reflecting layers separated by a half-wave layer of magnesium fluoride. The outer aluminium layer is protected from oxidation by a magnesium fluoride coating, approximately 400 Å thick. Curve *A* represents a filter peaking at 1825 Å. Below 1800 Å the finesse decreases because of the falling reflectivity of the aluminium layers, but at approximately 1660 Å the rapidly increased absorption of the 'Spectrosil' substrate leads to a sharp cut-off.

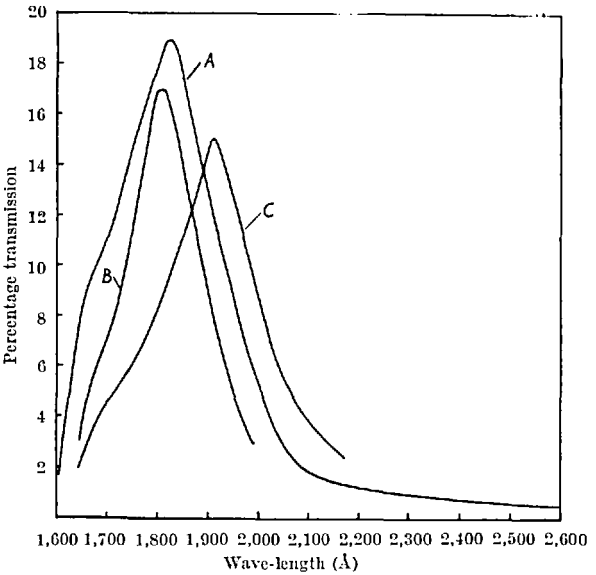


Fig. 1. Transmission curves of first-order Fabry–Perot type filters

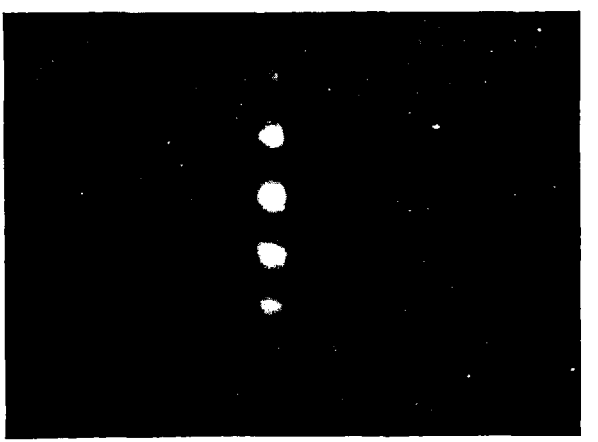


Fig. 2. Fabry–Perot interferogram of λ1849 HgI. Interferometer spacing, 0·15 mm

The transmission profile above 1800 Å corresponds to a half-width of 225 Å and a finesse (N) of 8. The recorded peak transmission of 0·19 when corrected for absorption in the substrate becomes 0·21, giving for the aluminium films a mean reflectivity $R = 0{\cdot}68$, transmissivity $T = 0{\cdot}15$, and an absorption $A = 0{\cdot}17$.

Table 1. Optical Properties of Aluminium Films derived from Fig. 1

Curve	N	R	T	A	$(R + T)$
A	8	0·68	0·15	0·17	0·83
B	8·5	0·69	0·135	0·175	0·825
C	8·5	0·70	0·12	0·18	0·82

Curve B is the same filter tilted through 8° to displace the peak wave-length to 1805 Å, and curve C represents another filter with a peak transmission of 0·15 (corrected 0·165) at 1910 Å. Because of an error in monitoring the second aluminium layer the performance of this filter is not optimum. The optical properties of the aluminium films derived from the longer wave-length half-profiles of these curves are summarized in Table 1.

The transmission curves below 2000 Å were measured on a vacuum Seya monochromator. Curves A and B were obtained when the filter was six weeks old and had been frequently exposed to ultra-violet light. Curve C was determined on the day following the manufacture of this filter. The longer wave-length tail of curve A was measured on a Perkin–Elmer 350 spectrophotometer. For this filter the transmission falls to 0·4 per cent at 2600 Å and to 0·3 per cent at 2800 Å. Greater contrast and a narrower band-width could be obtained with a second-order filter provided a selective detector[9] is used to suppress the longer wave-length peak. Alternatively, two filters could be used in series or deposited as a double filter[10] on the same substrate.

So far as we know these are the only results reported for interference filters < 2000 Å apart from Schroeder[10], who reports a double filter with a half-width of 200 Å but a peak transmission of only 0·7 per cent at 1900 Å.

Finally, 'Spectrosil' Fabry–Perot plates were coated. Fig. 2 shows fringes of λ1849 of HgI obtained with a 'Spectroline' 11*SC*–1 lamp. The line was isolated by a 'Spectrosil' prism spectrograph purged with nitrogen. A single-stage magnetically focused image converter, with a 'Spectrosil' window and cathode substrate, constructed for this work greatly facilitated detection and recording of the fringes (the imperfection in one of the fringes is caused by a defect in the image converter phosphor). The fringe finesse of about 5 is mainly limited by the quality and adjustment of the interferometer plates, which are, of course, very critical at these short wave-lengths. To confirm this, fringes of λ2537 were recorded and a finesse of 7 directly proportional to the increase in wave-length was obtained, showing that the defects finesse dominates. These are the first reported Fabry–Perot interferograms below 2000 Å. A high-quality interferometer is being constructed and we hope to extend the spectral range to 1600 Å or less so as to permit the utilization of the instrument, either in its oscillating form[11] or in its spectrographic method of use[8], for plasma diagnostic spectroscopy in this spectral region, in addition to space research applications.

We thank Prof. J. D. McGee for his advice, Prof. W. R. S. Garton for lending us equipment, and Mr. D. S. Widner for making the filter measurements on the Seya monochromator. Assistance from the British National Committee for Space Research for the purchase of equipment and the support of one of us (C. O. L. J.) is gratefully acknowledged. One of us (S. M.) is supported by a Colombo Plan fellowship.

D. J. Bradley
B. Bates
C. O. L. Juulman
S. Majumdar

Department of Physics.
Imperial College of Science and Technology,
London, S.W.7.

[1] Jacquinot, P., *J. Opt. Soc. Amer.*, **44**, 761 (1954).
[2] Dunham, T., *Vistas in Astronomy*, **2**, 1223 (Pergamon Press, London, 1956).
[3] Bradley, D. J., *Proc. Roy. Soc.*, A, 262, 529 (1961).
[4] Honica, G., and Krebs, K., *Z. Physik*, **156**, 117 (1959).
[5] Hass, G., and Wayonlis, J. E., *J. Opt. Soc. Amer.*, **51**, 719 (1961).
[6] Chabbal, R., *J. Rech. C.N.R.S.*, **24**, 138 (1953).
[7] Hunter, W. R., *Optica Acta*, **9**, 255 (1962).
[8] Bradley, D. J., Bates, B., and Juulman, C. O. L., *Proc. Sixth Conf. Phénomènes d'Ionization dans le Gaz*, **4**, 79 (Paris, 1963).
[9] Dunkelman, L., Fowler, W. B., and Hennes, J., *App. Optics.*, **1**, 695 (1962).
[10] Schroeder, D. J., *J. Opt. Soc. Amer.*, **52**, 1380 (1962).
[11] Bradley, D. J., *Proc. Conf. Optical Instruments and Techniques*, 31 (Chapman and Hall, London, 1961).

Printed in Great Britain by Fisher, Knight & Co., Ltd., St. Albans.

JAPANESE JOURNAL OF APPLIED PHYSICS VOL. 4, SUPPLEMENT I, 1965
PROCEEDINGS OF THE CONFERENCE ON PHOTOGRAPHIC AND SPECTROSCOPIC OPTICS, 1964

The Fabry-Perot Interferometer in the Middle and Vacuum Ultraviolet

D. J. BRADLEY, B. BATES, C. O. L. JUULMAN, and S. MAJUMDAR
Department of Physics, Imperial College, London S. W. 7, England

The factors affecting the performance of Fabry-Perot interferometers in the middle and vacuum ultraviolet are considered. Improvement of performance in the middle ultraviolet to 2000 Å and extension of the useful spectral domain of the instrument into the vacuum ultraviolet are reported.

The preparation and optical properties for ultraviolet multiple beam interferometry of double layer aluminium-magnesium fluoride semi-transparent reflecting coatings are discussed. Fabry-Perot type Al-MgF_2 interference filters for these spectral regions are also described and an interferogram of λ1849 of HgI obtained with an ultraviolet sensitive image converter is illustrated. Applications of these techniques to space research and to laser and plasma spectroscopy are mentioned.

Introduction

The Fabry-Perot interferometer is being increasingly employed for diagnostic spectroscopy of plasma discharges and laser sources both in its oscillating form[1)-3)] and in the classical etalon method of operation with image tube and photographic detection.[4)-7)] For orbiting astronomical telescopes and photometers the considerable advantages of the interferometer[8)] in luminosity, speed of recording and compactness over prism and grating instruments are also of importance.[9),10)] For all these applications it is important to extend the range of multiple beam interferometry, including interference filters, as far into the vacuum ultraviolet as possible. This will be particularly needed for spectroscopic examination of laser light higher harmonics (the ruby laser light fourth harmonics occurs at about λ1735), where the high resolving power of the interferometer is essential, and for space research applications. The two factors affecting the extension of the spectral range are the transmission and optical quality of the interferometer flats and the availability of suitable reflecting coatings.

The Optical Flats

It is desirable for maximum luminosity that the defects finesse N_D of the flats should not exceed the reflecting finesse N_R of the coatings.[11)] Fuzed quartz seems to be the most suitable material for attaining the high optical surface finish required at short wavelengths both for a high microdefects finesse (which for a given surface decreases with decreasing wavelength) and low scattering. This material, if completely pure, should be transparent down to about 1490 Å but in practice, for the best quality commercially available, a transmittance of $> 50\%$ is obtained down to 1670 Å for a 5 mm path required for a Fabry-Perot flat. If polished with care a surface finish of r.m.s. roughness of approximately 3 Å can be achieved.[12)] Etalon plates can be easily worked to match better than $\lambda/150$ in the green over 6 cm diameter. Cultured quartz can be obtained with a transmittance of 50 to 60% at 1600 Å for a 10 mm path but this material is more difficult to optically polish.

For fuzed quartz the surface roughness can be neglected in calculating the final defects finesse N_D. If the flats are adjusted parallel to $\lambda/150$ also, then N_D is about 18 at 1800 Å. For a smaller diameter aperture a correspondingly higher defects finesse should be obtained. If spherical mirrors are employed then the aperture required is greatly reduced.[13)]

Thus a defects finesse in the range 16–24 is attainable with flats transmitting a useful fraction of the light in the spectral region 1600–2400 Å.

The Reflecting Coatings

The limitation to date in extending the spectral range of the interferometer has been in obtaining suitable reflecting coatings. No high index material, transmitting below 2400 Å for multilayer dielectric coatings, has been

discovered so far.[14] However, reported measurements[15] on the optical properties of semi-transparent aluminium films down to 2200 Å, when analysed by us, showed that aluminium improves in performance for multiple-beam interferometry with decreasing wavelength, provided a reflecting finesse of 30 is adequate. This is illustrated in figure 1,

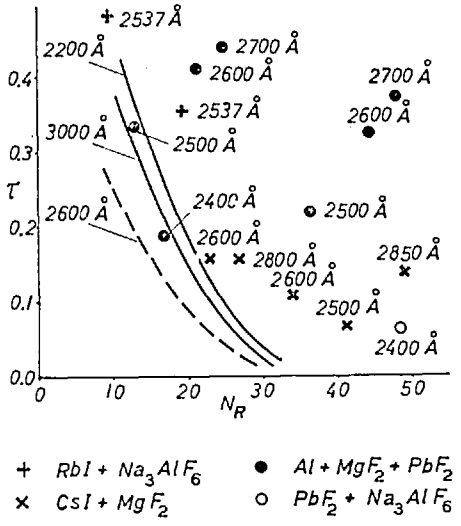


Fig. 1. Al, Al-dielectric multilayers and dielectric multi-layers in the ultraviolet spectral region. Al 2200 Å and 3000 Å;[15] Al 2600 Å;[16] Al-MgF_2-PbF_2 multilayers;[26] CsI-MgF_2 multilayers;[27] RbI-Na_3AlF_6 multilayers;[28] PbF_2-Na_3AlF_6 multilayers.[14]

which includes plots of the interferometer transmission τ as a function of the reflecting finesse N_R for aluminium films based upon the results of Hass and Waylonis.[15] It can be seen that for a given value of N_R the peak fringe transmission τ is greater at 2200 Å than for 3000 Å for all values of N_R. The points corresponding to various dielectric and dielectric-aluminium multilayer combinations for wavelengths > 2400 Å, also given in the figure, indicate their superiority over aluminium films for the longer wavelengths. The curve for 2600 Å derived from earlier results on aluminium films[16] shows the advance obtained with improved evaporation techniques.

Since, as we have seen, the defects finesse decreases with decreasing wavelength so that the reflecting finesse required decreases also, N_R=20 will be adequate at 2200 Å.

Previous to this analysis improvements[17] in the evaporation technique of depositing opaque aluminium films, overcoated with thin layers of magnesium fluoride to prevent oxidation and to enhance reflectivity in the vacuum ultraviolet, led us to believe[9] that a similar improvement could be obtained in the performance of semi-transparent aluminium films so as to permit extension to this spectral region for interference spectroscopy from an earth satellite. Our first results[4] indicated that thinner aluminium films similarly overcoated are suitable for multiple-beam interferometry down to 1900 Å. Since then we have further studied the optical properties of such films down to 1800 Å and employed them in Fabry-Perot type interference filters and for interference spectroscopy.

Method of Film Preparation and Optical Measurements

Aluminium of 99.99% purity is rapidly evaporated from heated tungsten wire filaments in an automatically controlled evaporation plant evacuated by a mercury diffusion pump. The reflectivity of a metal film is controlled by a shutter actuated by a reflectance monitoring unit, while the thickness of the magnesium fluoride overcoating is similarly controlled by monitoring the front surface reflection from a glass plate during the evaporation. In both cases the monitoring light is of wavelengths 4300–4500 Å. The aluminium is evaporated in about 3 seconds at a deposition rate of the order of 100 Å per second. The MgF_2 evaporation begins within about 20 seconds after the completion of the aluminium evaporation and takes about 50 seconds to complete. The initial pressure is about 5×10^{-6} mm of Hg though there is a slight increase during the aluminium evaporation. The results obtained are quite reproducible provided care is taken in cleaning both the aluminium and substrate.

The "Spectrosil" B substrates, usually 30 mm diameter discs 2 mm thick and polished to plate glass finish (2 fringes) are ultrasonically cleaned in detergent, then immersed in isopropyl alcohol with a final isopropyl alcohol vapour wash. The aluminium wire is cleaned in 50-50 hydrochloric acid, washed in water and then in acetone. Before evaparation, glow discharge cleaning is

carried out.

The reflectance and transmission of samples are measured at 10° incidence on a reflectometer attached to a nitrogen purged "Optica" CF4 grating spectrophotometer. An area 2 mm×6 mm of a coating is measured but the variation in reflectance over a disc does not usually exceed ~0.5%. As a check, reflectances and transmittances were also measured at normal incidence by the method of Giacomo[18] and the results were in fair agreement with the reflectometer values within the error in R and T of ±0.5%.

Optical Properties of Coatings

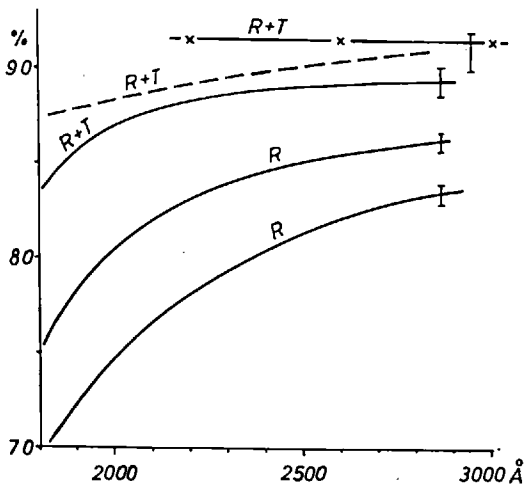


Fig. 2. Aluminium films. $(R+T)$ curve for back surface — — — — —. × Points at 2200 Å, 2600 Å, 3000 Å Hass and Waylonis.[15]

Figure 2 shows the reflectance R and the sum of the reflectance and transmittance $(R+T)$ for two thicknesses of aluminium film as measured within 24 hours of their preparation. The corresponding $(R+T)$ values obtained by Hass and Waylonis[15] for films measured within one hour after evaporation and with about the same R values at 2200 Å are indicated at λ 2200, λ 2600 and λ 3000. There should be little change in the reflectance at wavelengths longer than 1900 Å within 24 hours.[19] The back surface reflectance for the thicker of our films was also measured and the $(R+T)$ curve obtained after correction for the substrate refractive index and absorption is given. At 2200 Å the $(R+T)$ values obtained for both back and front surfaces of our films are 2-3% less than the Hass and Waylonis value.

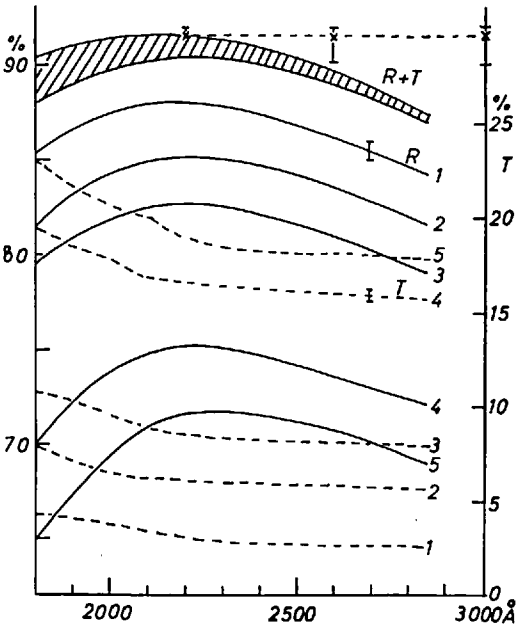


Fig. 3. Al-MgF_2 double layers. × Points at 2200 Å, 2600 Å, 3000 Å. Aluminium films Hass and Waylonis.[15]

Figure 3 gives R, T and $(R+T)$ curves for five samples of aluminium overcoated for optimum performance at 1850-1900 Å. As for figure 2, the reflectances and transmissions, measured within 24 hours, have been corrected for substrate absorption and reflection at the uncoated substrate face. The thickness of the MgF_2 overcoating is determined from the usual relation:

$$\lambda/2 = 2n.d - (\lambda/2\pi)\beta \qquad (1)$$

where β is the phase change on reflection at the MgF_2-Al interface. The value of β was calculated by substituting the values for the optical constants n_1, k_1 of aluminium, derived by extrapolation from the results of Hass and Waylonis,[20] in the formula[21]

$$\tan\beta = -2nk_1/(n_1^2+k_1^2-n^2) \qquad (2)$$

n is the refractive index of MgF_2.

The shaded area in figure 3 shows the spread in the $(R+T)$ values for the five samples, similar to that in the Hass and Waylonis values for 3000 Å for aluminium alone.

The performances of the various types of reflecting coatings for Fabry-Perot interferometry are compared in figure 4. The superiority of the double layers at 1900 Å

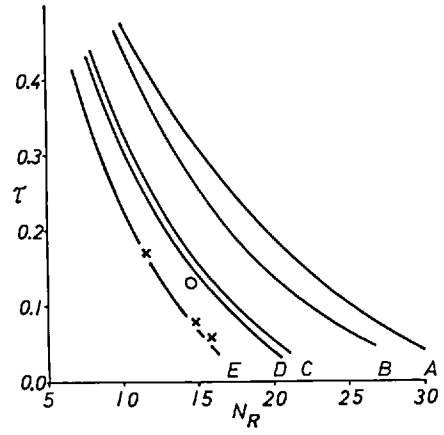


Fig. 4. Al and Al-MgF_2 reflecting coatings.
Curves A: Al at 2200 Å, Hass and Waylonis.[15]
B: Al-MgF_2 double layers at 1900 Å.
C: Calculated curve for Al at 1900 Å.
D: Al at 2200 Å.
E: Al at 1900 Å.
× Points back surface of Al-MgF_2 at 1900 Å.
○ Point back surface of Al at 1900 Å.

is clear but it should be noted that the curve corresponding to the back surfaces of these coatings reveals a performance inferior to the back surface of a single aluminium film. Why this is so is not clear, but it may be due to strain in the double coating.[22] It is interesting to compare these curves with the curve for pure aluminium calculated from the optical constants, derived as for formula (2). This suggests that the double layers are not optimum and from figure 2 it is likely that the aluminium layer is mainly at fault.

$N_R-\tau$ curves are very sensitive to variations in absorption in a coating. Using the relation[11]

$$\tau=[1-A/(1-R)]^2 \qquad (3)$$

it can be seen, for example, that for $N_R=17$, corresponding to $R=0.83$, the two values $T=0.07$ and $T=0.05$ give respectively $\tau=0.17$ and $\tau=0.09$, i.e. a difference in absorption of 2% results in a factor of nearly two in peak transmission.

It is hoped to increase the optical performance of the double layers for multiple beam interferometry by improved evaporation technique including a higher vacuum, with special attention to water vapour, and control of the substrate temperature.[15] This we feel will be specially important for coatings to be employed down to 1600 Å.

However, the performance of our present double layers at 1850 Å is as good as or better than that obtained previously with aluminium coatings, even in the near ultraviolet and visible. We have obtained Fabry-Perot interferograms of λ 1849 of HgI. Such coatings, might also prove suitable for a laser cavity working at these short wavelengths.

Fabry-Perot Interferogram at λ 1849

"Spectrosil" plates matched to λ/70 in the green were coated with Al-MgF_2 double layers designed to give optimum performance

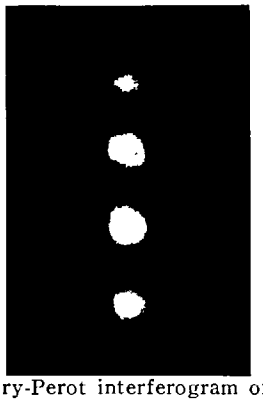


Fig. 5. Fabry-Perot interferogram of λ 1849 HgI. Interferometer spacing 0.15 mm.

at λ 1849. Figure 5 shows fringes of λ 1849 of HgI obtained with a "Spectroline" 11 SC-1 lamp. The line was isolated by a "Spectrosil" prism spectrograph purged with nitrogen and the interferogram was recorded by a single-stage magnetically focused image converter[23] with a "Spectrosil" window, S-9 photocathode, and a phosphor screen output. The image converter, specially constructed by us for this work, greatly facilitated detection and recording of the fringes (the imperfection in one of the fringes is due to a defect in the phosphor screen). The linear resolution of the image tube of 30 line pairs/mm was more than adequate for the fringes. An etalon separation of 0.15 mm was easily achieved with aluminium foil spacers and this arrangement proved to be stable.

The recorded fringe finesse of about 5 is mainly limited by the quality and adjustment of the interferometer plates. To confirm this, fringes of λ 2537 were also recorded and a finesse of 7, directly proportional to the increase in wavelength, was obtained, showing that the defects finesse dominates.

A high quality 6 cm diameter Fabry-Perot interferometer with plates of "Spectrosil A" matched to better than $\lambda/150$ in the green has now been constructed and we hope to extend the spectral range below 1700 Å for diagnostic spectroscopy and space research applications, employing the instrument both in its oscillating form and in its spectrographic method of use. Image intensifiers incorporating time resolution devices and solar blind photocathodes are being developed for this work.[6]

Fabry-Perot Type Interference Filters

For satellite and rocket photometry it is important to obtain interference filters capable of operation at wavelengths below 2000 Å. Such filters could also be used to isolate line structures for higher resolution study by the interferometer (e.g. λ 1640 of HeII). We have already reported[24] on the transmission characteristics of first order interference filters deposited on "Spectrosil" substrates. These filters consist of two aluminium reflecting layers separated by a magnesium fluoride spacing layer of thickness d given by

$$(m-1)\lambda = 2nd-(\lambda/2\pi)2\beta \qquad (4)$$

where n and β are the same as in equations (1) and (2) above, and m is an integer. The outer aluminium layer is protected from oxidation by a magnesium fluoride overcoating.

In figure 6, curve A is the transmission characteristic of a filter peaking at 1825 Å. Below 1800 Å the finesse decreases because of the falling reflectivity at the Al-MgF_2 interfaces, but at about 1660 Å the rapidly increasing absorption of the substrate leads to a sharp cut-off. Above 1800 Å the transmission profile corresponds to a halfwidth of 225 Å and a finesse of 8.

Curve B is the transmission characteristic of the same filter tilted through 8° to displace the peak wavelength to 1805 Å. Also indicated on the figure is the halfwidth of 115 Å for a filter with peak transmission of 19% at 1825 Å, composed of two double-layer Al-MgF_2 reflectors separated by a vacuum gap. The halfwidth and peak transmission are calculated from the results shown in figure 3.

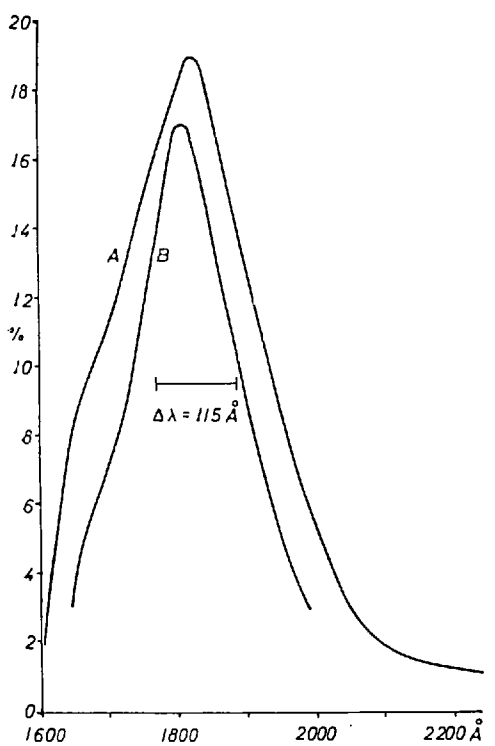


Fig. 6. Transmission curves of first-order Fabry-Perot type filter.

Conclusion

The feasibility of multiple beam interferometry down to 1800 Å has been demonstrated and we hope to extend the spectral range to 1600 Å for diagnostic spectroscopy and space applications. Employing lithium fluoride or sapphire substrates interference filters should be feasible to about 1500 Å. Interferometric determination of wavelength standards in this spectral region is now possible with extension to shorter wavelengths by the Combination Principle.[25]

Acknowledgements

We thank Professor J. D. McGee for his advice and encouragement, Professor W. R. S. Garton for helpful discussion and the generous lending of equipment, and Mr. D. S. Widner for making the filter measurements in the Seya monochromator. Assistance from the British National Committee for Space Research for the purchase of equipment and the support of one of us (C. O. L. J.) is gratefully acknowledged. One of us (S. M.) is supported by a Colombo Plan Fellowship.

References

1) S. Tolansky and D. J. Bradley: N. P. L. Symposium on Interferometry (H. M. S. O., London, 1959).
2) N. J. Peacock and E. T. Hill: U. K. A. E. A. Culham Laboratory Report on Time-Resolved Interferometric Measurements of Emission Line Profiles (U. K. A. E. A. Culham Laboratory, Culham, 1964).
3) D. R. Herriot: Applied Optics **2** (1963) 865.
4) D. J. Bradley, B. Bates, and C. O. L. Juulman: Proc. Sixth Conf. Phénomènes d'Ionization dans le Gaz **4** (C. I. P. I. G., Paris, 1963), p. 79.
5) G. M. Malyshev, G. T. Razdobarim, and L. V. Sokolova: Soviet Physics – Doklady **7** (1963) 701.
6) D. J. Bradley, B. Bates, C. O. L. Juulman, and S. Majumdar: Applied Optics **3** (1964) 1461.
7) D. J. Bradley, A. W. De Silva, D. E. Evans, and M. J. Forrest: Nature **199** (1963) 1281.
8) P. Jacquinot: Reports on Progress in Physics **23** (1960) 267.
9) D. J. Bradley: *Proceedings of the Conference on Optical Instruments and Techniques* (Chapman and Hall, London, 1961), p. 31.
10) T. Dunham: *Vistas in Astronomy*, Vol. 2 (Pergamon Press, London, 1956), p. 1223.
11) R. Chabbal: J. Rech. C. N. R. S. **24** (1953) 138.
12) H. E. Bennett and J. O. Porteus: J. Opt. Soc. Am. **51** (1961) 123.
13) D. A. Jackson: Proc. Roy. Soc. **A 263** (1961) 289.
14) G. Honica and K. Krebs: Z. Physik **156** (1959) 117.
15) G. Hass and J. E. Waylonis: J. Opt. Soc. Am. **51** (1961) 719.
16) J. C. Burridge, H. Kuhn, and A. Pery: Proc. Phys. Soc. B **46** (1953) 963.
17) G. Hass and R. Tousey: J. Opt. Soc. Am. **49** (1959) 593.
18) P. Giacomo: Compt. Rend. **235** (1952) 1627.
19) P. H. Berning, G. Hass, and R. P. Madden: J. Opt. Soc. Am. **50** (1960) 586.
20) D. J. Schroeder: J. Opt. Soc. Am. **52** (1962) 1380.
21) J. M. Bennett: J. Opt. Soc. Am. **54** (1964) 612.
22) L. G. Schulz and F. R. Tangherlini: J. Opt. Soc. Am. **44** (1954) 357.
23) J. D. McGee: Reports on Progress in Physics **24** (1961) 167.
24) D. J. Bradley, B. Bates, C. O. L. Juulman, and S, Majumdar: Nature **202** (1964) 579.
25) B. Edlén: Reports on Progress in Physics **26** (1963) 181.
26) Z. Lés, F. Lés, and L. Gabla: Acta Physica Polonica **23** (1963) 211.
27) A. Stendel: J. Phys. Radium **19** (1958) 312.
28) R. Lennuier: J. Phys. Radium **19** (1958) 319.

DISCUSSION

Mangus, J. What size, diameter, plates are you using?

Bradley, D. J. We have now 6 cm plates flat to $\lambda/150$ in the green.

Hartman, P. L. What material are you hoping to use for 4th harmonic generation of ruby light?

Bradley, D. J. Crystal quartz.

Reprinted from APPLIED OPTICS, Vol. 3, page 1461, December 1964
Copyright 1964 by the Optical Society of America and reprinted by permission of the copyright owner

Time Resolved Photoelectric Spectrography by Electron-Optical Image Detection of Etalon Interferograms

D. J. Bradley, B. Bates, C. O. L. Juulman, and S. Majumdar

The application of a Fabry–Perot etalon combined with an electron-optical image detector to obtain simultaneously time, spatial, and spectral resolution of plasma and laser sources is discussed, and comparison is made with oscillating Fabry–Perot interferometers. Matching of the interferometer to the image tube is considered, and optimum conditions are determined. Four types of image tubes were tested and the effects of signal-induced background and noise are described. Finally, the interpretation of time-resolved interferograms of wavetrains of very short duration, such as obtained from laser giant pulses, is dealt with, and extension of the interferometer spectral range in the vacuum uv reported.

Introduction

The superior angular dispersion and large light gathering power of photoelectric interferometric spectrometers are being increasingly exploited for plasma diagnostic spectroscopy. In particular, the oscillating Fabry–Perot interferometer has proved to be a powerful tool for time-resolved spectroscopy, and the technique has been extended to laser spectroscopy where the high spectral resolving powers required can be obtained by interferometric means only. The advantages and optical principles of the oscillating interferometer for time-resolved spectroscopy have been previously discussed,[1,2] and instruments employing electromechanical[1,3–5] and piezoelectric drives[6–8] have since been fully developed. However, this method of use of the interferometer suffers from the serious disadvantage that time and wavenumber dispersion are superposed. It is thus necessary to scan at a speed N times greater than the rate of change of the phenomena studied (where N is the interferometer finesse) which leads to a decrease in the signal-to-noise ratio attainable with a given source. Also, continuous monitoring is not possible, and, since a point source is utilized, simultaneous spatial and time resolutions are not obtained.

With the development of Q-spoiled laser systems[9] with outputs lasting <20 nsec and spectral widths[10] <0.01 cm^{-1}, time-resolved interferometric spectroscopy in the nanosecond region is now required. At these speeds, time-sequential spectral scanning results in a distorted recorded profile because of Doppler shifts at the moving mirror. However, the increase in the time resolution limit by the factor N (usually about 20) is the most serious limitation, since the time resolution limit set by the source itself cannot be achieved, as will be shown, and time resolution is obtained only at the expense of spectral resolving power, and the study of phenomena such as multimoding would not be possible.[10]

The development of image intensifiers[11] combining the high quantum efficiencies of photocathodes with the information capacity of the photographic plate led us to explore the possibility of employing the Fabry–Perot interferometer in combination with an image-tube detector for time-resolved spectroscopy to overcome the limitations of the oscillating instrument, and reports of our preliminary investigations have been made.[12,13] We now wish to summarize these, and more recent results employing electronography, to comment further on the optimum conditions of matching the interferometer and the image tube, and to discuss the application of the method to laser spectroscopy.

The Photoelectric Spectrographic Method

The Fabry–Perot ring pattern superposed on a slit image, as in the classical photographic method of use, is swept across the output phosphor of an image tube to give a continuous time record, since wavenumber and time dispersions are now crossed. We have initially tested the system with a rotating mirror system (Fig. 1). The slit-ring pattern was swept across the photocathodes of four different types of image tube. The time resolution limit of 2 μsec was set entirely by the intensity of the mercury arc source. For laser and plasma source, electron-optical sweeping[14,15] or a multiple-beam image tube[15] may be employed.

The advantages of the method are immediately obvious. The only limit to time resolution is now the

The authors are with the Physics Department, Imperial College, London, England.

Received 25 March 1964.

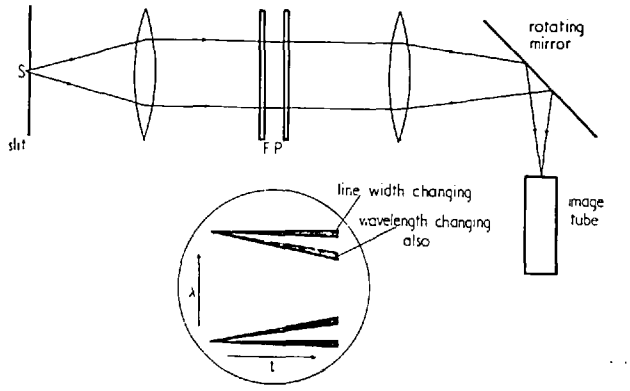


Fig. 1. Principle of the method.

intensity of the source, and maximum spectral resolution of laser modes is then possible. Secondly, a continuous time record is obtained with wavenumber and time dispersions crossed, and, since there is normally a one-to-one correspondence between source and ring pattern, simultaneous spatial resolution is achieved, also crossed with the time dispersion. Finally, there is a gain in luminosity depending upon the order of the fringe employed, and, just as for the scanning interferometer, because of its superior angular dispersion, the Fabry–Perot spectrograph has a gain in illumination over grating spectrographs, and this gain increases with resolving power.[16]

The Interferometer

As usual, it is necessary to match the linear resolution g of the image tube to that of the projected fringe half-width. This requires, for the pth ring from the center, a focal length of $f = 2gN\sqrt{ps\nu}$; N is the finesse, ν the wavenumber, and s the interferometer separation. Maximum use is made of the image-tube photocathode area if the interferometer is tilted and only half of the ring pattern employed. For a cathode of linear dimension l, the maximum number of rings is then $(p_2 - p_1) = (l/gN)[1 - (l/4gNp_2)]$ if the half-width of the p_2th ring from the center is matched to g. Angular dispersion decreases from the center, so it is best to start with the first ring out. Then $p_1 \leqslant 1$. Also, for a given image tube, the maximum number of rings depends only on the finesse.

The angular width α of the slit is determined by the usual relation $\alpha = 2/\sqrt{Ns\nu}$, giving a linear width $a = 4g\sqrt{Np_2}$. Spectral resolving power of the swept image is little affected by ring curvature for a slit of this width. Since the linear diameter D_p, of ring p, is equal to $4gN\sqrt{pp_2}$, then the maximum height of the fringe chord is $(a/2)^2/D_p = g\sqrt{p_2/p}$, the half-width of fringe p, so that the effect of ring curvature does not vary from fringe to fringe. A typical value of g is 100 μ, so that for a 2-cm photocathode two hundred time-resolution elements are obtained on each of the fringes.

The gain in luminosity over the oscillating Fabry–Perot spectrometer arises from the fact that the fringes are continuously and simultaneously recorded, not just $(1/N)$ of an order at a time. If m fringes are utilized, the total gain is mN. However, there is a loss in luminosity, since only a fraction of a fringe $(= 1/\pi\sqrt{Np})$ of a complete ring is recorded for a slit of width a. So for each fringe the gain G in luminosity is $= (1/\pi)\sqrt{N/p}$. This gain decreases with increasing p and has its maximum value at $p = 1/2N$ (the central fringe). For $p = 1$, $N = 10$, the gain is about unity.

It is not very useful to consider the total gain in luminosity,[14] for, while the density of each fringe remains constant, because of the parabolic dispersion of the interferometer, the elementary resolution area decreases from the central fringe outward, so the information rate decreases. This also follows from the decrease in luminosity for increasing p. Since the width of the fringe p is $g\sqrt{p_2/p}$, the information decreases as $1/\sqrt{p}$. The angle subtended by a slit of width a situated at position of fringe p_2 is $\alpha = a/R_{p_2} = 2/\sqrt{Np_2}$ (Fig. 2), so a sector slit of angular width α will have a linear width $\alpha R_p = 4gN\sqrt{p}$ at fringe p. Such a sector slit then provides the same amount of information from each fringe, and, more importantly, gives an increased number of time-resolution elements per linear length of each higher order fringe, the interferometer being tilted to use only one-half of the fringe pattern. A similar argument also applies when the interferometer is employed as a polychromator with photomultiplier detection.

The Image Detector

This comparison of the two methods of use of the interferometer is based on the assumption that the signal-to-noise ratio of a photomultiplier and an image tube with photographic recording of the output can be made equal. Unfortunately, this is not always true of all image tubes presently available. Though tube background is usually negligible for rapid time-resolved spectroscopy, with some tubes signal-induced background and noise can be serious.

The system was first tested with a five-stage magnetically focused transmission secondary-emission image intensifier (20th Century Electronics Type IPM 29/25) of the type developed at Imperial College.[11,17] This tube had a linear resolution of 30 lp/mm, a 20-mm photocathode of 20-μA/lm sensitivity and a blue light

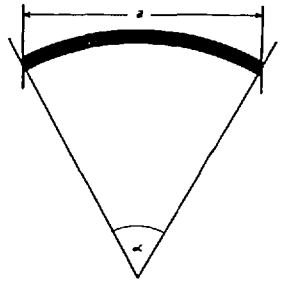


Fig. 2. Slit angle.

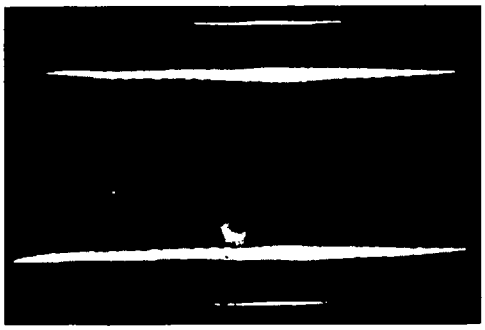


Fig. 3. λ5461 high-pressure mercury lamp. Single-stage image tube. Time resolution 6×10^{-4} sec; spectral resolution 3.3×10^5 sec.

gain of 10^5 at 33 kV with a tube background of 10^3 scintillations sec^{-1} cm^{-2}. An interferometer separation of 0.4 mm and coatings of 85% reflectivity gave a spectral resolving power of 32,000 for λ5461 HgI of a high-pressure mercury lamp. The slit-width of 125 μ was magnified to 250 μ on the tube photocathode, giving eighty time-resolution elements per fringe which, with a mirror speed of 100 cps, corresponds to a 2×10^{-6} sec time resolution limit. Even with a tube voltage of only 26 kV, the signal-induced background and noise and the wide spread in the multiplication factor for individual photoelectrons resulted in such a decrease in the effective signal-to-noise ratio in the recorded image as to make it unsuitable for diagnostic spectroscopy.

The signal-induced noise is mainly due to unfocused penetrating primary electrons, whereas the signal-induced background arises from focused photoelectrons from light reflected back from the first dynode. The photocathode transmits some of the incident light, and this is, of course, common to most types of image intensifier. Thicker photocathodes should help to reduce the effect which would be expected to be wavelength-dependent also. The magnitude of the penetrating primaries' effect is dependent on such factors as the thickness and structure of the dynodes. It is to be hoped that both these effects can be greatly reduced, but meanwhile signal-induced noise limits the use of transmitted secondary-emission image intensifiers for swept time-resolved spectroscopy.

A single-stage magnetically focused tube was employed to test the relative importance of signal-induced background arising from back reflected light. The aluminum-backed phosphor screen of this tube is 20 cm from the photocathode compared with 7 cm between photocathode and first dynode of the transmitted secondary-emission tube. The gain of such a tube with F 1 optical coupling to a photographic recorder is about 5 or with contact print recording about 50.[11] Figure 3 shows a swept scan of λ5461 of the high-pressure mercury lamp. Spectral resolving power is now 3.2×10^5, and the time-resolution limit is 6×10^{-4} sec with sixty time elements on each fringe. Variations in intensity and half-width arise from source instability. A microphotometer trace of the two central fringes is shown in Fig. 4. Penetrating primary electrons are absent, of course, and the smaller solid angle subtended at the photocathode by the phosphor output screen reduces the effect of back reflected light.

Next a three-stage magnetically focused cascaded phosphor-photocathode image intensifier of the type developed at Imperial College by McGee and Catchpole[18] was employed as detector. This tube originally had a blue light gain of 80,000 at 45 kV, but the gain had dropped somewhat. Optical coupling to the phosphor output was again an F 1 system. Figure 5 shows a microphotometer tracing of a swept scan of λ5461. A slit-width of 0.5 mm on the phosphor screen corresponds to a time-resolution limit of 10 μsec with fifty resolution elements per fringe. A faster scan giving 3-μsec resolution was also obtained, but the density was not so high. Spectral resolving power is again 3.2×10^4. The signal-to-noise ratio of the cascaded phosphor-photocathode tube is much superior to that of the transmitted secondary-emission multiplier tube.

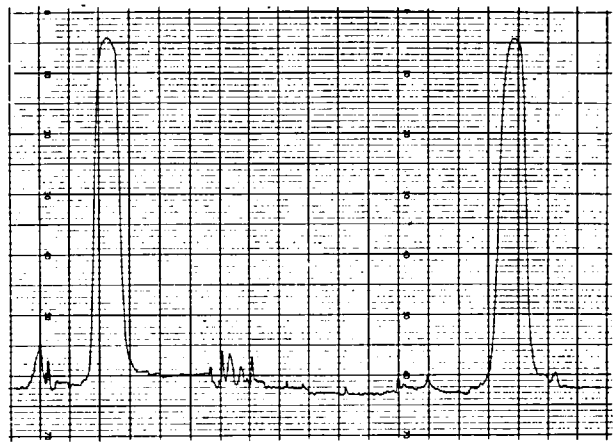


Fig. 4. Microphotometer trace of Fig. 3.

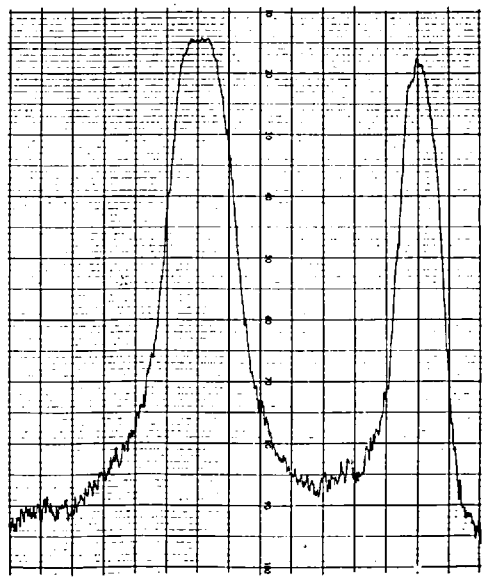


Fig. 5. Microphotometer trace of λ5461 fringes. Cascaded image intensifier. Time resolution 10^{-5} sec, spectral resolution 3.2×10^4 sec.

Electronography

Finally a Lenard window image tube, also developed by McGee[19] at Imperial College, was employed. This particular tube had a low cathode sensitivity of ~16 μA/lm but was otherwise satisfactory. The mica window was 5 mm × 30 mm and about 4 μ thick, and the tube was operated at an over-all voltage of 40 kV. The Ilford G5 nuclear emulsion was mounted on a Melinex strip, and the method of operation of the tube was as described by McGee.[19]

The slit-width of 300 μ was magnified 3× on the photocathode, and the interferometer was tilted to obtain five fringes across the 5-mm width of the mica window. A Philips low-pressure mercury lamp (Type 93109) was employed as light source, and the λ5461 line was isolated by a filter. Figure 6 shows the fringes recorded for exposures of 0.02 sec and 0.04 sec. Signal-induced background is completely absent across the whole of the 30 mm of the window, and the excellent recording of the pattern is indicated by the absorption line in the middle of the fringes.

Because of the low sensitivity of this particular tube, it was not possible to obtain a time resolution of <1 msec with the Philips lamp, without resorting to track counting. A tri-alkali cathode and the employment of Ilford Ilfex emulsion should reduce this limit to ~20 μsec. A tube with a phosphorphotocathode sandwich gain stage would increase the speed by a further factor of 50× to 100×, but with some loss of linear resolution. For spectroscopy in general, the Lenard window has outstanding signal-to-noise performance with, in addition, the great advantage of a linear density-exposure relationship.[11]

Time-Resolved Interferograms from Pulsed Wavetrains

By employing electron-optical sweeping and multiple beam image tubes, it should prove possible to obtain nanosecond time resolution of laser sources, and it is interesting to consider the type of interferogram recording expected. Consider a constant-amplitude wavetrain of length Δl and spectral width $\Delta\nu \cong c/\Delta l$. Even for a perfect interferometer, the finesse is no longer determined by the reflectivity of the coatings, since the number of interfering beams is limited by the length of the wavetrain, and the intensity distribution in the transmitted pattern is now the same as that of the Lummer–Gehrcke interferometer,[20]

$$I(p) = \frac{1 + G_p \sin^2 p\delta/2}{1 + F \sin^2 \delta/2} (1 - R^p)^2 I_0,$$



Fig. 6. λ5461 low-pressure mercury lamp fringes. Lenard window electronographic image tube. Exposures 1/50 and 1/25 sec.

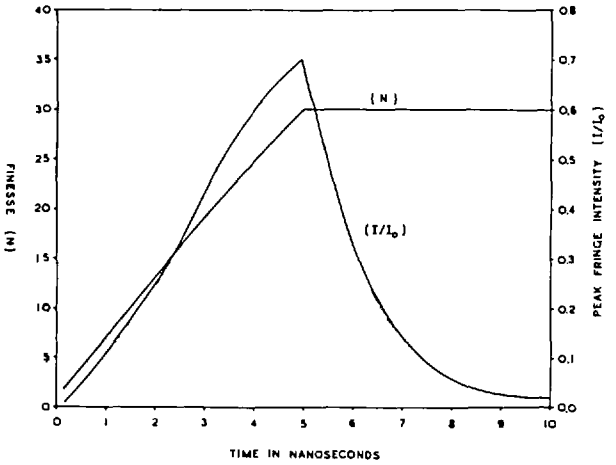


Fig. 7. Time variation of finesse and peak fringe intensity of interferogram of 150-cm wavetrain.

where $G_p = 4R^p/(1 - R^p)^2$; $F = 4R/(1 - R)^2$; and p is the number of interfering beams.

To obtain a recorded spectral width equal to that of the source width (assuming a perfect etalon), it is necessary that the interferometer finesse equal the number of interfering beams. The condition is easily obtained from Fig. 7.70 of ref. 20. Taking, for example, a typical laser giant pulse wavetrain[10] lasting 5 nsec so that Δl = 150 cm, then an interferometer reflectivity of 0.94 gives a finesse N = 30. A plate separation of 2.5 cm then produces thirty interfering beams and a fringe width of 200 Mc/sec as required.

However, it takes 5 nsec for the interference pattern to build up to its maximum intensity and finesse. Although the finesse remains constant after this, the intensity of the fringe maxima will decrease rapidly and continuously as the earlier transmitted beams cease to contribute to the interferogram. For our particular example, the rate of decrease will be by R^2 every 1.7 × 10^{-10} sec (5/30 nsec) and after a further 5 nsec the fringe peak is only 0.02 I_0 [$I_0 \rightarrow (T/1-R)^2$]. The time variation of both finesse and peak fringe intensity to be expected in this elementary case is shown in Fig. 7.

Discussion

The combination of a Fabry–Perot interferometer and an image intensifier provides a powerful diagnostic tool for laser and plasma sources, providing as it does simultaneous spectral, spatial, and time resolution. No other system seems capable of the high temporal and spectral resolving powers required.

Recent developments in coating techniques[21] make possible the extension of the spectral range of the interferometer into the vacuum ultraviolet region. An automatic evaporation plant has been constructed for this purpose. Aluminum films are evaporated in about 3 sec and immediately, without breaking the vacuum, overcoated with magnesium fluoride to both prevent oxidation of the metal and enhance reflectivity. We have now succeeded in obtaining Fabry–Perot fringes

at λ1849 and an interference filter with a bandwidth of 200 Å and 19% peak transmission at this wavelength.[22]

Finally, we would like to point out that when only an isolated line without any neighboring satellites is being examined, as is frequently the case in plasma diagnosis, high reflecting powers, as normally employed for hyperfine structure work, of >85%, are not always necessary. Luminosity can often be greatly increased by reducing the reflectivity of the interferometer coating (to as low as 75%) and at the same time maintaining the spectral resolving power by increasing plate separation.

We wish to thank J. D. McGee for his interest, encouragement, and helpful discussion during the course of this work and, in particular, for the loan of both cascade and Lenard window image tubes. S. Majumdar is supported by a Colombo Plan Fellowship and C.O.L Juulman by the British National Committee for Space Research.

References

1. S. Tolansky and D. J. Bradley, *N.P.L. Symposium on Interferometry* (Her Majesty's Stationery Office, London, 1959), p. 375.
2. D. J. Bradley, Proc. Roy. Soc. (London) **A262**, 529 (1961).
3. D. J. Bradley, *Proceedings of Conference on Optical Instruments and Techniques* (Chapman and Hall, London, 1961), p. 31.
4. D. J. Bradley, J. Opt. Soc. Am. **52**, 222 (1962).
5. D. R. Herriot, Appl. Opt. **2**, 865 (1963).
6. J. Cooper and J. R. Greig, Nature **195**, 371 (1962).
7. J. V. Ramsay, Appl. Opt. **1**, 411 (1962).
8. N. J. Peacock and E. T. Hill, "Culham Laboratory Report", U.K.A.E.A. Culham, England (1962).
9. F. J. McClung and R. W. Hellwarth, Proc. IEEE **51**, 46 (1963).
10. D. J. Bradley, A. W. Desilva, D. E. Evans, and M. J. Forrest, Nature **199**, 1281 (1964).
11. J. D. McGee, *Reports on Progress in Physics* (The Physical Society, London, 1961), Vol. 24, p. 167.
12. D. J. Bradley, Institute of Physics and The Physical Society Spectroscopy Group, London meeting abstracts (1962).
13. D. J. Bradley, B. Bates, and C. O. L. Juulman, *Proc. of VI Conf. Phenomenes d'Ionization dans les Gaz, Paris (1963)*, (Centre d'Etudes Nucleaires, Saclay, France, 1963), Vol. 4, p. 791.
14. G. M. Malyshev, G. T. Razdobarim, and L. V. Sokolova, Soviet Physics-Doklady **7**, 701 (1963).
15. D. J. Bradley and S. Majumdar, to be published.
16. P. Jacquinot, *Reports on Progress in Physics* (The Physical Society, London, 1960), Vol. 23, p. 267.
17. W. L. Wilcock, D. L. Emberson, and B. Weekley, Nature **185**, 370 (1960).
18. J. D. McGee and C. E. Catchpole, British I.E.E. Conf. Rept., Series 5, p. 182 (1962).
19. J. D. McGee and B. E. Wheeler, *Advances in Electronics and Electron Physics* (Academic, London, 1962), Vol. 16, p. 47.
20. M. Born and E. Wolf, *Principles of Optics* (Pergamon, London, 1959), pp. 340–346.
21. W. R. Hunter, Optica Acta **9**, 255 (1962).
22. D. J. Bradley, B. Bates, C. O. L. Juulman, and S. Majumdar, Nature **202**, 579 (1964).